Graz University of Technology

Birgit Ungerböck

Application of Optical Sensor Materials to Microfluidic Devices (Lab on a Chip)

DIPLOMARBEIT

zur Erlangung des akademischen Grades einer Diplomingenieurin
der Studienrichtung Allgemeine Technische Chemie
erreicht an der

Technischen Universität Graz

Univ.-Prof. Dipl.-Chem. Dr. rer.nat. Ingo Klimant
und
Univ.-Ass. Dipl.-Chem. Dr. rer.nat. Torsten Mayr

2010

Contents

1 INTRODUCTION 5

2 THEORETICAL BACKGROUND 7

2.1 BASIC PRINCIPLES OF PHOTO-LUMINESCENCE 7
2.1.1 JABLONSKI DIAGRAM 7
2.1.2 LIFETIME 8
2.1.3 QUENCHING 11
2.1.3.1 Dynamic quenching 12
2.1.3.2 Static quenching 12
2.2 FLUORESCENCE MICROSCOPY 14
2.2.1 ASSEMBLY OF A FLUORESCENCE MICROSCOPE 14
2.2.2 IMAGING CALIBRATION SCHEMES 15
2.2.2.1 FRIM (Fluorescence ratiometric imaging) 15
2.2.2.2 FLIM (Fluorescence lifetime imaging 15
2.3 LIGHT HARVESTING 17
2.4 MICROFLUIDIC SYSTEMS – GENERAL ASPECTS 18
2.4.1 DEFINITION 18
2.4.2 HISTORY OF MICROFLUIDICS 18
2.4.3 FABRICATION OF MICROFLUIDIC DEVICES 19
2.4.3.1 Polymer micromachining 19
2.4.3.2 Polymer materials for microfabrication 21
2.4.4 APPLICATIONS OF MICROFLUIDICS 21
2.5 OPTICAL SENSORS IN MICROFLUIDIC DEVICES 22
2.5.1 DETECTION OF OXYGEN IN MICROFLUIDIC SYSTEMS 23
2.5.2 OPTICAL PH-SENSING IN MICROFLUIDIC SYSTEMS 24

3 MATERIALS AND METHODS 26

3.1 CHEMICALS AND MATERIALS 26
3.1.1 CHEMICALS 26
3.1.2 OPTICAL FILTERS 27
3.1.3 MICROFLUIDIC DEVICES 27
3.1.4 FLOW-THROUGH-CELL 29

3.1.5 PREPARATION OF GLUCOSE-OXIDASE-FILMS 29
3.2 INSTRUMENTATION 30
3.3 SOFTWARE 31

4 PRACTICAL PART 32

4.1 INTEGRATION OF OXYGEN-SENSING FILMS 32
4.1.1 INTRODUCTION 32
4.1.2 EXPERIMENTAL PROCEDURE 33
4.1.2.1 Preparation of oxygen-sensing films 33
4.1.2.2 Measurements 33
4.1.2.3 Estimation of film thickness 34
4.1.3 RESULTS AND DISCUSSION 35
4.1.3.1 Spectral characterisation and adaption of optical systems 35
4.1.3.2 Optimisation of the light-harvesting dye system regarding brightness 37
4.1.3.3 Photobleaching 38
4.1.3.4 Calibration 43
4.1.3.5 Application in microfluidic devices 48
4.1.4 CONCLUSION 51
4.2 OXYGEN-SENSITIVE PSPVP-NANOSENSOR PARTICLES 53
4.2.1 INTRODUCTION 53
4.2.2 EXPERIMENTAL PROCEDURE 53
4.2.2.1 Staining of the nanoparticles 53
4.2.2.2 Emission and excitation spectra 54
4.2.3 RESULTS AND DISCUSSION 54
4.2.3.1 Spectral characterisation 54
4.2.3.2 Adaption of optical systems 55
4.2.3.3 Application 55
4.2.3.4 Ratiometric imaging 57
4.2.4 CONCLUSION 59
4.3 MAGNETIC NANOPARTICLES 60
4.3.1 INTRODUCTION 60
4.3.2 EXPERIMENTAL PROCEDURES 62
4.3.3 RESULTS AND DISCUSSION 63
4.3.3.1 Adaption of the optical system 63
4.3.3.2 Spectral characterisation 64
4.3.3.3 Calibration: 65
4.3.3.4 Application 65

4.3.4 CONCLUSION 74
4.4 OPTICAL PH-SENSING FILMS 75
4.4.1 INTRODUCTION 75
4.4.2 EXPERIMENTAL PROCEDURE 77
4.4.2.1 Preparation of sensor films 77
4.4.2.2 Calibration curve measurements 77
4.4.2.3 Phosphate buffer preparation 78
4.4.3 RESULTS AND DISCUSSION 79
4.4.3.1 Adaption of optical system 79
4.4.3.2 pH dependency of emission spectra 80
4.4.3.3 Calibration using the color camera 80
4.4.4 CONCLUSION 82

5 CONCLUSION AND FUTURE OUTLOOK 83

5.1 FLIM 83
5.2 FRIM APPLYING A MONOCHROME CAMERA 83
5.3 FRIM APPLYING A COLOR CAMERA 84
5.4 INTEGRATION OF DIFFERENT SENSOR MATERIALS 84

6 APPENDIX 86

6.1 REFERENCES 86
6.2 LIST OF FIGURES 89
6.3 LIST OF TABLES 91
6.4 MATLAB-SCRIPTS 91

1 Introduction

Microfluidic systems are defined by the small volume that is processed by these systems (10^{-9} to 10^{-18}l) [1]. Their promising advantages like reduced reagent consumption, laminar flow, enhanced heat transfer, parallelization and low cost led the new technology of the mid-20th century from gas chromatography [2] and a general miniaturized total analysis system (μTAS) [3] to various research fields including chemistry, biology, genomics, proteomics, pharmaceuticals and bio-defence.

When materials used for the fabrication of microfluidic devices changed from glass and silicon to elastomers like PDMS, life science research became a very important research field of the microfluidic technology. This is mainly due to the high biocompatibility of PDMS and laminar flow, which enabled new methods of studying cellular processes [4]. Moreover the change to polymeric substrates opened the road to mass fabrication and low-cost disposable devices. This can be traced back to the generally lower cost of substrate materials and to the fact that polymer microfabrication technologies are relatively simple compared to fabrication methods used for glass and silicon [5].

However, application of microfluidic devices in life sciences also shows many other conveniences compared to conventional technologies. Their similarity to natural conditions (fluid-to-cell volume ratio is close to physiological conditions), high controllability and reproducibility of environmental factors and the possibility of automation are convincing reasons to perform experiments in microsystems.

In addition to universally helpful components such as valves, mixers and pumps it is also necessary to integrate sensors into microfluidic devices to control or simply monitor certain analytes in the chip. Due to reduced analysis volumes this sometimes turns out to be a difficult task. Since optical sensors are sufficiently sensitive, scalable to smaller dimensions and rather low-priced there is a growing interest in integration of optical components into lab-on-a-chip-devices [6]. Luminescence based sensors are known to be robust, well suited for small volumes and they facilitate parallelisation and the determination of multiple parameters. Last but not least their flexibility finally allows performing 2-dimensional measurements by microscope-based detector set-ups.

Especially when microfluidic systems are used for biological investigations determination of the oxygen-concentration – as one of the most important metabolites is of high importance [7]. Oxygen-sensors can be used to indicate the physiological status of cells that can be

affected by various toxic agents. Thereby the observation of oxygen consumption of cells can for instance provide information in applications like pharmaceutical drug screening or environmental monitoring [8].

When small volumes are analysed optical sensors offer one important advantage over state-of-the-art electrochemical sensors [8]: they do not consume oxygen.

Moreover, apart from simply detecting averaged oxygen-levels in the chip it is also interesting to accomplish space-resolved quantitative analysis of the oxygen-distribution. Space resolved measurements can give information about oxygen gradients in biofilms or about a heterogeneous chemical distribution (for example caused by a variable gas-permeability of PDMS) which can lead to difficulties in developing tissues [9]. Luminescence based sensors combined with referencing methods (see chapter 0) provide a dedicated possibility to accomplish such 2D-measurements.

For this diploma thesis three different designs of optical luminescent sensors (films, nanosensor particles and magnetic nano sensor particles) for monitoring dissolved oxygen and sensor foils for pH-sensing are prepared, optimised concerning emission intensity and integrated into microfluidic devices. Oxygen sensors base upon collisional luminescence quenching principle, whereas the basic principle pH-sensing is the change of the fluorescent response of a pH-sensitive dye. Signal read-out is accomplished off chip by imaging techniques on a fluorescence microscope. Two different referencing methods (fluorescence lifetime imaging and fluorescence ratiometric imaging; see chapter 2.2.2) with the application of two different cameras (monochrome camera (Sensicam) and a color camera (AVT Marlin F-201C)) are tested for 2D-imaging (overview see figure 1.1).

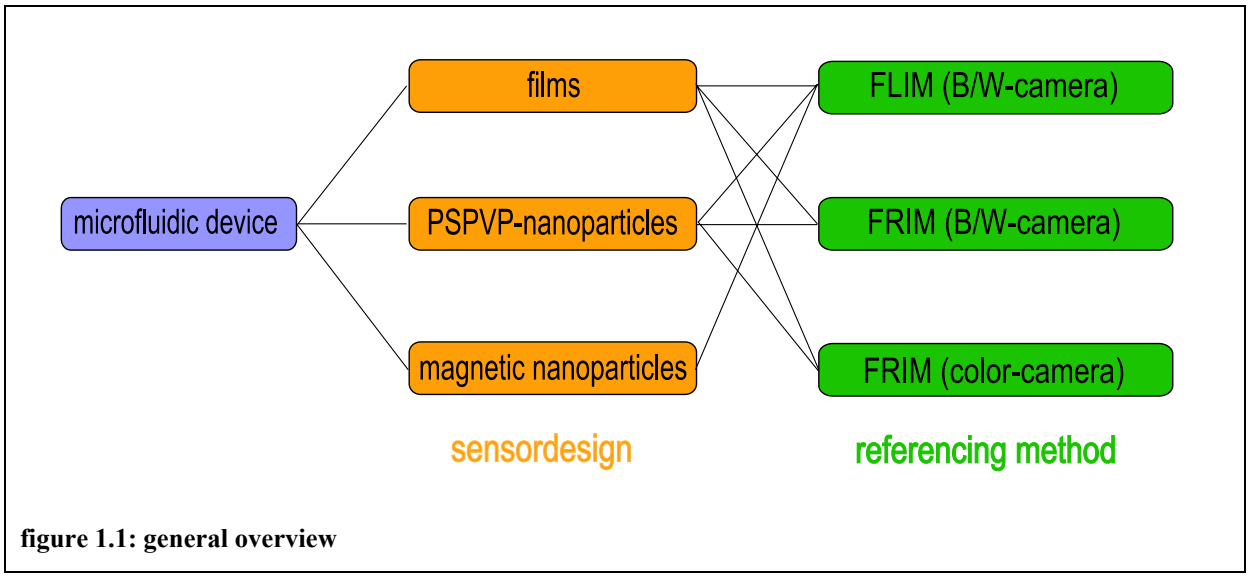

figure 1.1: general overview

2 Theoretical Background

2.1 Basic principles of photo-luminescence

There is a growing interest in integration of optical components into lab-on-a-chip-devices. This trend is mainly due to the fact that these components are easy to miniaturize and to the high sensitivity exhibited by the use of optical sensors [6]. Especially in molecular and cellular imaging, photoluminescence methodology faced an enormous rise.
This chapter will focus on the basic principles of photo-luminescence.

2.1.1 Jablonski diagram

The Jablonski diagram is suitable for the visualization of the main-processes concerning transitions between electronic states of a molecule, which are responsible for the phenomena of photoluminescence (see figure 2.1).

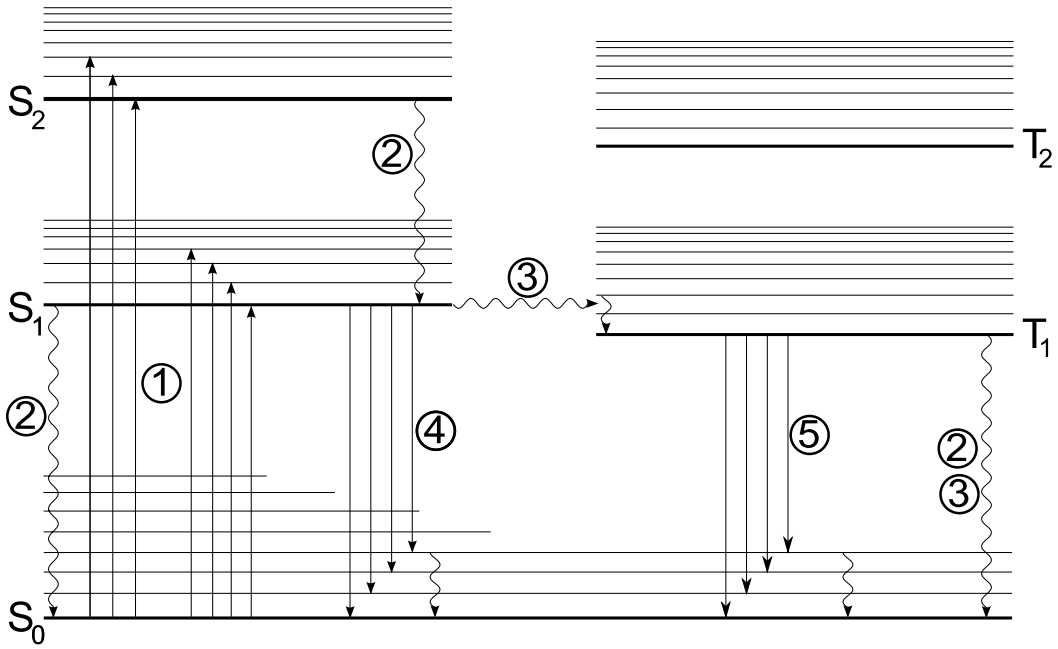

figure 2.1: Jablonski diagram with possible transitions
(1) absorption of a photon, (2) internal conversion, (3) intersystem crossing, (4) fluorescence, (5) phosphorescence

As one can see, transitions occur between the singlet electronic states S_0, S_1, S_2, … (electrons have opposite spin) and the triplet electronic states T_1, T_2, …(two electrons have parallel spin). Each electronic state has further energy-levels, the vibrational sub-levels.
Possible processes between these all these energy-levels (visualized by arrows) include absorption of a photon (1), internal conversion, intersystem crossing (3), fluorescence (4), phosphorescence (5) and triplet-triplet-transitions. Deactivation from an excited state can happen by the emission of a photon (radiative) or by other processes (non-radiative) (2), where the excess energy is transferred to surrounding molecules.
It is worth mentioning, that radiative deactivation always takes place at higher wavelengths than excitation. Absorption of a photon usually occurs from the lowest vibrational level of S_0 to one of the vibrational levels of an excited electronic singlet state. The fluorescent molecule is always deactivated from the lowest vibrational level of S_1. This leads to an offset of the energy, respectively the wavelength, also called the Stokes shift (gap between the maximum of the absorption band and the maximum of fluorescence).
What also deserves closer attention is the process called intersystem crossing. It is the transition between the isoenergetic singlet and triplet states, which is in principle forbidden. Spin-orbit coupling, however, enables this forbidden transition. Hence, radiative deactivation of the excited triplet-state, called phosphorescence, can occur. Due to the again forbidden transition T_1 to S_0 phosphorescence is a very slow process compared to fluorescence. (cf. [10])

2.1.2 Lifetime

One of the most important characteristics of a luminescent substance is the luminescent lifetime.
"The lifetime of the excited state is defined by the average time the molecule spends in the excited state prior to return to the ground state." [10]
To advance to the final mathematical description of the term lifetime we have to introduce some rate constants (k_r and k_{nr}) that describe various possible ways to deactivate the excited state S_1.
k^S_r: rate constant for radiative deactivation S_1->S_0 with emission of light
k^S_{IC}: rate constant for non-radiative deactivation S_1->S_0 without emission of light
k^S_{nr}: overall rate constant for non-radiative deactivation from S_1; $k^S_{nr} = k^S_{IC}+k_{ISC}$

For deactivation from T_1 we have:

k^T_r: rate constant for radiative deactivation T_1->S_0 with emission of light

k^T_{nr}: rate constant for non-radiative deactivation T_1->S_0

(see also figure 2.2)

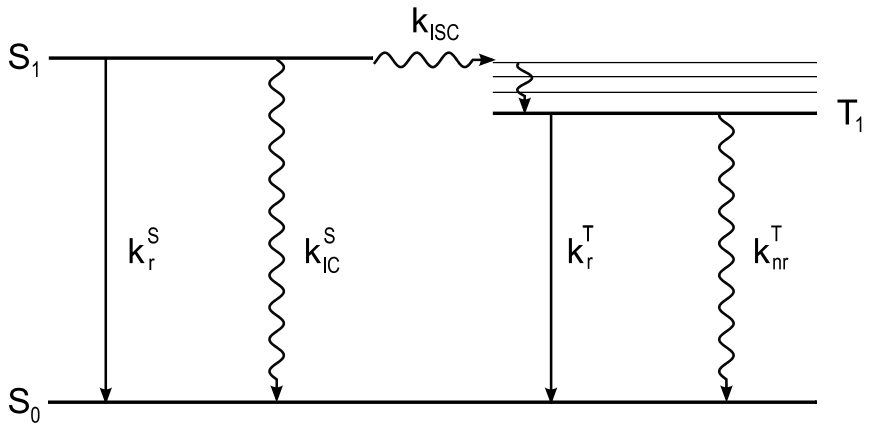

figure 2.2: definition of rate constants

At that point deactivating processes due to intermolecular interactions are neglected (for integration of intermolecular interactions see chapter 2.1.3).

If $[A^*]$ is the concentration of the luminophore A in the excited state, we can express the rate of deactivation from the excited state S_1 by the following equation:

$$-\frac{d[A^*]}{dt} = (k_r^S + k_{nr}^S)[A^*] \qquad (1)$$

Integration of this equation leads to the following mathematical term:

$$[A^*] = [A^*]_0 \exp\left(-\frac{t}{\tau_S}\right) \qquad (2)$$

with τ_S, the lifetime of the excited state S_1

$$\tau_S = \frac{1}{k_r^S + k_{nr}^S} \qquad (3)$$

As said before, the lifetime is the average time the molecule spends in the excited state. This means that only few molecules emit exactly at $\tau_S = t$ because the process of emission is a random process [10].

So far we only discussed deactivation from the excited state S_1. By intersystem crossing a fraction of molecules can reach the triplet state as was mentioned by $k_{nr} = k_{IC}+k_{ISC}$ and then relax from T_1 to S_0 by phosphorescence.

Similarly to the fluorescence lifetime we finally yield

$$\tau_T = \frac{1}{k_r^T + k_{nr}^T} \qquad (4)$$

Usually lifetimes of fluorescence reach a value between tens of picoseconds to hundreds of nanoseconds, whereas lifetimes of the excited triplet state show a tendency to much higher values.

Since the luminescent intensity I at a time t is proportional to the concentration of molecules that are in the excited state, the intensity decreases according to a single exponential decay. (see figure 2.3)

$$I(t) = k_r \left[A^*\right]_0 \exp\left(\frac{t}{\tau_S}\right) \qquad (5)$$

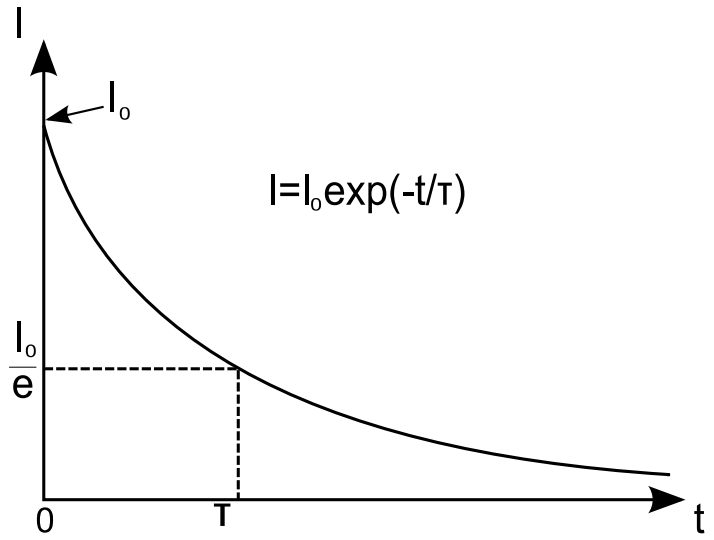

figure 2.3: decay of luminescence intensity

(cf. [11])

2.1.3 Quenching

As mentioned in chapter 2.1.2 so far interactions with surrounding matter or molecules were neglected. However, in the majority of cases, interaction plays an important role in luminescence phenomena.
Apart from decrease of luminescence intensity because of internal conversion and intersystem crossing there are several ways to deactivate the excited state without emission of light and so to lower the luminescence intensity, all combined by the term "quenching" [10]. This decrease of intensity is not always unwanted, as you can obtain important information on the surrounding matter.

For the phenomenon of quenching several photophysical processes exist, that are listed below:

- Collision with heavy atoms or paramagnetic species
- Electron transfer
- Excimer formation (dimers in the excited state)
- Exciplex formation (complexes in the excited state)
- Proton transfer
- Energy transfer

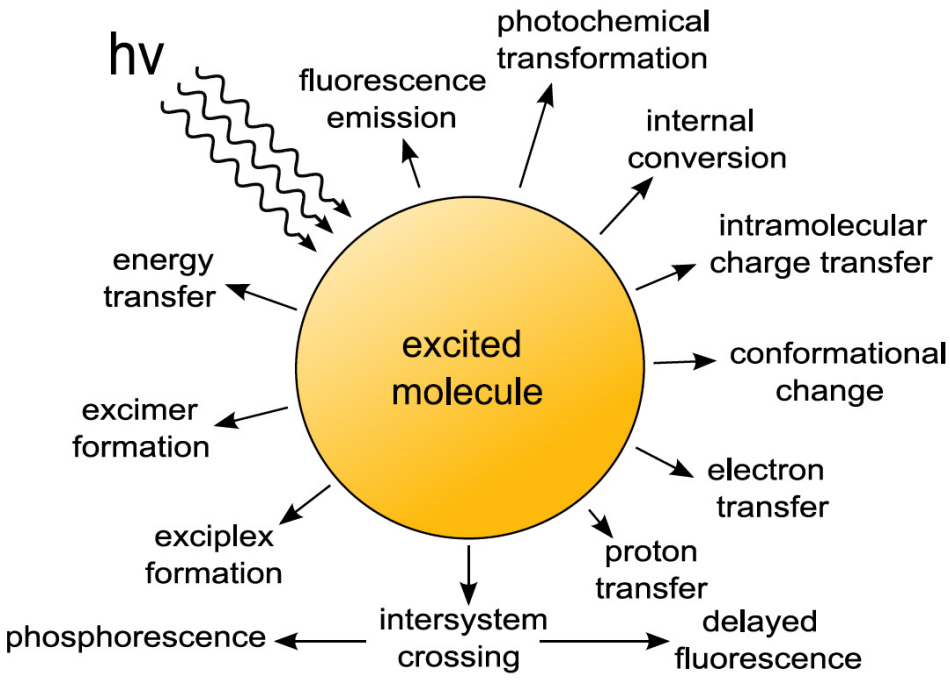

figure 2.4: possible de-ecxitation pathways of excited molecules

All of these processes have two consequences in common: A faster decrease of intensity than in the absence of a quencher and a decrease of the quantum yield.
As described above several mechanisms of quenching exist. In the context of my diploma theses two types of quenching will be discussed in detail: dynamic and static quenching.

2.1.3.1 Dynamic quenching

Dynamic (or collisional) quenching is a result from collisions of the luminescent molecule and the quenching molecule. Diffusion of the quencher (one of the best known is oxygen), which is not in large excess, to the excited luminophore happens during the lifetime of the excited state. As a consequence the process is diffusion-controlled. Contact of luminophore and quencher then leads to the deactivation of the excited state without emission of light.
Dynamic quenching causes a decrease of intensity, quantum yield and finally the decrease of the lifetime of the excited state and is described by the Stern-Volmer equation:

$$\frac{\Phi_0}{\Phi} = \frac{I_0}{I} = \frac{\tau_0}{\tau} = 1 + K_{SV}[Q] = 1 + \tau_0 k_q [Q] \quad (6)$$

Φ/Φ_0... quantum yield in presence/absence of the quencher
I/I_0.....intensity in presence/absence of the quencher
τ/τ_0.....lifetime of the excited state in presence/absence of the quencher
K_{SV}.....Stern-Volmer quenching constant
[Q].....concentration of the quencher
k_q.....bimolecular quenching constant

In equation (6) the bimolecular quenching constant k_q was assumed to be a constant. Considering transient effects and a time-dependence of k_q, however, leads to more complex solutions than equation (6).

2.1.3.2 Static quenching

Two circumstances can lead to static quenching: On the one hand this can be the existence of a sphere of effective quenching, which plays a role in viscous media or in rigid matrices, where the luminophore and the quencher have fixed positions to each other while the luminophore is in the excited state.
On the other hand the formation of a ground-state non-fluorescent complex leads to quenching. When the complex is excited through absorption of a photon, deactivation of the

excited state takes place immediately without emission of light. Although the intensity can be described by almost the same equation as dynamic quenching (see equation (7)), the lifetime of the excited state is not affected and $\tau_0/\tau = 1$.

$$\frac{I_0}{I} = 1 + K_S[Q] \qquad (7)$$

I/I_0……intensity in presence/absence of the quencher

K_S.....constant for static quenching

[Q] .....concentration of the quencher

(cf. [10,11])

2.2 Fluorescence microscopy

Fluorescence microscopy is a very popular technique for application in life sciences. Most commonly it is used for investigation of living cells and tissues in respect of metabolic parameters like pO_2, pH or other important analytes.

2.2.1 Assembly of a fluorescence microscope

One of the most important components of a fluorescence microscope is the light source, which produces – in contrast to a standard microscope - UV-visible light (mercury or xenon lamp; LEDs). Furthermore a fluorescence microscope consists of a set of filters and a detection system.

Very often fluorescence microscopy is performed using the epifluorescence configuration, which means that emission an excitation pass the same objective. This configuration has the advantage that most of the excitation light leaves the optical path away from the detection system.

The filter system consists of the emission and excitation filter and the dichroic mirror. The Excitation filter transmits the range of wavelengths that is used to excite the fluorophore, whereas the emission filter rejects the excitation and transmits the emission light. The dichroic mirror or beam splitter has two functions: On the one hand it reflects the excitation light to focus on the microscopic sample and on the other hand it transmits the emission light coming from the sample going to the detector [10].

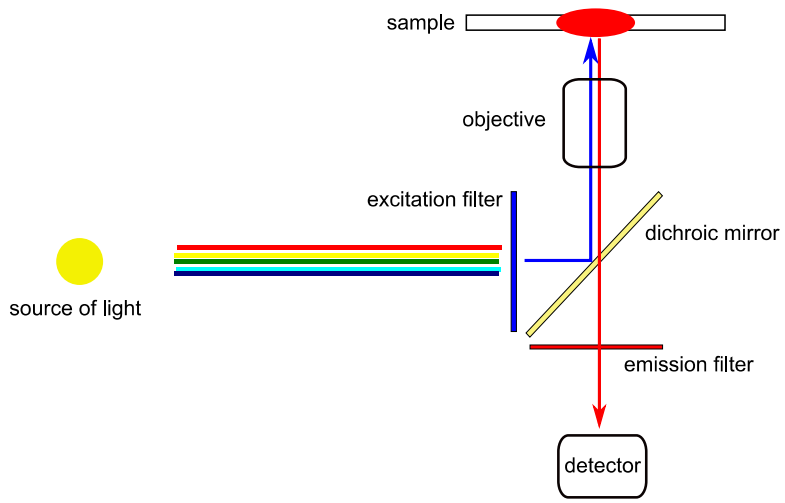

figure 2.5: Assembly of an epifluorescent microscope

Fluorescence is observed by eye, photographic film or CCD (charge-coupled device) camera, whereat CCD-cameras are promising detectors for imaging systems due to enormous advances in CCD-technology in the past concerning sensitivity, resolution, size and costs [12].

2.2.2 Imaging Calibration schemes

The original signal that is obtained by fluorescence microscopy is the intensity of the emitted light. Unfortunately this original information often can not be used for obtaining the requested information about the investigated sample due to inhomogeneities of the light source, inhomogeneous sensitivity of the detection system or concentration gradients of the fluorescent probes. In order to finally obtain the wanted information it is necessary to reference out these intensity fluctuations. For fluorescence microscopy several methods for the correction of the original images exist, for example fluorescence ratiometric imaging (FRIM) or fluorescence lifetime imaging (FLIM). (cf. [10])

2.2.2.1 FRIM (Fluorescence ratiometric imaging)

FRIM is a method that is able to provide quantitative information about the concentration of the observed analyte. Its principle is to measure the intensity of two different wavelengths of the emitted light and then to calculate the ratio between these intensities. That way the ratio depends on the concentration of the analyte and not on the concentration of the luminophore.
However, the disadvantage of this method is that the ratio can be influenced by scattering, leaching or bleaching. (cf. [12])

2.2.2.2 FLIM (Fluorescence lifetime imaging

Measuring the luminescence lifetime is especially convenient for imaging techniques as lifetime is not influenced by scattering, reflection, concentration of the luminescent dye or some interactions with environment. Furthermore it is barely affected by photobleaching.

Lifetime can be detected using two different methods: the time domain or the frequency domain approach, where the luminophore is excited either by a pulsed or a sinusoidal modulated light source. (cf. [10,12])

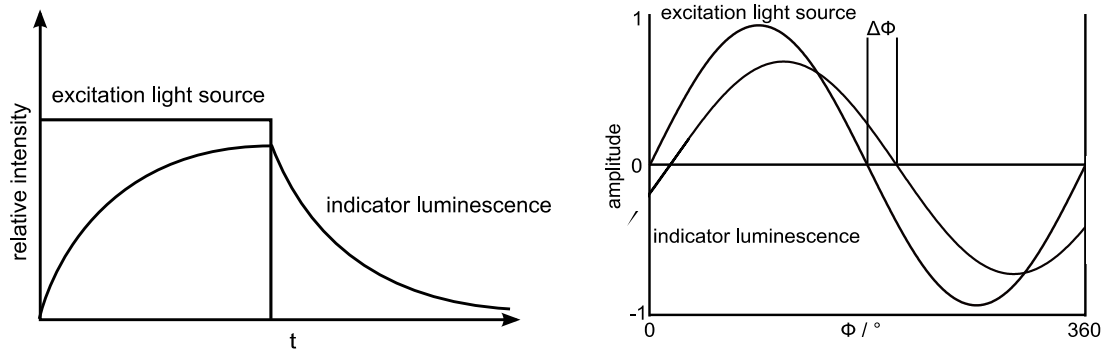

figure 2.6: Time-domain and frequency-domain approach

FLIM is especially interesting when using Rapid lifetime determination (RLD, see figure 2.7). In this approach the luminescent probe is excited by a square-shaped light pulse and emission is measured in two different gates. Assuming a single-exponential decay, two different gates (D_1 and D_2) at two delay times t_1 and t_2 are adequate to calculate the lifetime via the following formula [11].

$$\tau = \frac{t_2 - t_1}{\ln(D_1 / D_2)}$$

Because of low intensities the microscopic images are accumulated on the CCD-Chip by repeated pulse excitation.

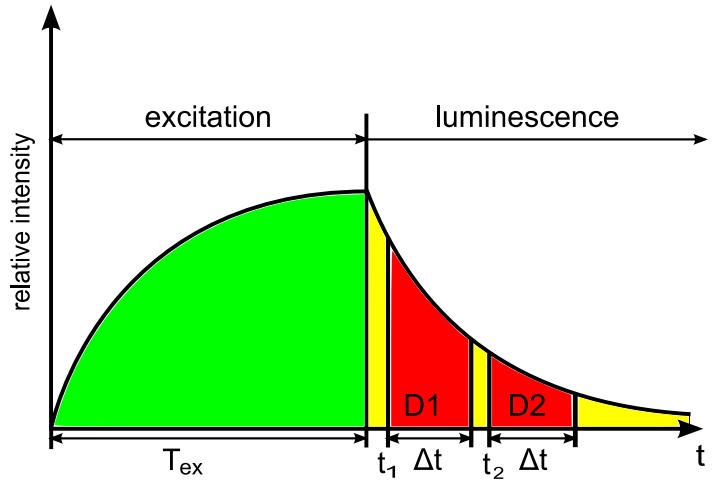

figure 2.7: Scheme of rapid lifetime determination

2.3 Light harvesting

High luminescent emission is one of the major interests in optical sensors. The higher the intensity of the emitted light, the better the overall sensor performance, including a better signal-to-noise-ratio, less influence of background luminescence and the possibility to reduce the thickness of sensing films.

Apart from increasing the indicator dye concentration, which sometimes causes self-quenching, one of the simplest ways to enhance the brightness of reagent mediated sensors is the principle of light harvesting.

By employing a so-called antenna-dye with a high extinction coefficient, energy can be absorbed to a greater extent and then be transferred to the so-called indicator (analyte sensitive dye) by energy transfer. Application of the antenna dye in high concentrations involves the energy transfer from many surrounding donor molecules to one acceptor molecule sensitive to the analyte. The energy transfer is enabled by an overlap of emission and absorption spectra.

This concept leads to very efficient absorption of light and high emission intensities. The principle of light harvesting can also be seen in figure 2.8.

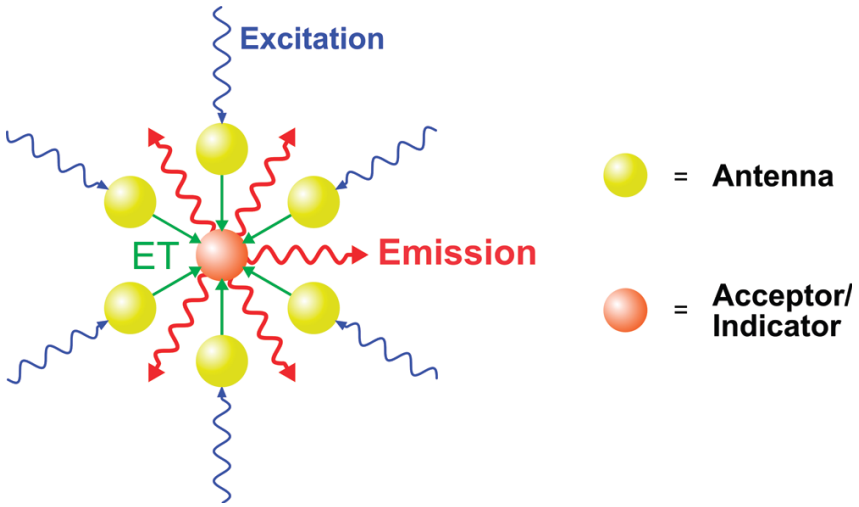

figure 2.8: Principle of light harvesting:
Antenna dye molecules collect light and transfer the energy to an analyte-sensitive acceptor (indicator) dye. (taken from [13] **with permission of Torsten Mayr)**

Using light harvesting as a way to improve the signal intensity results as well in an extended Stokes' shift and hence to a higher flexibility concerning for example the light source. Moreover one can use the remaining green fluorescence to apply ratiometric measurements (see chapter 2.2.2: FRIM). (cf. [13])

2.4 Microfluidic systems – General Aspects

2.4.1 Definition

Microfluidic systems are defined by the volume processed by these systems. Usually 10^{-9} to 10^{-18} L of fluid are pumped through channels in the scale of tens to hundreds of micrometers. Synonyms for the term "microfluidic systems" are for example "Lab-on-a-Chip", miniaturized total analysis system (μTAS) or microfluidic analysis system, which can be subsumed by the generic term microelectromechanical systems (MEMS).
The application of microfluidic systems in analysis involves many advantages compared to macro scale laboratory analysis like low consumption of samples and reagents, short times for analysis and separations and detection with high resolution and sensitivity. Furthermore, the integration of various functional units serving as different operating procedures leads to complete analysis systems on only one chip and one can observe phenomena, which wouldn't be observable in the macroscopic scale. (cf. [1])

2.4.2 History of Microfluidics

The development of microfluidic systems traces back to the mid-20th century with the awareness, that reducing column diameters and packed column particle sizes can improve performance of gas and liquid chromatography [14,15]. Also in the field of capillary electrophoresis reduction of capillary size was shown to be advantageous.
Moreover there was enormous scientific interest in microelectronic industry. Hence the processing of technologies like photolithography, etching and bonding techniques experienced an important boom. These technologies facilitated the processing of miniaturized patterns.
The combination of these above mentioned developments facilitated the origin of microfluidics.
The first analysis system based on silicon (miniature GC air analyzer on a silicon waver) was published 1979 [2], but it took another ten years until the term micro Total Analysis System (μTAS) was impressed by Manz et al. [16].
Soon researchers found out, that the application of microfluidic systems is not only confined to separation techniques, but a variety of other applications. Microfluidic technology became

important in many fields, where reduced reagent consumption, laminar flow, enhanced heat transfer and parallelization only cited as examples were shown to be advantageous.
Nowadays microfluidic devices are applied in many research fields, including chemistry, biology, genomics, proteomics, pharmaceuticals and bio-defence. (cf. [17])

2.4.3 Fabrication of Microfluidic Devices

The development of microfluidics traces back to a boom in the microelectric industry as the microelectric industry provided a solution for fabrication of miniaturized systems. Thus, microfluidic systems can also be seen as a part of microelectromechanical systems (MEMS).
As the use of photolithography and etching processes were standard processing steps to process silicon [18] ad rather well-known, silicon was the initial material, which was used for fabricating microfluidic devices. Soon, however, research also focused on glass substrates [19,20] since its transparency allows a better visualization of on-chip processes and bonding to other substrates is simpler than it is for silicon.
The use of silicon and glass also exhibits some drawbacks that trace back to the relatively high costs of these materials, multiple fabrication steps involving harmful wet chemistry (e.g. HF), unfavourable surface chemistry (attachment of biomolecules to silicon surfaces) [5] and the fact that high aspect ratio structures are difficult to fabricate with glass as a substrate.
Today, many applications are based on polymers, amongst others polymethacrylmethacrylate (PMMA), polycarbonate (PC), parylene (paraxylylene), polydimethylsiloxane (PDMS), SU-8 and biodegradable polymers, that are employed in construction of microfluidic channels [17]. Generally polymers are moldable to complex shapes and dimensions and satisfy different needs like low cost, low electrical and thermal conductivity and compatibility with biological materials. Moreover different methods are known that can be used in the polymeric microfabrication process and that provide an opportunity for mass production [5].
(cf. [17])
The following chapter gives a brief description of microfabrication technologies using polymers.

2.4.3.1 Polymer micromachining

Microfabrication methods can be divided into replication methods that can be used for mass production, and serial/individual device techniques.

Replication technologies base upon the micromachining of a master mold (inverse structure of the final microfluidic device) which is then replicated into the polymeric substrate. Methods for master fabrication include micromachining methods like sawing, cutting, milling and turning, electroplating methods (photolithography with subsequent treatment in a galvanic bath) or well known silicon micromachining like wet etching or reactive ion etching.

Replication processes involve hot embossing, injection molding and casting [5].

Hot embossing [21] is used to transfer the negative structure of the master mold to a thermoplastic polymer. In this process the polymer and the master are placed in the embossing system and heated above the glass transition temperature of the substrate under vacuum. Then the master is pressed against the substrate with a controlled force.

Another possibility to form thermoplastic materials is a technique called **injection molding** [22] . The raw polymer material is melted in a heated screw (above the glass transition temperature of the substrate) and transported to the mold cavity where the master mold is located. The melt is then injected into the mold cavity and the whole system is cooled.

Casting is usually used for non-thermoplastic materials like epoxies and elastomers (e.g. PDMS) [17] . A mixture the uncrosslinked polymer and a crosslinker are poured over the master mold in its liquid form. After the relatively long curing process (few hours) the complete elastomer can be peeled off the mold.

Sometimes there is also the need for the rapid fabrication of single devices. For that purpose several methods exist which allow a direct fabrication of the final device. Important processes involve laser-based technologies, optical lithography in deep resists, stereolithography and layering techniques [5].

Laser-based technologies use laser ablation, typically applying an excimer laser [23] combined with a mask or aperture. This method can be used for a variety of polymers (PS, PC, PET, etc.) [24].

Lithographic techniques can be used for microfabrication either by the use of stereolithography, where a photocuring polymer cures at exposure to focused laser light or by directly patterning thick photosensitive polymeric layers like SU-8. The thickness of the used resists allows the direct formation of microchannels. Several processes starting with the deposition of a SU-8-layer which is then irradiated with UV-light have been proposed [5].

Layering techniques deal with the use of sacrificial layers that are covered with layers of the wall and cover polymers and then etched.

In the majority of cases these microfabrication techniques produce open systems with microchannels positioned on the surface of the substrates. This entails the need for additional

bonding technology to obtain complete devices. Bonding techniques include lamination [24], gluing, application of heat and pressure, laser welding and ultrasonic welding [5].

2.4.3.2 Polymer materials for microfabrication

Various types of polymers can be used for microfabrication, depending on the microfabricating technology. Thermoplastic polymers melt above the glass transition temperature and can be processed by techniques like hot embossing or injection molding. Amongst others PMMA and PC are the most popular polymers used for microfluidic systems [5].

Photosensitive polymers are another important group of polymers applied in microfabrication processes. Different methods of lithography are used for patterning of these materials. One of the most popular substrates is SU-8, an epoxy polymer that becomes insoluble under exposure to light (negative resist).

A third group of polymers have to be applied in a premature form. This is the case for parylenes (in-situ-polymerisation) and PDMS, the most widely used substrate in academic microfluidic research. For fabrication of microfluidic devices the elastomeric form of PDMS is used. Base solution of PDMS and a curing crosslinker are mixed and poured over the master mold [17].

In PDMS advantageous properties like ease of fabrication, transparency in the UV-visible wavelength range, flexibility and low costs are combined [25,26].

2.4.4 Applications of Microfluidics

Microfluidic devices are applied in various research fields. However, most applications concentrate on biological sciences, which can be drawn back to the high biocompatibility of these systems. Some of the most common application areas are genetic analysis of DNA and RNA, proteomics, cellular assays and drug delivery and compatibility.

Microfluidic systems are especially suitable for investigations of cell cultures, because the extracellular fluid-to-cell (volume) ratio is close to physiological conditions [9].

One of the main advantages using microfluidic cell cultures and assays is the fact, that they exhibit high controllability and reproducibility. Moreover, they serve as a rapid instrument to accomplish high-throughput-screenings due to serial processing and parallelization of cellular assays [27].

For example microfluidic devices have been used to investigate cell physiology in different environments by controlling the surface shape of the device. There have also been investigations of cell morphology, bacteria immobilization and dynamic bacteria population [28].

Nowadays, the technology of microfluidic systems is on the verge of commercialisation. Some companies already produce and sell microfluidic devices (e.g. Micronics, Caliper Life Sciences, Agilent, Micronit Microfluidics,…), but the field is still at an early stage of development.
Although a range of applications exists, microfluidics didn't make the commercial breakthrough so far, although there seems to be enormous potential regarding healthcare alone. In this field importance of preventing diseases instead of treating them increases and there will be the need for employing technologies that are able to do high-throughput-screenings.
Today the hindrance for a breakthrough seems to be cost. The implementation of different processes and the whole equipment that you need on one chip is at the moment too expensive. Moreover, there is the necessity to invest into user-friendliness of these systems.
Supposably, however, sooner or later the advantages of microfluidic technology will win recognition, which then will lead to commercial success of these systems.
(cf. [17])

2.5 Optical Sensors in Microfluidic Devices

Due to reduced analysis and detection volumes in microfluidic devices detecting certain analytes in lab-on-a-chip-devices often emerges to be a difficult task. Thus, researchers face the challenge to find adequate detection methods that are sufficiently sensitive, scalable to smaller dimensions and rather low-priced.
Since electrochemical sensors do not meet all these requirements, there is a developing interest in integration of optical components into microfluidic devices. [6]. In general, optical sensors can be easily miniaturized and read-out from the outside. Due to their sensitivity and selectivity, especially luminescence based sensors turn out to be an excellent analytical method for microsensing systems [29]. By reduction of the fluorescent background due to reducing the size of the detection volume sensitivity can even be enhanced in microfluidic applications [30]. Moreover, optical sensors are robust, facilitate parallelisation and the

determination of multiple parameters, well suited for small volumes and relatively nonperturbing. Finally the flexibility of the sensor design allows performing 2-dimensional measurements by microscope-based detector set-ups.

Basically optical sensing systems can be divided into the on-chip and the off-chip approach. These approaches differ by the kind of integration of the optical sensing system into microfluidic devices. Off-chip technology combines macroscopic optical sensing systems that are coupled to the microfluidic system whereas the on-chip approach deals with the integration of micro-optical components into microfluidic devices [6].
Information about the investigated system can be obtained by observing various optical parameters. Common detection systems are mostly based on absorbance- [31,32] or luminescence-measurements [33-35], but also other parameters like reflectance [36] or refractive index [37] are applied to receive analytical information.

2.5.1 Detection of Oxygen in Microfluidic Systems

Determination of the oxygen-concentration is of high importance - especially when microfluidic systems are used for biological investigations. Oxygen is part of a variety of metabolic processes and for this reason one can obtain a lot of useful information by monitoring oxygen in a bioreactor. For example extracellular oxygen indicates the ability of the cell for respiratory activity [7]. Thereby oxygen-sensors can be used to indicate the physiological status of cells and provide information in applications like pharmaceutical drug screening or environmental monitoring [8]. Cellular oxygen consumption is a measure of metabolic activity so that influences of toxic agents on cells can be observed by detecting the pO_2 level.

State-of-the-art-techniques for sensing oxygen include the two main technologies amperometric electrochemical and optical oxygen sensing based on oxygen quenching of fluorescent dyes. Although amperometric approaches [8] are rather sophisticated, monitoring oxygen in microfluidic bioreactors by optical measurements entails several advantages: besides the previously mentioned benefits luminescent sensors do not consume oxygen (in contrast to amperometric sensing approaches).
As mentioned in chapter 2.1.3 dynamic quenching causes a decrease of intensity, quantum yield and finally the decrease of the lifetime of the excited state. These changes of intensity or

lifetime can be used to determine dissolved oxygen (DO) levels, whereas lifetime measurement is preferred due to it's independence of influences by photobleaching, dye concentration and optical drifts or inhomogeneities.

Several examples of integrated optical oxygen sensors based on collisional quenching principle are reported in scientific literature. Most of them apply sensor patches [38,39], where an average oxygen-concentration can be detected.

However, apart from simply detecting averaged oxygen-levels in the chip it is also interesting to accomplish space-resolved quantitative analysis of oxygen-distribution. Space resolved measurements can give information about oxygen gradients in biofilms or about a heterogeneous chemical distribution (for example caused by a variable gas-permeability of PDMS) which can lead to difficulties in developing tissues [9].

Concerning imaging techniques luminescent dyes can either be applied dissolved [9] or immobilized in or on a matrix [40,41]. Immobilization of the dye facilitates handling and prevents wastage of the dye, which must be applied in high amounts.

Read-out of the luminescence signal can be read-out by a CCD-chip of a camera – for instance coupled with fluorescence microscopy. As mentioned in chapter 2.2.2 original images often can not be used for obtaining the requested information about the investigated sample due to inhomogeneities of the light source, inhomogeneous sensitivity of the detection system or concentration gradients of the fluorescent probes. This is the reason, why referencing methods like FLIM or FRIM are very important. For further information see chapter 2.2.2.

2.5.2 Optical pH-Sensing in Microfluidic Systems

In life sciences it is of high importance to have information about the pH value. For instance the pH influences cell activity and stability in a bioreactor. Moreover the knowledge of pH in addition to the knowledge of other important metabolites can help understanding the complex processes in heterogeneous living communities [42].

Different principles of optical pH-sensing exist; for instance pH-dependency of absorption spectra and dependency of the luminescent lifetime [10]. Also in microfluidic systems the basic principle of optical sensing of pH is the change of the fluorescent response of a pH-sensitive dye [43].

Typical pH-sensitive dyes are for example fluorescein and HPTS (1-hydroxypyrene-3,6,8-trisulfonate). These substances are wavelength-ratiometric pH-indicators which show different absorption spectra in their acidic and basic form.

3 Materials and Methods

3.1 Chemicals and Materials

3.1.1 Chemicals

table 1: list of used chemicals

Abbreviation	IUPAC-name	supplier	Additional notes
acetone	propanone	Fisher Scientific	
CHCl3	chloroform	Fisher Scientific	
GOX	glucose oxidase	FLUKA	
Ir(Cs)2(acac)		Quelle Sergey paper	
Macrolex Yellow	3-(5-chloro-2-benzoxazolyl)-7-(diethylamino)-2H-1-Benzopyran-2-one	Simon und Werner GmBH	
microscope slides		Roth	76 * 26 mm
Mylar polyester foil			
nitrogen		Air Liquide	
PS	polystyrene	ACROS	average MW 250,000
PSPVP	Poly(styreneblockvinylpyrrolidone) emulsion in water (38% w/w)	Aldrich	
PtTFPP	Platinum(II)-5,10,15,20-tetrakis-(2,3,4,5,6-pentafluorphenyl)-porphyrin	Frontier Scientific	
synthetic air		Air Liquide	
THF	Oxacyclopentane	Fisher Scientific	
TiO_2 P170		Kemira, Finnland	ultrafine

Microorganisms and media:

Escherichia coli K12 ATCC 23716 (Miller Hinton Medium)
Candida albicans ATCC 10231 (Worthbroth Medium)
Pichia pastoris ATCC 28485 (YPD Medium)

Microorganisms and media were provided by the Austrian Institute of Technology GmbH (AIT), Health & Environment, Nano Systems (working group of DI Dr. Peter Ertl).

3.1.2 Optical filters

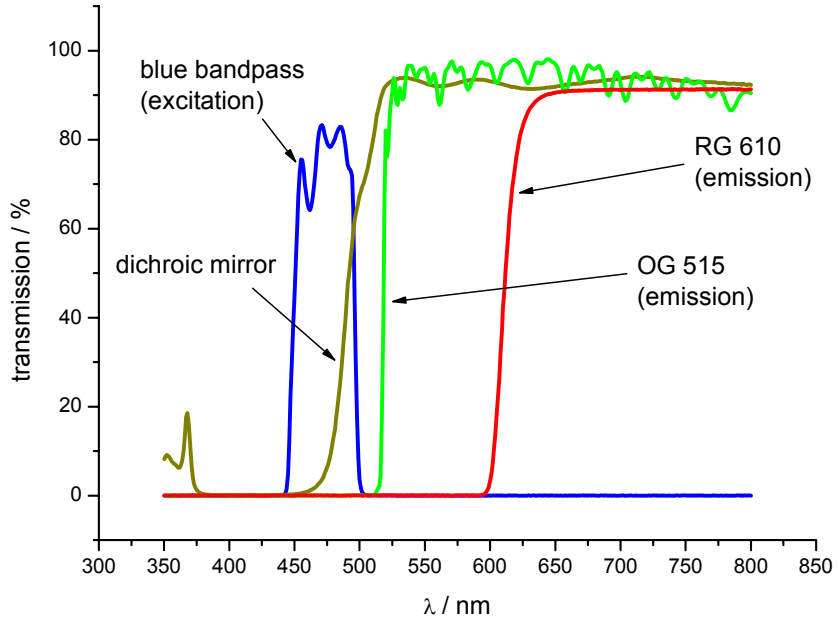

figure 3.1: optical filters used for measurments on the fluorescence microscope

3.1.3 Microfluidic devices

Microfluidic devices were derived from the Austrian Institute of Technology GmbH (AIT), Health & Environment, Nano Systems (working group of DI Dr. Peter Ertl). The preparation was carried out according to the following procedure.

A glass slide (microscope object carrier) with or without an oxygen-sensitive fluorescent layer serves as a substrate for the microfluidic chips. The fluidic channels are formed in a PDMS (Polydimethylsiloxane) layer as an imprint of a silicon master mold. The mold is placed in a Petri dish and covered with a 3mm thick layer of liquid PDMS. Air inclusions are removed by repeated degassing in an evacuated exsiccator. After baking at 60°C for 4 hours, the PDMS with the fluidic channels is cut and peeled off the mould. At in- and outlets of the fluidic holes are punched into the PDMS (diameter <500µm). As a fluidic interface, a glass slide featuring holes for the in- and outlets of the microfluidic channels is covalently bonded to the PDMS. Oxygen plasma (Femto plasma asher, Diener Electronic; 30s, 40% power) is used for surface activation. Fluidic connections are assembled by attaching 1cm long pieces of TYGON tubes to the predrilled glass slides (2 component epoxy adhesive, Loctite 9492). The PDMS is then attached to the substrate: A small amount of liquid PDMS (approximately 200µL) is dropped

onto a clean glass slide and a thin layer is generated by spinning the slide at 5000U/min for 300s (acceleration 50%). Then the fluidic is carefully dipped into the layer of liquid PDMS and transferred to the glass substrate. The assembled chip is put into an oven (60°C for 4 hours) to harden the PDMS film.

Silicon master mould: To fabricate the silicon master mold a silicon wafer with a 750nm silicon oxide layer, formed by thermal oxidation, is used as substrate material. The thermal oxide, used as hard mask for the KOH silicon etching, is patterned by etching with a buffered HF (BHF) for 14 minutes. After stripping the photo resist (AZ MIR^{TM}701 positive photo resist) the substrate is etched in a 40% KOH solution at a constant temperature of 80°C for 25 minutes resulting in an etch depth of 20µm. For different etch depths (10-60µm) the time is varied. After rinsing in DI-water, the hard mask is stripped by BHF etching.

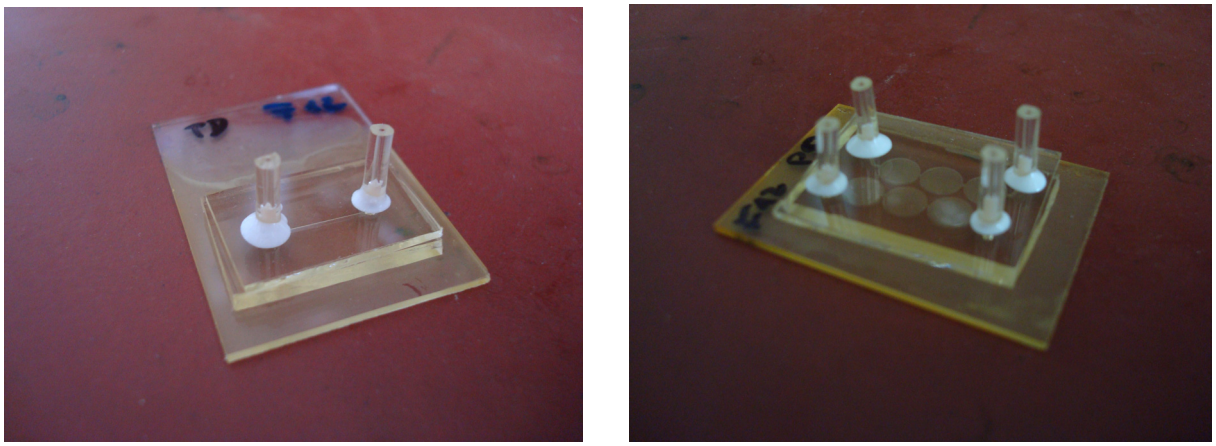

figure 3.2: microfluidic devices (different designs) with integrated oxygen sensing film

3.1.4 Flow-through-cell

The flow-through-cell used for experiments with nano sensor particles was obtained from Günter Mistlberger. In the middle of the cell there is a round hole that can be closed from below with a microscope glass-slide covered with Loctite Superkleber. From below the hole was covered with a circular glass slide covered with immobilized glucose oxidase to simulate a biofilm which consumes oxygen.

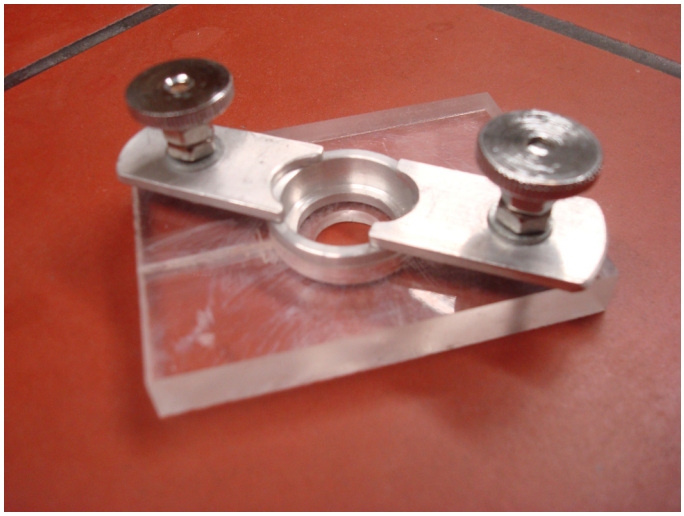

figure 3.3: flow-through-cell used for experiments with nano sensor particles

3.1.5 Preparation of glucose-oxidase-films

Two solutions had to be prepared. Solution 1 contained 1 mL of deionised H_2O, 75 µL glycerol, 50 mg glucose-oxidase, and 50 mg bovine serum albumin. Solution 2 was a mixture of 950 µL deionised H_2O and 50 µL glutaraldehyde.

Thin circular glass-slides were first cleaned with acetone and coated with a 10% (w/w) solution of RL 100 in chloroforme (spacer thickness 20 µm). After evaporation of the solvent the glass slides were coated again with a mixture from 1 mL solution1 and 0.5 mL solution 2. Coating steps were accomplished using a home-made knife coating device.

3.2 Instrumentation

Emission and excitation spectra were acquired on a Hitachi F-7000 fluorescence spectrometer (www.inula.at) equipped with a red-sensitive photomultiplier tube (PMT) R 928 from Hamamatsu (www.hamamatsu.com). The Emission spectra were corrected for the sensitivity of the PMT.

Absorption spectra were measured at a Cary 50 UV-vis spectrophotometer (www.varian.com).

The modular luminescence lifetime imaging system MOLLI [44] was adapted for application in an inverted fluorescence microscope.

Images were obtained using an epifluorescent microscope (Zeiss Axiovert 25 CFL), equipped with a 50 W mercury arc lamp for fluorescence excitation. For luminescence lifetime imaging light emitting diodes (LEDs) are integrated exchangeably into the filter cube of the microscope as triggered e xcitation light sources.

A monochrome CCD camera (Sensimod, PCO, Kehlheim, Germany) and a color CCD camera (AVT Marlin F-201C) were connected to the microscope.

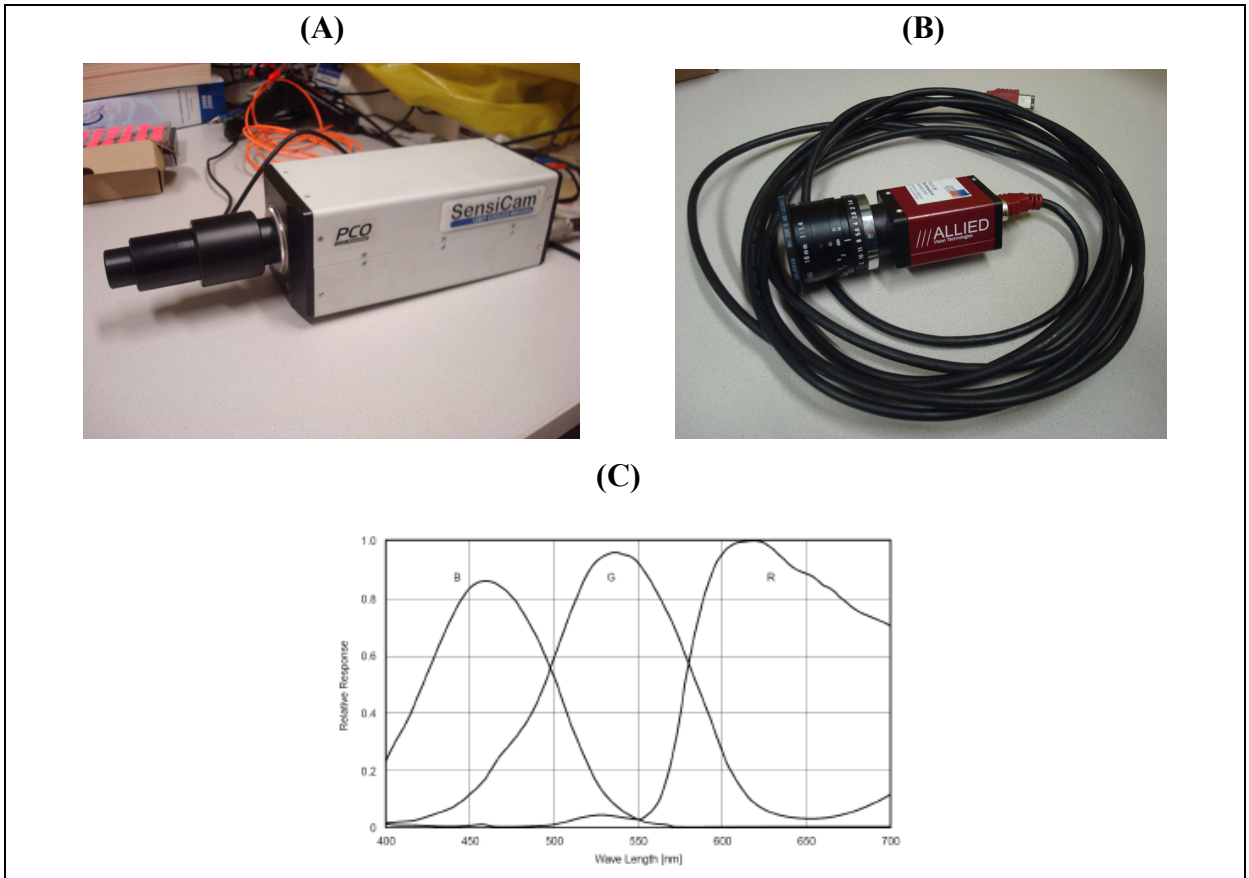

figure 3.4: (A) monochrome CCD camera (Sensimod), (B) color CCD camera (AVT Marlin F-201C) and (C) spectral sensitivity of Marlin F-201C without cut filter and optics

A “triggerbox” (assembled by Björn Grunwald, MPI Bremen, Germany) is used as pulse generator for camera and LED. An additional signal amplifier box (Biocam, Regensburg, Germany) together with an external power source (Thurlby Thandar, TSX1820D) is inserted between triggerbox and LED.

The trigger box and CCD camera are connected to a PC. The whole imaging process including triggering and image acquisition is controlled by the software Look@Molli v.1.83 (Björn Grunwald, MPI Bremen, Germany) (see 3.3).

3.3 Software

Look@Molli v.1.83 (Björn Grunwald, MPI Bremen, Germany)

The software Look@Molli v.1.83 controls triggering and image acquisition using the monochrome camera. It allows variegating different parameters like referencing methods, excitation time, temporal width of recording time and integration time (see figure 3.5).

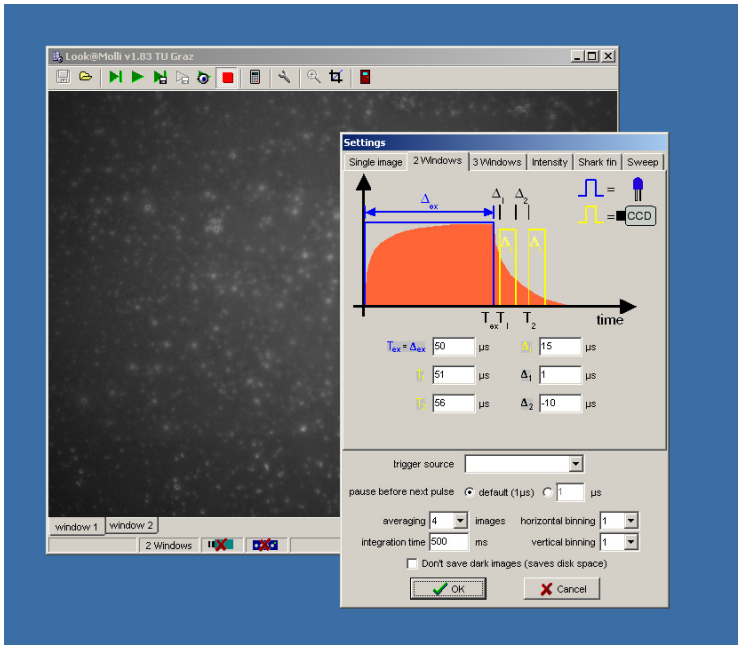

figure 3.5: sreenshot Look@Molli v.1.83

Matlab R2008a (v.7.6.0.324):

Various Matlab-scripts were adapted from the dissertation of Dipl.-Ing. Christoph Moser [45] and slightly modified whereas others were created all new.

Matlab-scripts used for this diploma-thesis are listed in the appendix (see chapter 6.4).

4 Practical Part

4.1 Integration of Oxygen-sensing Films

4.1.1 Introduction

Several possibilities exist concerning the design of optical oxygen sensors. Only to list some options, optical sensors can be integrated into a sample vessel using films coated on a substrate, sensor patches, which can be fixed inside a sample vessel or nanoparticles, which are simply added to the sample. All these different designs entail specific benefits but also show some drawbacks.
Sensor spots, for instance, can be used to measure several parameters in parallel, but require additional production effort. Furthermore sensor patches only give analytical information about one selected region of the sample vessel or microfluidic system.
Integration of optical sensors using luminescent dyes immobilized in sensor foils exhibits several advantages over other sensor designs. The dyes are protected against possibly interfering media compounds and dye consumption can be reduced [40]. Moreover sensor films exhibit high homogeneity of dye distribution and hence a very homogeneous emission intensity,

Oxygen-sensitive films used for the application in microfluidic devices are prepared based on the principle of light harvesting, optimised concerning dye concentration and tested for their applicability in microfluidic systems.
The dye system uses Macrolex Yellow (MY) as antenna dye and Pt(II)-meso-Tetra(pentafluorophenyl)porphine (PtTFPP) as the oxygen-sensitive indicator.

4.1.2 Experimental procedure

4.1.2.1 Preparation of oxygen-sensing films

The respective amounts of the dyes Macrolex Yellow (MY) and Pt(II) meso-Tetra(pentafluorophenyl)porphine (PtTFPP), of TiO_2 P170 and of polystyrene (PS) were weighed in, filled to overall 4 g with $CHCl_3$ and dissolved carefully. These stock-solutions then were diluted to the finally wanted concentration of polystyrene.

To ensure finely dispersed TiO_2-particles TiO_2-containing mixtures were placed in an ultrasonic bath for ten minutes.

Mylar-foils and microscope slides were cleaned carefully with acetone and lint-free tissues. 200 ml of the mixtures then were coated on these carriers with a very precise doctor knife (15 µm).

4.1.2.2 Measurements

Absorption-, excitation- and emission-spectra were recorded of all the sensor films. Films with TiO_2 were not investigated in respect of absorption-spectra.

Absorption-spectra were taken three times at different spots of the films. Then the mean spectrum was calculated.

Emission and excitation spectra of each film were acquired on a Hitachi F-7000 fluorescence spectrometer.

Measurements were made in oxygen-saturated and oxygen-free solutions in deionised water.

Solutions were deoxygenated by dissolving α-D-glucose and glucose oxidase in deionised water (c(glucose) = 0,25 mol/l; c(glucose oxidase) = 200 µg/ml).

Bleaching experiments of the films were carried out using a Zeiss fluorescence microscope. Each measurement was done three times focussing on different spots of a sensor film.

table 2: Measuring setup for photobleaching

Light source	HBO 50/AC
Irradiation time	10 min
Image every	30 s
Excitation filter	Blue BP
Emission filter	RG 610
IT	variable

4.1.2.3 Estimation of film thickness

Film thickness was estimated via absorption measurements using the Lambert-Beer-law. Calculation was made using the extinction at 452 nm and the molar extinction coefficient of Macrolex Yellow ε = 39050 $lmol^{-1}cm^{-1}$.

$$E = -\ln\left(\frac{I}{I_0}\right) = \varepsilon \cdot c \cdot d \qquad (8)$$

4.1.3 Results and Discussion

4.1.3.1 Spectral characterisation and adaption of optical systems

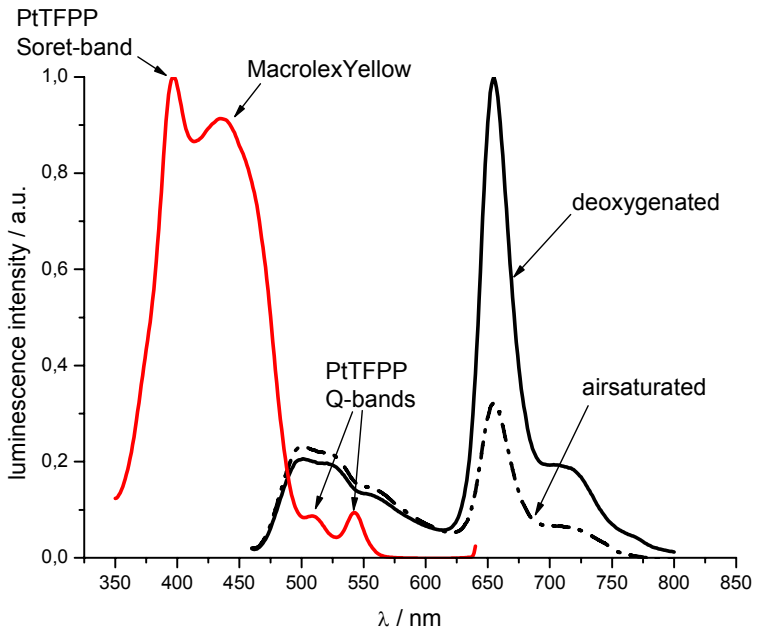

figure 4.1: excitation and emission spectra of oxygen-sensitive film (4% MY, 1% PtTFPP and 30% TiO_2 in PS coated from 2% PS in $CHCl_3$) in air-saturated (dashed line) and deoxygenated (solid line) solution; λ_{EM} = 650 nm; λ_{EX} = 450 nm. Ratio of deoxygenated to oxygenated intensity at 655 nm = 3,10

For measurements on the fluorescence microscope adequate optical filters have to be selected that fit to excitation and emission spectra of the dye system. Furthermore investigations on the applicability of the color camera must be made.

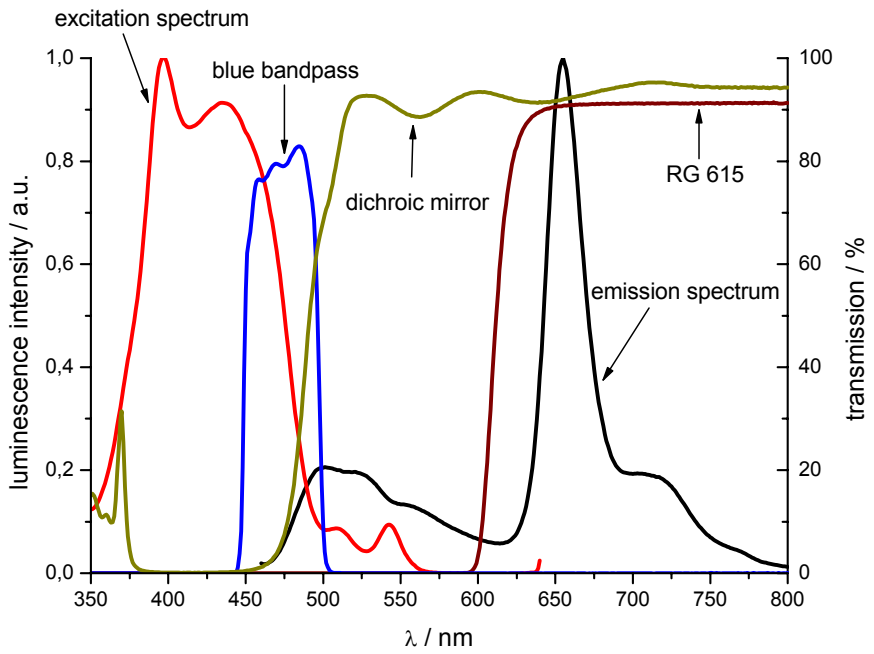

figure 4.2: excitation and emission spectra of oxygen-sensitive film (4% MY, 1% PtTFPP and 30% TiO2 in PS coated from 2% PS in CHCl3) with adequate optical filters (blue BP and RG 610) and dichroic mirror; λ_{EM} = 650 nm; λ_{EX} = 450 nm

The transmission spectrum of the blue bandpass filter (blue BP) shows a good overlap with the excitation spectra.

The red longpass filter opens at approximately 600 nm and cuts most of the emission signal of the antenna dye. Moreover it is fitting to the selected excitation filter as excitation light which passes the dichroic mirror is not transmitted. On the contrary, emission signal of the indicator dye (λ_{max} = 650 nm) is fully transmitted.

The dichroic mirror reflects a large part of the excitation light and orients it towards the sample on the microscope. Luminescence light from the sample is then transmitted by the dichroic mirror and also by the red longpass emission filter (RG 610).

The applicability of the color camera depends on the question if the color channels of the camera fit to the emission spectra of the dye system. Hence it was necessary to compare the sensitivity of the camera channels with emission spectra of the sensor film.

Since excitation of the sensor film remains the same emission filter and dichroic mirror of the former adapted system can be used.

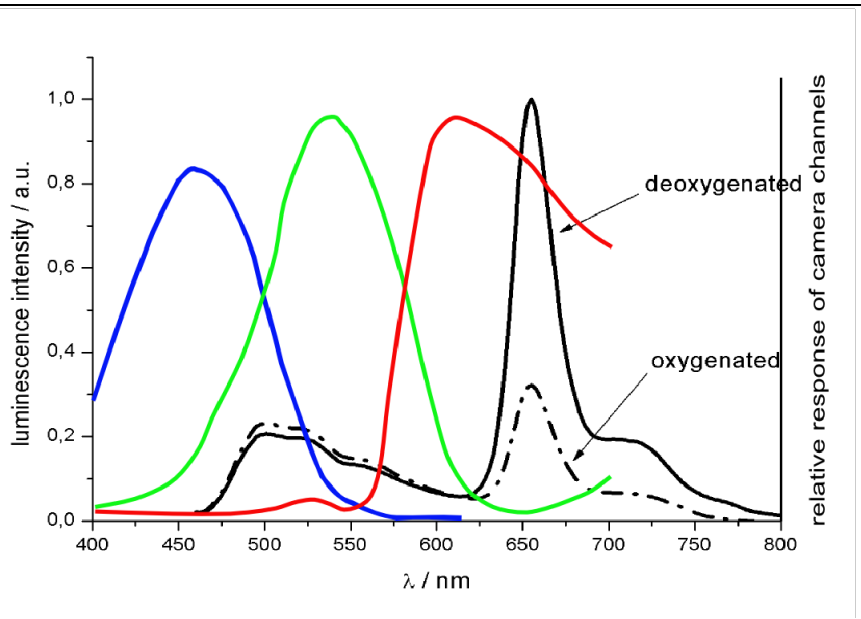

figure 4.3: comparison of the color channels of the camera with an excitation spectrum (F12); relative response of blue, green and red channel are displayed in the respective color

The color camera turned out to be perfectly convenient for the applied dye system. The green channel covers the range of wavelengths where Macrolex Yellow emits and luminescence emission of PtTFPP can be detected by the red channel. However, it must be mentioned that there is some cross-sensitivity. Green and red channel are not fully separated. As a consequence we can assume that the red channel will detect a combined signal from MY- and PtTFPP-emission. The blue bandpass filter was used as excitation filter. OG 515 was used to separate emission light from excitation light that passes the dichroic mirror.

4.1.3.2 Optimisation of the light-harvesting dye system regarding brightness

During preliminary tests on the fluorescence microscope we found out, that especially FLIM measurements require very high luminescence intensities to achieve highly homogenous lifetime images. This fact can be traced back to the principle of RLD (rapid lifetime determination, see chapter 2.2). Especially the second gate is located in a region of the luminescence decay curve where most molecules already have been deactivated. Hence intensities of the second gate were rather low. For that reason we had to add high amounts of the signal intensifier TiO_2 to obtain convenient signal intensities. Principle of signal enhancement by TiO_2 is an increase of the optical path length.

For optimisation of the dye concentration emission spectra of different sensor films were compared. Unfortunately the comparison did not give the desired information because

deviation of the measurements exceeded the effect of different dye concentration. Maybe this can be traced back to the agglomeration of TiO_2-particles in the sensor layers and a resulting inhomogeneous intensity distribution.
Best results on the fluorescence microscope were obtained with films containing 4% Macrolex Yellow, 0.5% and 1% PtTFPP and 30 % (w/w) TiO_2 with a film thickness about 1 µm (coated from 2% (w/w) polystyrene-solutions in chloroform).
By contrast, in preliminary tests applying FRIM emission intensity did not play an important role because of the high sensibility of FRIM measurements. However, FRIM is not able to reference bleaching effects and we had to notice that the chosen dye system is not as stable as expected. For that reason bleaching effects of the films were further investigated.

4.1.3.3 Photobleaching

Photobleaching poses a strong limitation for the use of optical sensors. Several methods have been developed to reduce the influences of bleaching on experimental results, for instance FLIM or the introduction of small molecules that serve as scavenger for reactive radicals, which are known to cause the degradation of dye molecules [46]. However, addition of auxiliary substances complicates the fabrication of sensors and FLIM deals with relatively low intensities compared to direct intensity measurements (for instance FRIM).
On the other hand FRIM is strongly affected by bleaching effects. For that reason it is important to obtain signals which are as stable as possible. As FRIM should be applied for sensors presented in this work it is important to explore the influences of several parameters of the applied sensors.

To optimize bleaching effects, the influence of various parameters of the sensor films was investigated. Important parameters are the thickness of the sensing film, concentration of antenna and indicator dye and the amount of added signal intensifier (TiO_2). In the following section influences of these parameters are discussed.

Photobleaching at variable film thickness

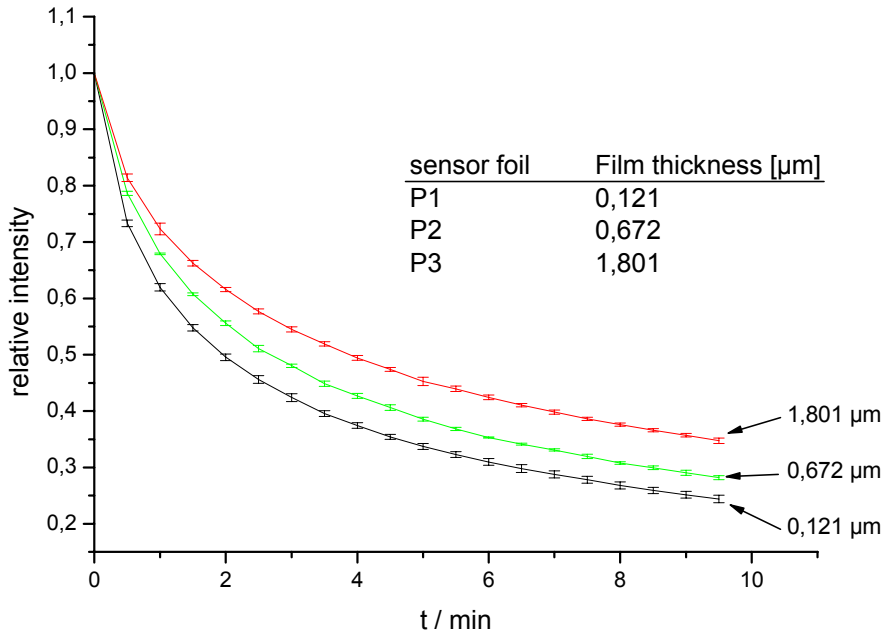

figure 4.4: Photobleaching at variable film thickness;
standard deviations refer to values averaged over three measurements; films containing 4% MY and 1% PtTFPP

Reduction of film thickness apparently leads to stronger photobleaching. Probably the reason can be found in the fact that high thickness leads to high absorption of excitation light in surface near film regions directly exposed to irradiation. Then areas, that are far from the light source (weakly or not irradiated), are influenced less by bleaching effects.

Photobleaching at variable antenna dye concentration

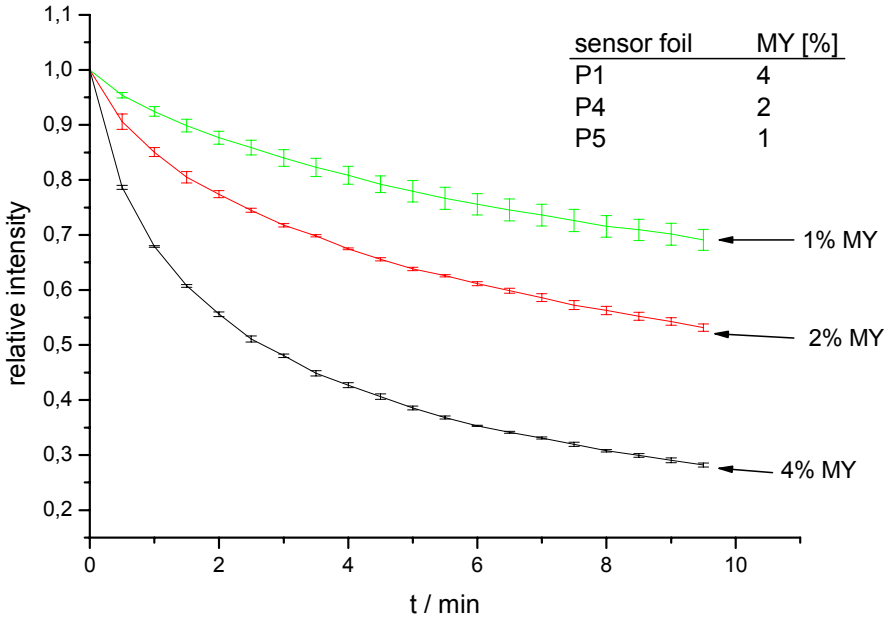

figure 4.5: photobleaching at variable MY concentrations;
standard deviations refer to values averaged over three measurements; films containing 1% PtTFPP; film thickness approximately 0,650 µm

Concentration of Macrolex Yellow seems to play an important role in photobleaching. figure 4.5 shows clearly that lower levels of MY lead to a reduction of photobleaching effects.

Photobleaching at variable PtTFPP concentration

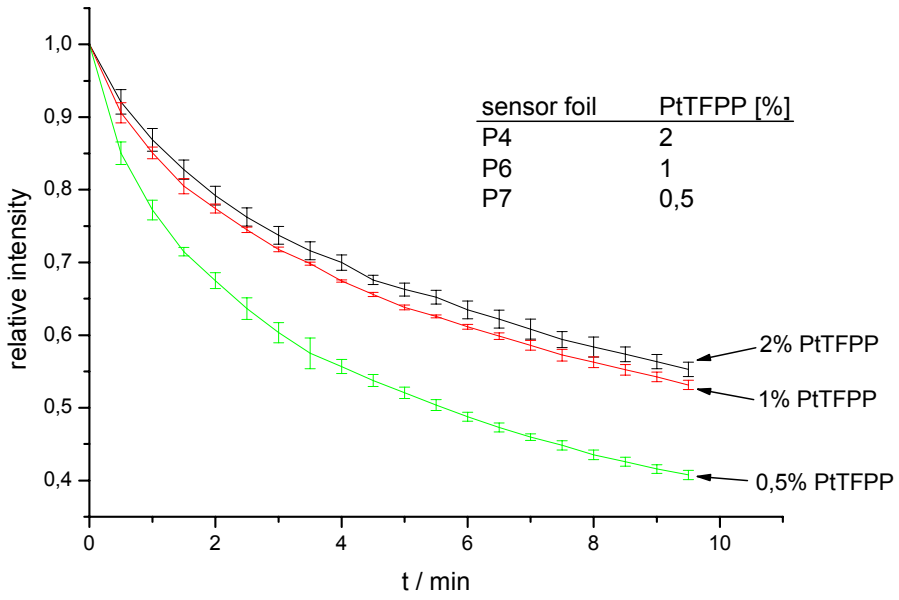

figure 4.6: photobleaching at variable PtTFPP concentrations;
standard deviations refer to values averaged over three measurements; films containing 2% MY; film thickness approximately 0,650 µm

Again photobleaching depends on the dye concentration. Higher concentration leads to reduction of photobleaching. Curiously at very low PtTFPP levels the concentration seems to have a stronger influence. Possibly this phenomenon can be traced back to the fact that at low PtTFPP levels the emission intensity of PtTFPP is so low that the signal recorded by the camera is influenced by the emission of MY.

Photobleaching at variable TiO2 concentration

Apart from investigations concerning dye concentration and film thickness also the influence of the amount of the signal intensifier TiO_2 was tested.

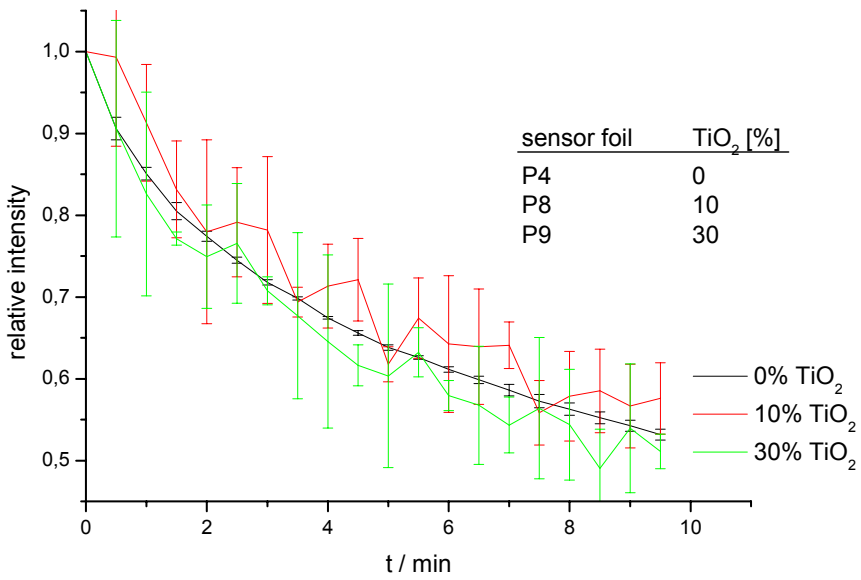

figure 4.7: photobleaching at variable TiO_2 concentration
standard deviations refer to values averaged over three measurements; films containing 2% MY and 1% PtTFPP; film thickness approximately 0,650 µm

We expected that TiO_2 destabilizes the dye system dramatically because it is well known to be a photocatalytic substance. However, addition of TiO_2 does not influence the stability of the emission signal. The fluctuations and high standard deviations of these measurements can be explained by low integration times used for these measurements due to high emission intensities of these films.

Variation of film parameters shows important effects on the photostability of the investigated sensor films. Some films showed bleaching rates of above 75 % during the observation period. On account of these results optimisation of sensor parameters is absolutely necessary.
Sensor films can be optimised concerning film thickness and dye concentration. Results showed that it is advantageous to increase film thickness while the antenna dye concentration should be reduced.
The bleaching curves show an enormous decrease of emission intensity at the beginning of the measurements and flatten after a certain time of irradiation. Thus a further possibility to

reduce bleaching effects during measurements is to condition the sensor films by "prebleaching". Prebleaching provokes that films are in the flattened region of the bleaching curves; accordingly the intensity signals show higher stability. For this purpose films are irradiated with a relatively strong light source for 30 min.

Other parameters, which were not investigated during these experiments, but lead to a reduction of photobleaching are the application of antenna dyes with higher stability, or simply the substitution of the very intense light sources like HBO 50/AC by ones that show lower intensities.

4.1.3.4 Calibration

Calibration using FLIM (Sensicam)

figure 4.8 shows the calculated lifetime images using the Matlab script alltau.

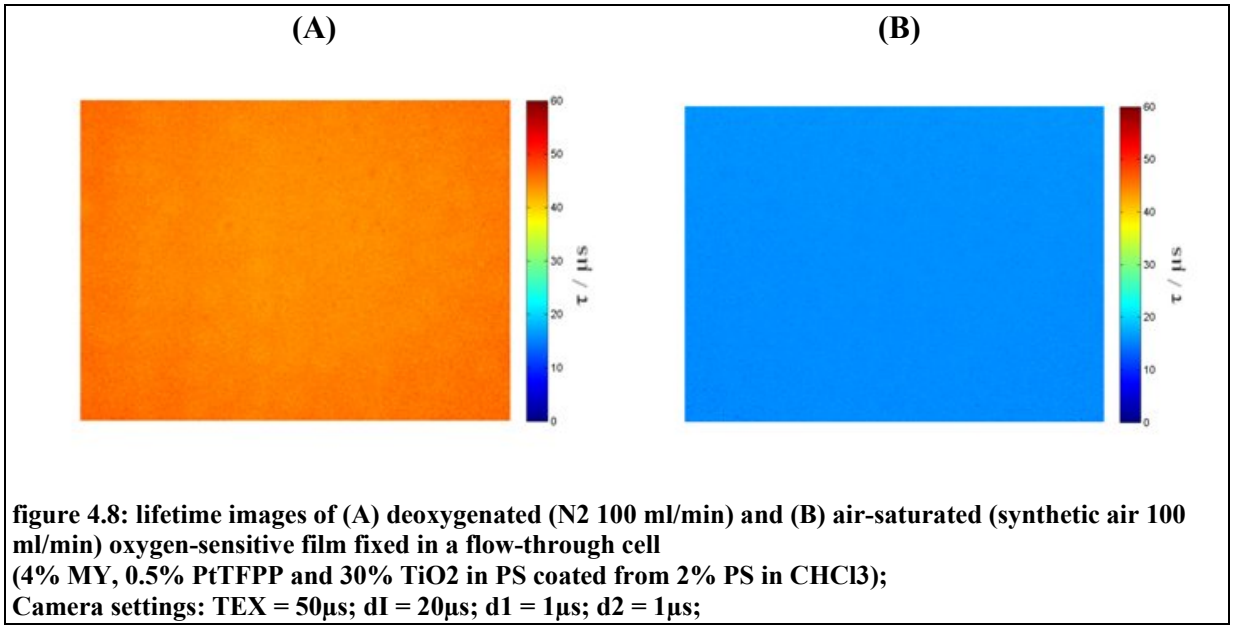

figure 4.8: lifetime images of (A) deoxygenated (N2 100 ml/min) and (B) air-saturated (synthetic air 100 ml/min) oxygen-sensitive film fixed in a flow-through cell
(4% MY, 0.5% PtTFPP and 30% TiO2 in PS coated from 2% PS in CHCl3);
Camera settings: TEX = 50µs; dI = 20µs; d1 = 1µs; d2 = 1µs;

The lifetime images show high homogeneity over the whole recorded area. The calculated values and standard deviation were plotted in a Stern-Volmer-plot (see figure 4.9).

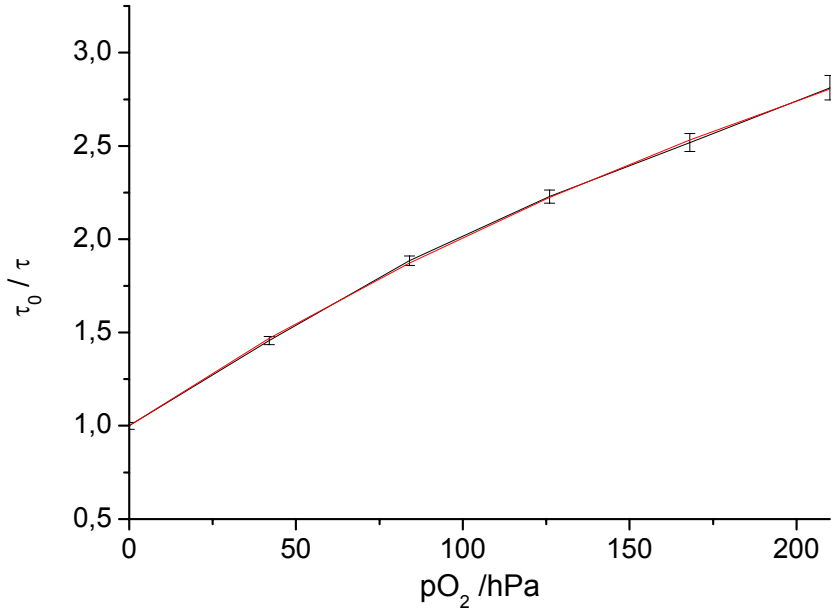

figure 4.9: Stern-Volmer plot of the calibration data obtained using the Sensicam; 4% MY, 0.5% PtTFPP and 30% TiO_2 in PS coated from 2% PS in $CHCl_3$ Standard deviation was calculated over the whole image area τ_0 = 47.2 µs; τ_0/τ = 2.8; f_1 = 0.863; K_{SV} = 0.0140 hPa^{-1}

The calibration curve has a slightly nonlinear developing. This behaviour is commonly known when luminescent dyes are dissolved in matrices. Dissolving the indicator leads to a fraction of indicator molecules which can be easily quenched and another fraction which is barely or not quenched [47]. At low pO_2 the calibration curve shows a higher increase of τ_0/τ because easily quenchable molecules are quenched by oxygen. The flattening of the curve at higher pO_2 is traced back that at high pO_2 also indicator molecules with a lower K_{SV} have to be quenched.

For this reason calibration data could not be fitted using the Stern-Volmer model. Instead calibration data were fitted using the commonly used simplified two-side-model [47, 48]

$$\frac{\tau}{\tau_0} = \frac{f_1}{1 + K_{SV}\, pO_2} + f_2 \qquad (9)$$

The values τ_0 (47.2 µs) and τ_0/τ (2.8) are comparable with values found in literature τ_0 = 49.0 µs and τ_0/τ = 2.9 for PtTFPP [13].

Calibration using FRIM (using the channels of a color camera)

Images were taken with a Marlin F201C. The color channels were separated using the Software ImageJ. Then the images were calculated using the Matlab script ratio (see chapter 3.3).

The following figures show the original images that were obtained after separating the three color channels.

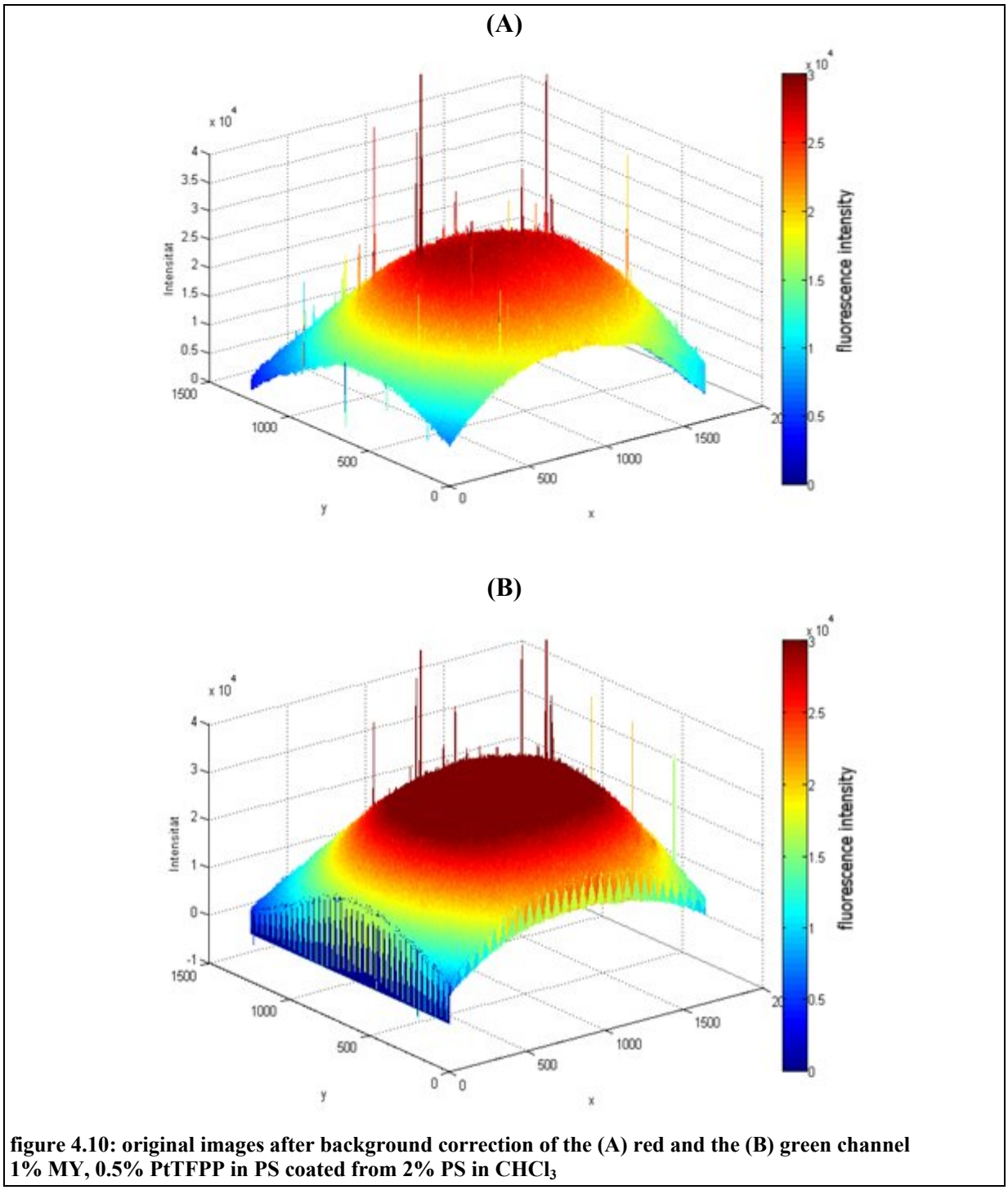

figure 4.10: original images after background correction of the (A) red and the (B) green channel 1% MY, 0.5% PtTFPP in PS coated from 2% PS in $CHCl_3$

The original images of the red and the green channel show an inhomogeneous distribution of the intensity. Possible reasons for that are an inhomogeneous light field or an inhomogeneous sensitivity of the CCD-chip of the camera.

The Matlab script ratio calculates the ratio of red to green channel. By this division the following images were obtained.

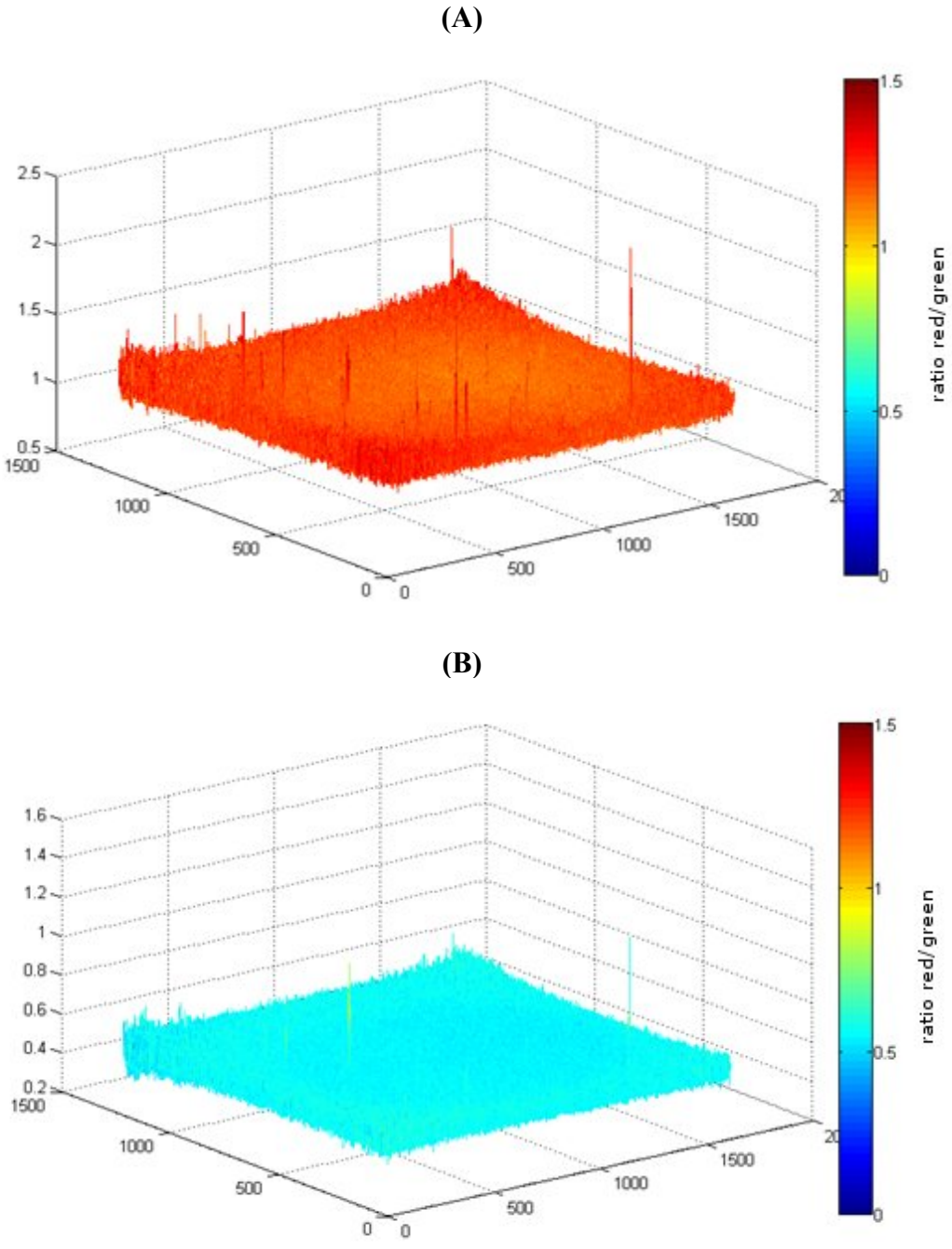

figure 4.11: ratiometric surface plots of (A) deoxygenated (N2 100 ml/min) and (B) air-saturated (synthetic air 100 ml/min) oxygen-sensitive film
1% MY, 0.5% PtTFPP in PS coated from 2% PS in $CHCl_3$

The calculated values and standard deviation were plotted in a Stern-Volmer-plot (see figure 4.12).

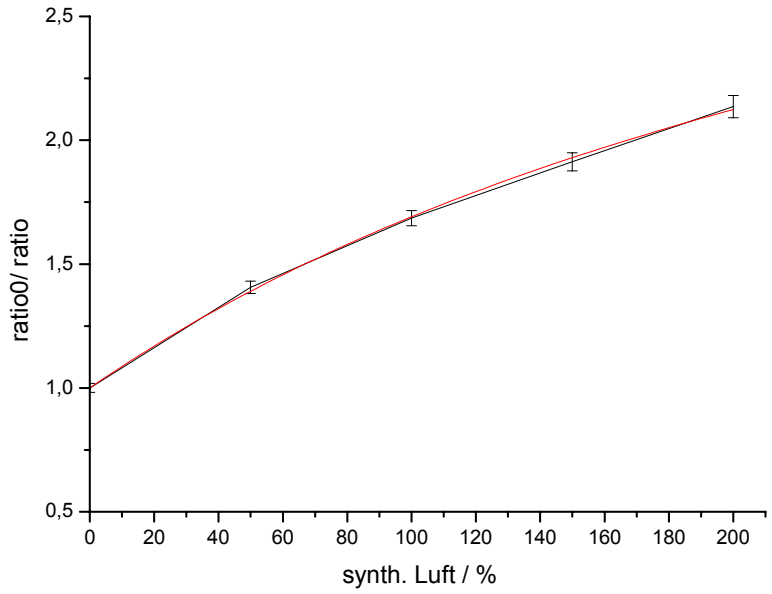

figure 4.12: Stern-Volmer plot of the calibration data obtained using the color camera
1% MY, 0.5% PtTFPP in PS coated from 2% PS in $CHCl_3$
Standard deviation was calculated over the whole image area
$Ratio_0 = 1.21 \pm 0.02$; $ratio_0/ ratio = 2.1$; $f_1 = 0.750$; $K_{SV} = 0.0114\ hPa^{-1}$

The calibration curve has a slightly nonlinear developing. The value $ratio_0/ ratio$ (2.1) is lower than the expected value found observed value in emission spectra of 3.10. Probably this is due to the overlap of green and red channel of the color camera.

Calibration data were fitted using the commonly used simplified two-side-model [48].

4.1.3.5 Application in microfluidic devices

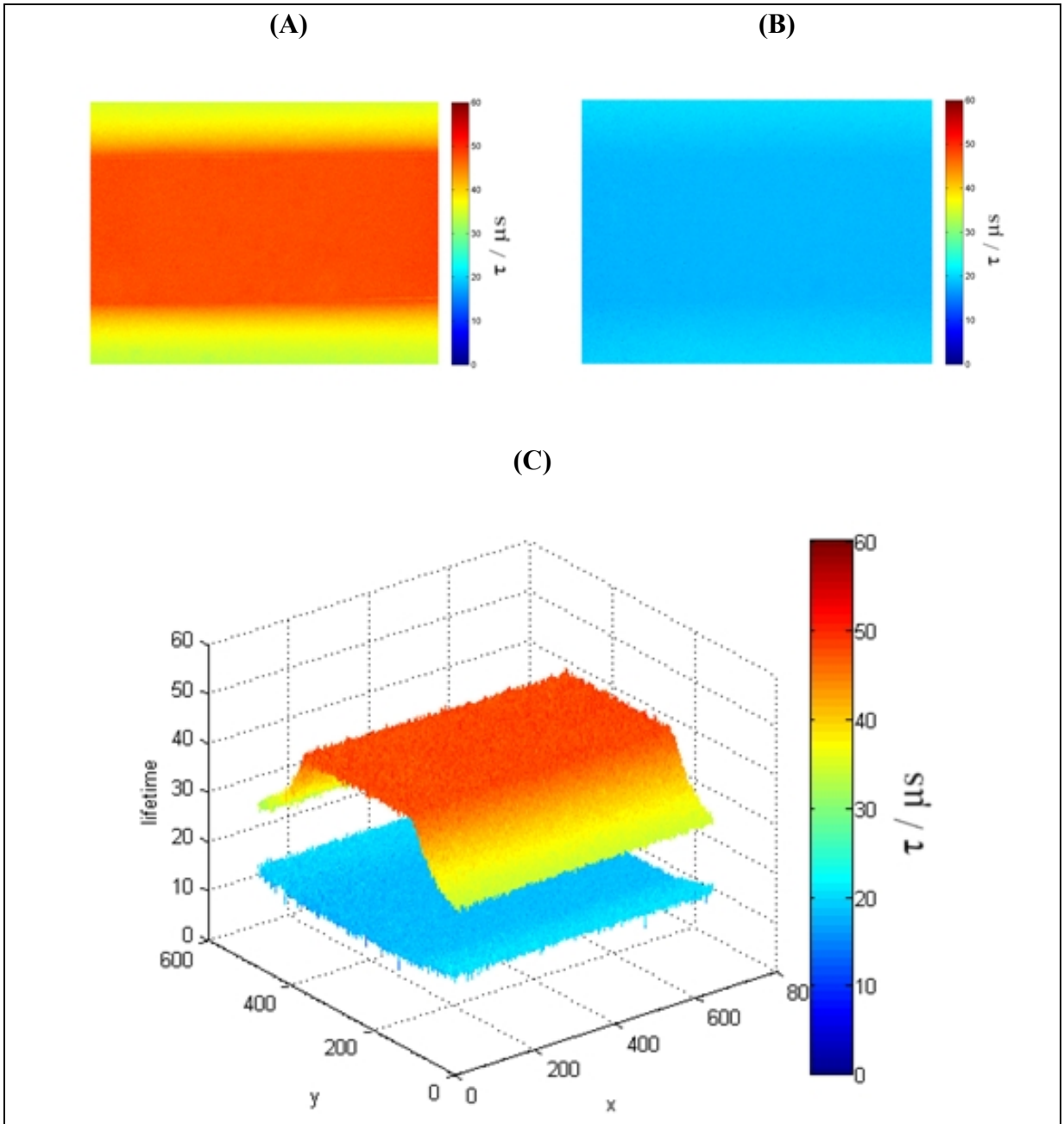

figure 4.13: lifetime images of a microfluidic channel flushed with (A) nitrogen and (B) synthetic air; (C) surface plot of (A) and (B)
(4% MY, 0.5% PtTFPP and 30% TiO2 in PS coated from 2% PS in CHCl3);
Camera settings: TEX = 50µs; dI = 20µs; d1 = 1µs; d2 = 1µs;

The obtained lifetime images are very homogenous. figure 4.13 (A) shows lifetime values outside the microfluidic channel of 35 to 45 µs. This phenomenon can be traced back to the high gas permeability of PDMS [49]. Gaseous nitrogen can easily diffuse into the polymeric material.

The oxygen-sensing films were also tested by application in microfluidic systems which were inoculated with different microorganisms.

(A)

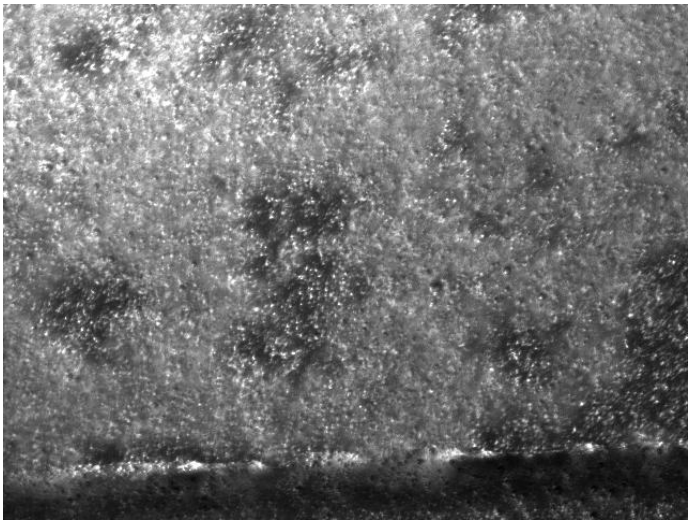

(B)

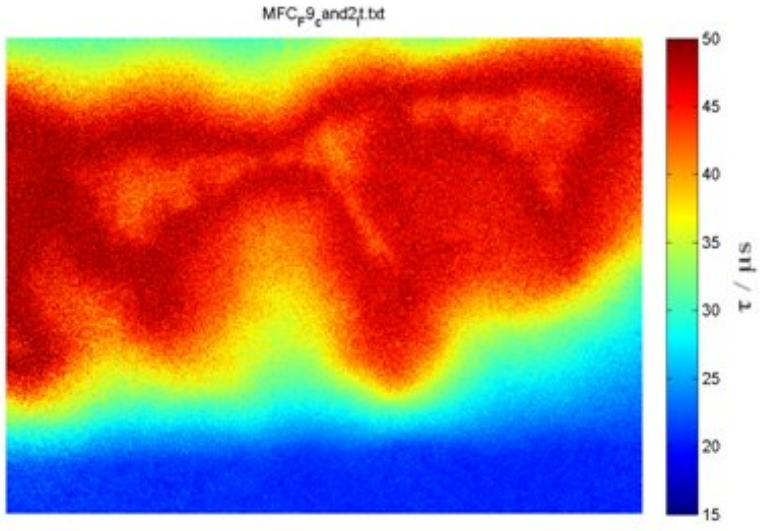

figure 4.14: (A) Transmitted light and (B) lifetime image of Candida albicans in microfluidic chip integrated sensor foil: 4% MY, 0.5% PtTFPP and 30% TiO_2 in PS coated from 2% PS in $CHCl_3$ T_{EX} = 50µs; dI = 15µs; d1 = 1µs; d2 = -10µs; averaging 16 images

Figure figure 4.14 (A) shows that the yeast grows along the whole channel. It only exhibits vacancies at some positions, including the right, lower corner.

Oxygen deficiency occurs exactly where the highest growth of Candida albicans can be seen.

Application of oxygen sensors in microfluidic systems requires not only taking single images, but monitoring oxygen levels over time. For that reason growth of Candida albicans was monitored.

The yeast strain was inserted into the microfluidic device. The following images were obtained 20 min, 65 min, 4 h 55 min and 7 h 50 min after inoculation.

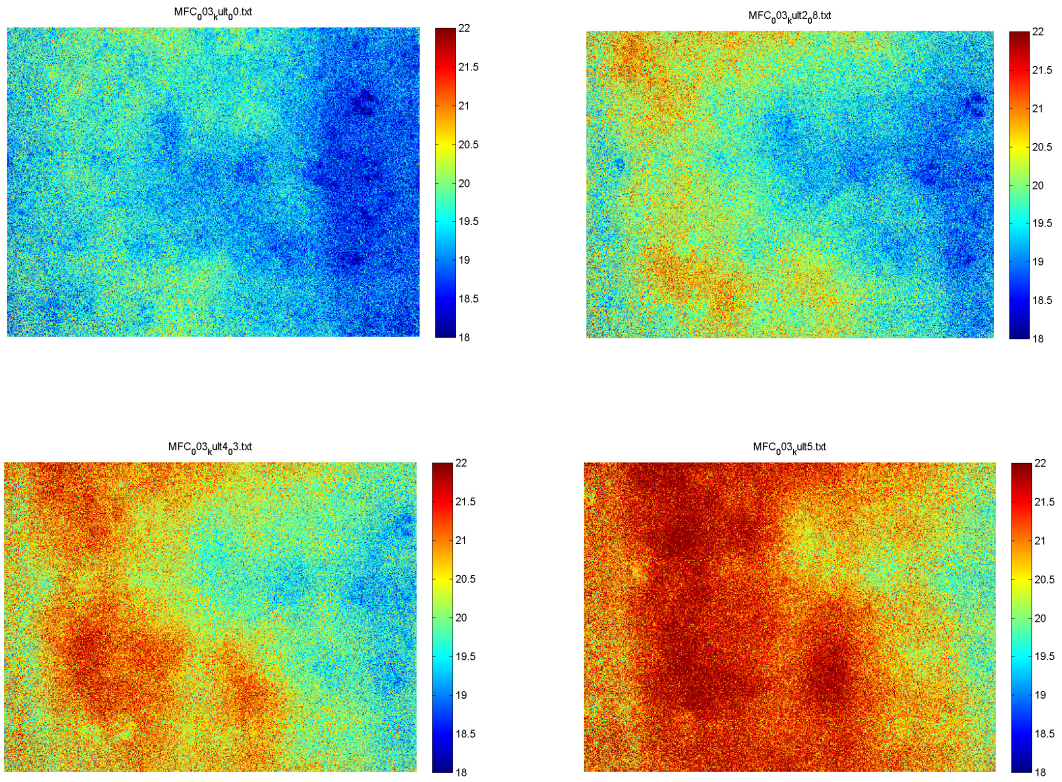

figure 4.15: Lifetime images taken 20 min, 1 h 5 min, 4 h 55 min and 7 h 50 min after inoculation with Candida albicans
integrated sensor foil: 4% MY, 1% PtTFPP and 30% TiO_2 in PS coated from 2% PS in $CHCl_3$
T_{EX} = 50µs; dI = 20µs; d1 = 1µs; d2 = 1µs; IT = 900ms

To observe lifetime of the inoculated microfluidic chip the average value of the lifetime over the channel width was calculated and plotted against time.

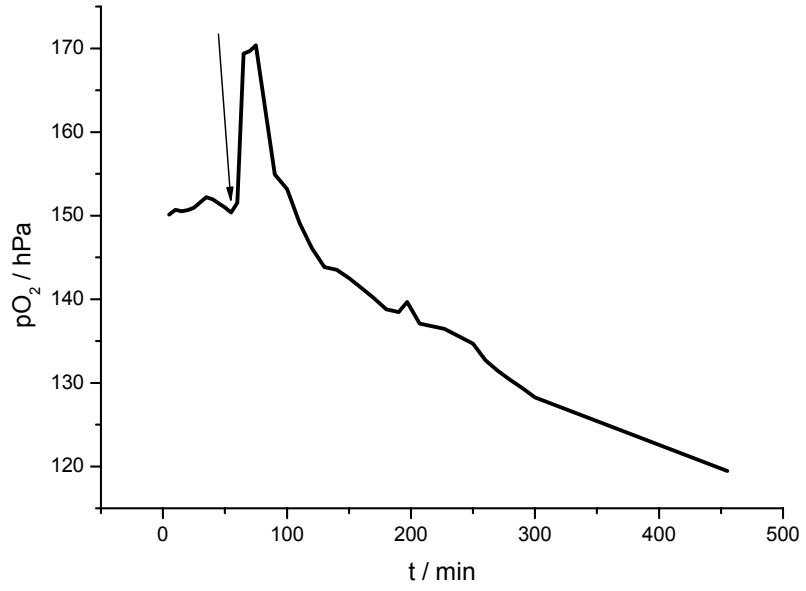

figure 4.16: pO_2 vs. time during cultivation of Candida albicans
integrated sensor foil: 4% MY, 1% PtTFPP and 30% TiO_2 in PS coated from 2% PS in $CHCl_3$
the arrow marks the moment when the channel is flushed with fresh, air-saturated media
pO_2 was calculated using $f_1 = 0.863$; $K_{SV} = 0.0140\ hPa^{-1}$

Initially the value of the pO_2 doesn't show any change. After 55 min the channel was flushed with fresh, air-saturated media. After the flush a rampant development of the lifetime can be observed, that fades to a constant increase of the lifetime over hours.
Supposable this constant decrease of pO_2 can be traced back to the growth of Candida albicans.

4.1.4 Conclusion

The integration of the presented films into microfluidic devices seems to be a promising possibility to monitor oxygen-consumption of cells. Inhomogeneities of the film can easily be referenced using FLIM (monochrome camera) as well as FRIM (color camera). The color camera turned out to be perfectly convenient for the applied dye system.
Calibration showed to follow the simplified two-site model and showed relatively low standard deviation.
Applying FRIM as referencing method using a color camera showed to be more difficult than measuring the lifetime due to the low photostability of the used dye system. Finding a solution to that problem is one of the most important challenges to facilitate the application of FRIM.

However, integrating sensor films into microfluidic systems is one more step in fabricating these devices. To facilitate a commercial application, sensor materials should be more flexible. A possibility to achieve more flexibility could be to use sensors that can be added to the surrounding medium and thus be used in every desired microfluidic system (see chapters 4.2 and 4.3).

4.2 Oxygen-sensitive PSPVP-nanosensor particles

4.2.1 Introduction

Nanosensor particles represent an easy-to-handle possibility to integrate sensors into microfluidic devices. One of their advantages over the application of sensor films or patches is the possibility to introduce them in almost every system without causing an additional fabrication step of the system they are applied in. Luminescent nanosensor particles can simply be added to a sample and allow similar detection methods as dissolved indicators (for instance microscopic applications), whereat they enable the application of dyes that are insoluble in water and hence inapplicable in water-based systems. Furthermore the dye is virtually enclosed in the nano particle and a transfer from the sample to the surrounding matter (for example PDMS in a microfluidic chip [50]) is inhibited compared to the application of dye solutions.
Oxygen-sensitive nanoparticles were reported by Kopelman and co-workers [51]. Borisov et al. presented an easy method to prepare stable and non-aggregating oxygen-sensitive nanobeads by staining poly(styrene-block-vinylpyrrolidone) nano particles with luminescent dyes. They demonstrated that their nanobeads are applicable for monitoring oxygen in bioreactors and for lifetime imaging [52].

Oxygen-sensitive nanobeads used for the application in microfluidic devices were prepared using the method of Borisov et al. Poly(styrene-block-vinylpyrrolidone) nano particles were stained with Macrolex-Yellow and PtTFPP, optimised concerning dye concentration and tested for their applicability in microfluidic systems.

4.2.2 Experimental procedure

4.2.2.1 Staining of the nanoparticles

The poly(styrene-block-vinylpyrrolidone) nano particle emulsion (approximately 520 mg; = 200 mg polymer) was diluted with 50 ml of water and 30 ml of tetrahydrofuran. The respective amounts of the dyes Macrolex Yellow (MY) and Pt(II) meso-Tetra(pentafluorophenyl)porphine (PtTFPP) were dissolved in 20 ml of THF. The solution containing the dyes was then added drop wise under heavy stirring into the particle

suspension. A rotary evaporator was used to remove all of the THF and the water to some extent. Then the suspension was diluted with water up to 20 ml overall volume (= 1% (w/w)).

table 3: composition of the nanosensor particles

Name	MY [%]	C545T [%]	PtTFPP [%]
P2	2		2
P3	4		2

4.2.2.2 Emission and excitation spectra

Emission and excitation spectra of the particles were acquired on a Hitachi F-7000 fluorescence spectrometer.

Measurements were made in oxygen-saturated and oxygen-free solutions in deionised water.

Solutions were deoxygenated by dissolving α-D-glucose and glucose oxidase in deionised water (c(glucose) = 0,25 mol/l; c(glucose oxidase) = 200 µg/ml).

4.2.3 Results and Discussion

4.2.3.1 Spectral characterisation

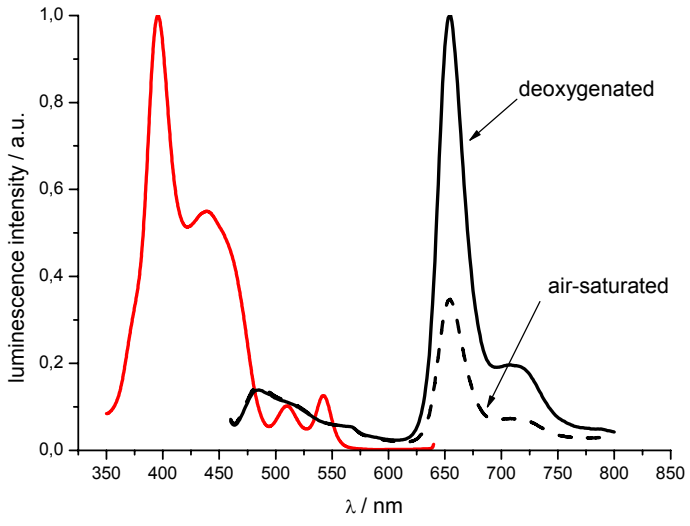

figure 4.17: excitation and emission spectra of P2 (2% MY and 2% PtTFPP) in air-saturated (solid line) and deoxygenated (dashed line) solution;
λEX = 450 nm, λEM = 650 nm. Ratio of deoxygenated to oxygenated intensity at 655 nm = 2.88.

4.2.3.2 Adaption of optical systems

Since the same dye system was applied as in chapter 4.1.3.1 the adaption of the optical system remains the same. Investigations on the fluorescence microscope can be made using the blue bandpass filter for excitation and the red longpass filter for emission.
The same applies to the applicability of the color camera.

4.2.3.3 Application

Lifetime Imaging

The small volume of the microfluidic chip caused some difficulties concerning the use of lifetime imaging. Application of the nanosensor particles emerged only to be possible using high concentrations to yield intensities, which are high enough for this method.
However, preliminary tests showed good performance when particles were added in high concentrations.
figure 4.18 shows a lifetime image of nanosensor particles P3 (4% MY and 2% PtTFPP) in a microfluidic chip. An undiluted particle suspension was inserted into the chip. Before the insertion the particle suspension was deoxygenated using glucose and glucose oxidase.

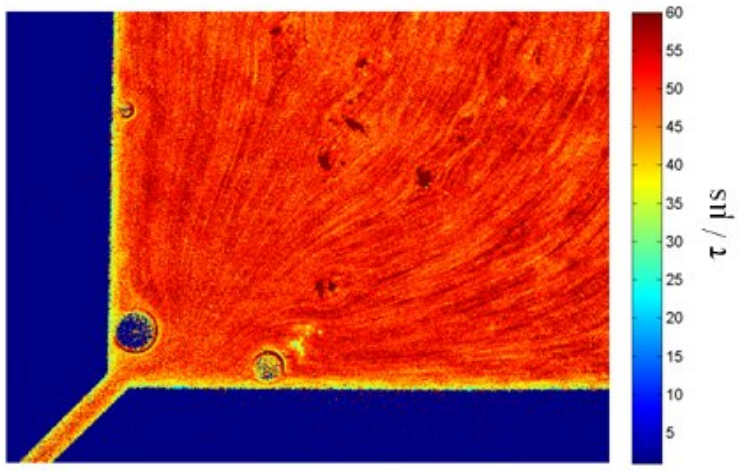

figure 4.18: preliminary test applying nanosensor particles P3 (4% MY and 2% PtTFPP) in a microfluidic chip; lifetime image
T_{EX} = 50µs; dI = 20µs; d1 = 1µs; d2 = 1µs; IT = 900ms

The preliminary test showed that application of nanosensor particles leads to very homogenous distribution of the lifetime. Stripes in the image can be traced back to the movement of the particles.

Application during cultivation of microorganisms

Nanosensor particles P3 (4% MY and 2% PtTFPP) were also tested concerning their applicability in a microfluidic device during cultivation of pichia pastoris.

For application during cultivation of pichia pastoris particles had to be diluted with media to a particle concentration of 0,5% (w/w). In spite of resulting low intensities some images (figures figure 4.19 and figure 4.20) were taken.

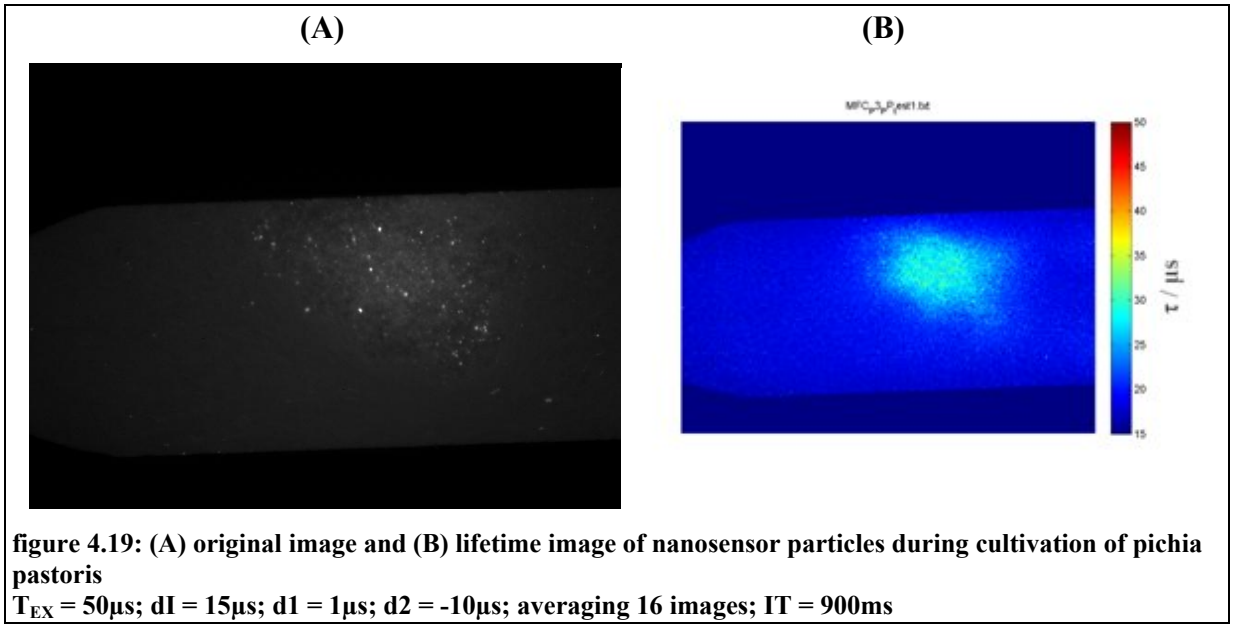

figure 4.19: (A) original image and (B) lifetime image of nanosensor particles during cultivation of pichia pastoris
T_{EX} = 50µs; dI = 15µs; d1 = 1µs; d2 = -10µs; averaging 16 images; IT = 900ms

Respirometric activity can clearly be seen. However, one can only suppose that lifetime values really reflect the pO_2 because intensities are too weak to get reliable information.

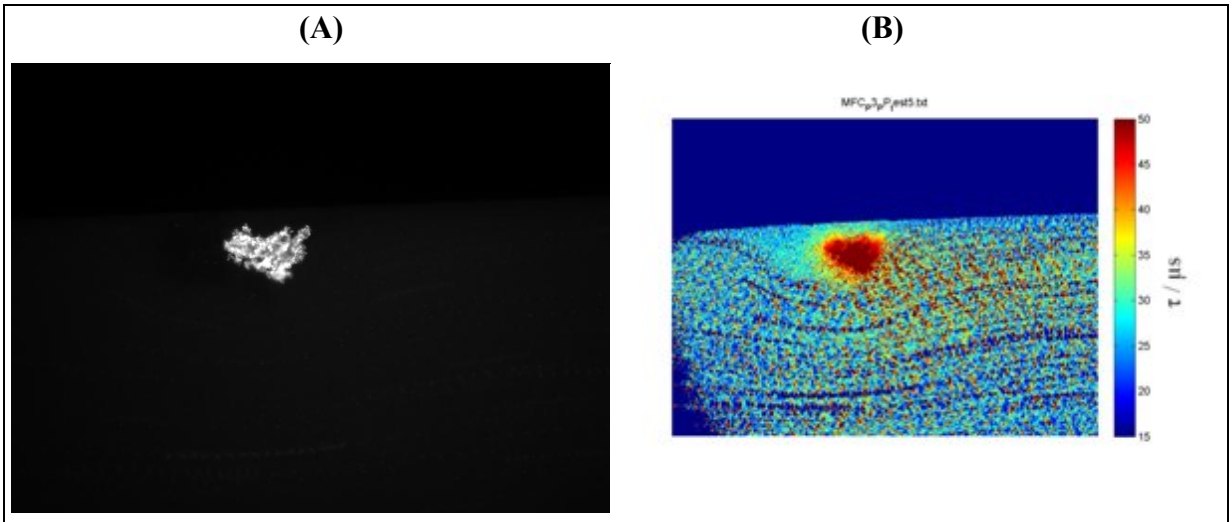

figure 4.20: (A) original image and (B) lifetime image of nanosensor particles during cultivation of pichia pastoris
T_{EX} = 50µs; dI = 15µs; d1 = 1µs; d2 = -10µs; averaging 16 images; IT = 900ms

In figure 4.20 the situation is even worse. Except for the high intensities directly located at the pichia pastoris colony intensities were even lower than in the figure before. This leads to the problem that values for lifetime can only be calculated directly around the colony.
The location of nanosensor particles mainly on or nearby the colony leads to the speculation that the particles tend to accumulate on the surface of microorganisms.

4.2.3.4 Ratiometric imaging

Ratiometric imaging involves the advantage that it is easier to obtain signal intensities that are high enough because images can be made during illumination. Preliminary tests showed that it is possible to apply nanosensor particles down to concentrations of 0.1% (w/w).
However, following images were taken using particle suspensions with 0.5% (w/w).

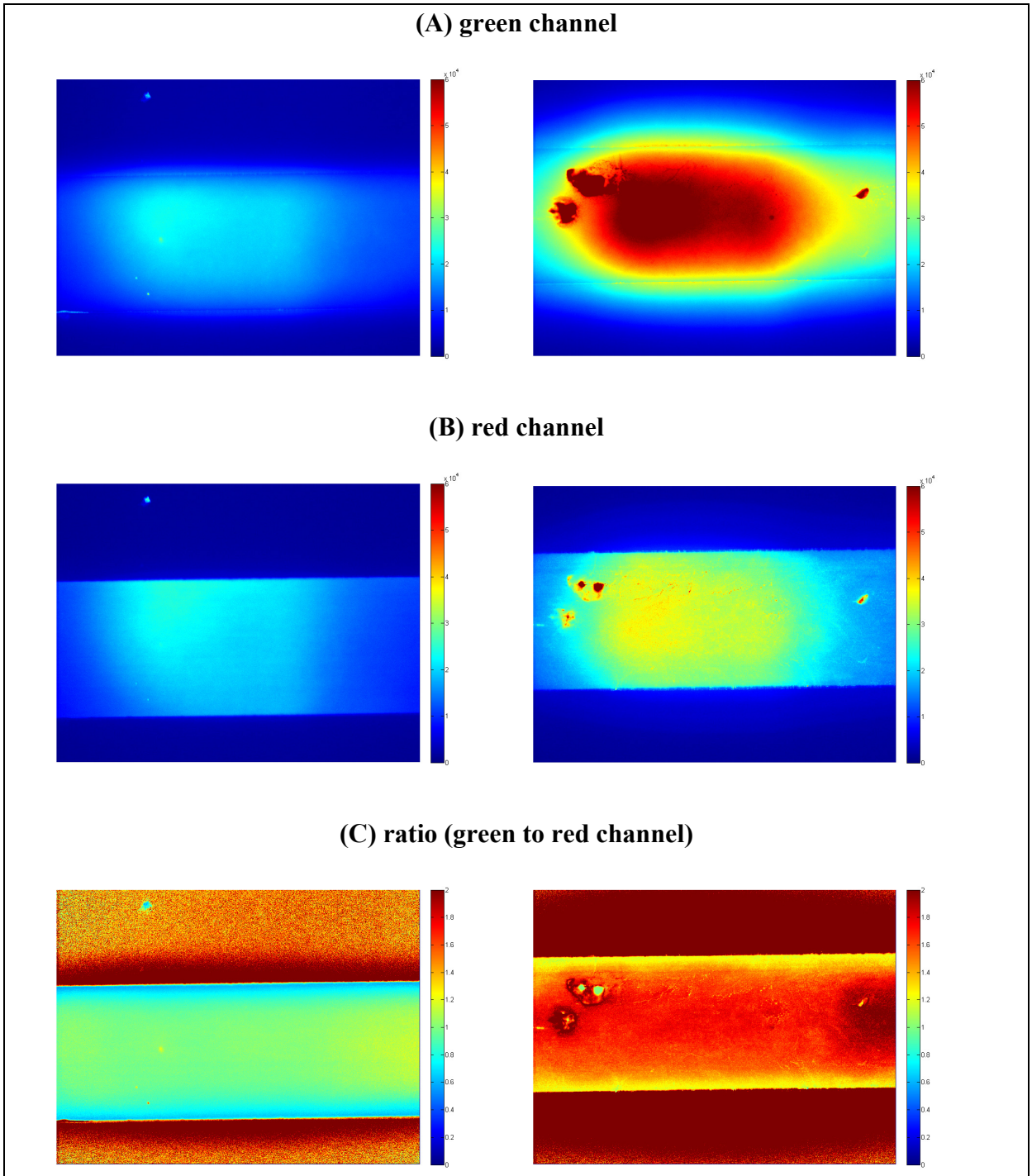

figure 4.21: luminescence intensity images of the (A) green and (B) red channel of the color camera and (C) ratio (green to red channel) of a microfluidic channel filled with air-saturated (left) and deoxygenated (right) particle suspensions P3 (4% MY and 2% PtTFPP)

The experimental output is contradictory to the theory. Usually the ratio of green to red channel should decrease at lower oxygen levels. What can be further seen is that emission intensity is not limited to the microfluidic channel.

Further experiments were performed to explain this unexpected behaviour. These tests showed that apparently a dye transfer from the particles to the surrounding PDMS takes place. Thereby the emission of the green channel gains intensity.
Since only the green emission increases it is possible that only Macrolex Yellow is transferred to the surrounding matter. This behaviour can be explained by the lower lipophilicity of Macrolex Yellow compared to PtTFPP. Whilst PtTFPP is located inside the highly lipophilic core of the particle Macrolex Yellow is located between shell and core. Hence it can be assumed that the problem could be solved by transferring the dye molecules further into the interior of the particles.

4.2.4 Conclusion

In principle nanosensor particles represent an easy-to-handle possibility to integrate sensors into microfluidic devices. However, application of oxygen-sensitive particles showed to evoke some unexpected difficulties. Low intensities, which can be traced back to the small detection volumes in a microfluidic device, caused problems using RLD. Difficulties due to a lack of intensity can be erased using ratiometric imaging for instance using the color channels of a color camera. The use of the color camera shaped up as a good alternative to lifetime imaging. However, further improvements must be made concerning the dye transfer from the particle to the PDMS.

4.3 Magnetic Nanoparticles

4.3.1 Introduction

Concerning the design of optical oxygen sensors several possibilities exist. Only to list some options, optical sensors can be integrated into a sample vessel using films coated on a substrate, sensor patches, which can be fixed inside a sample vessel or nanoparticles, which are simply added to the sample. All these different designs entail specific benefits but also show some drawbacks. Sensor films for instance usually exhibit high homogeneity of dye distribution and hence a very homogeneous emission intensity. On the other hand, however, integration of sensor films sometimes appears to be difficult. Integration of films causes one additional fabrication step and adhesion on the substrate depends on the used material. Moreover frequently applied fabrication techniques like photolithography may lead to a strong reduction of emission intensity. Sensor spots can be used to measure several parameters in parallel, but also require additional production effort. Furthermore sensor patches only give analytical information about one selected region of the sample vessel or microfluidic system. Application of nanosensor particles poses an easy-to-handle possibility to integrate sensors into microfluidic devices, but they must be applied in relatively high concentration to achieve high emission intensities (see chapter 4.2)
Magnetic optical particles combine the advantages of solid sensor spots with high intensities and relatively low consumption of dyes and nanoparticles, which are known to be convincing due to their simple application. Magnetic particles can be used for the in situ formation of sensor spots by collecting the particles with a magnet and then can be read out from the outside. In contrast to conventional sensor spots these spots can be moved in a vessel when there is the need to obtain analytical information of another region of the vessel.
Magnetic nanosensor particles seem to be especially applicable in microfluidic devices due to several reasons. First of all they can be easily integrated into microfluidic systems by adding them directly to the sample. For that reason the number of fabrication steps of one chip can be reduced. Furthermore it can be estimated that the separation of the particles is much easier due to small sample volumes.

This chapter deals with the application of magnetic oxygen-sensing nanoparticles in microfluidic devices. These particles containing an oxygen-sensitive ultra bright Ir(III)-

coumarin complex (structure and emission/excitation spectra see figure 4.22) [53] were provided by Günter Mistlberger [54].

(A)

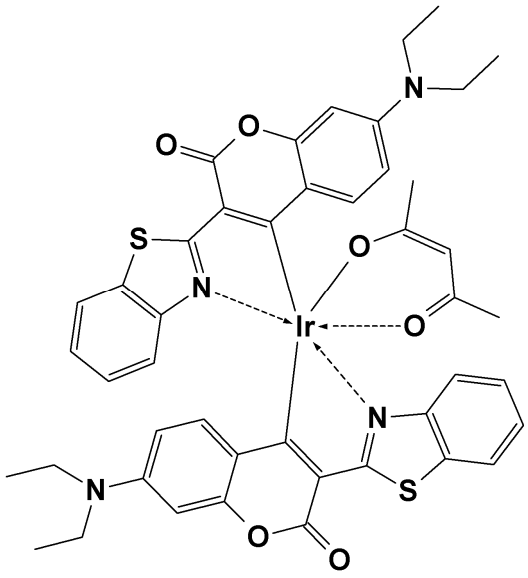

(B)

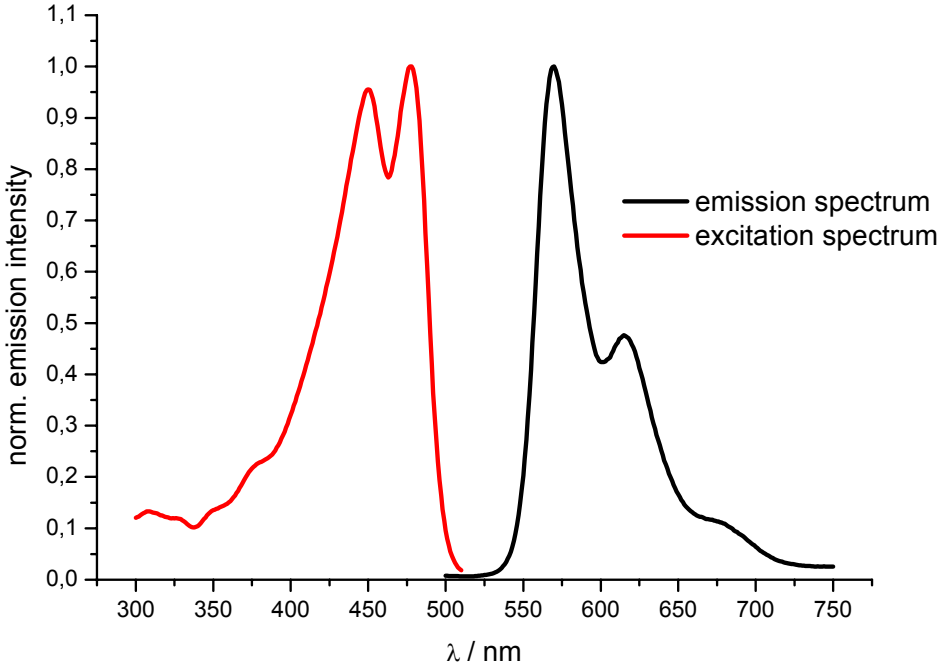

figure 4.22: (A) Structure of Ir(CS)2(acac) provided by Sergey Borisov and (B) corrected and normalised emission (λ_{EX} = 475 nm)and excitation spectra (λ_{EM} = 565 nm) of magnetic nanosensor particles;

4.3.2 Experimental procedures

Following table shows the properties of the provided nano sensor particles.

table 4: properties of magnetic nanosensor particles

z-av [nm]	186
PDI	0,029
c [mg/ml]	15,3 ± 0,07

Emission spectra were acquired on a Hitachi F-7000 fluorescence spectrometer. Measurements were made in air-saturated and oxygen-free solutions in deionised water.

Solutions were deoxygenated by dissolving α-D-glucose and glucose oxidase in deionised water (c(glucose) = 0,25 mol/l; c(glucose oxidase) = 200 µg/ml).

4.3.3 Results and Discussion

4.3.3.1 Adaption of the optical system

For measurements on the fluorescence microscope adequate optical filters have to be selected that fit to excitation and emission spectra of the dye system.

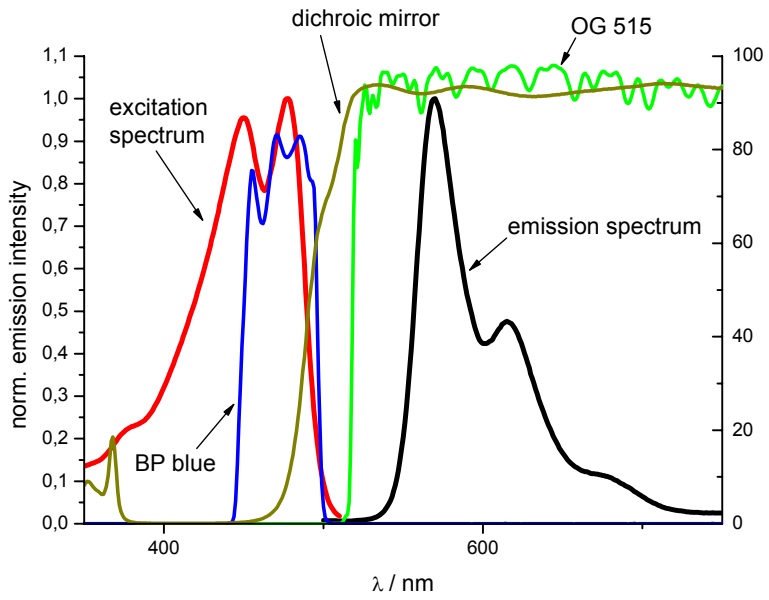

figure 4.23: corrected and normalised emission (λ_{EX} = 475 nm)and excitation spectra (λ_{EM} = 565 nm) of magnetic nanosensor particles with appropriate optical filters (BP blue, OG 515 and dichroic mirror;

The transmission spectrum of the selected filter (blue bandpass) shows even a better overlap with the excitation spectra than it did for the light harvesting system in chapter Spectral *characterisation and adaption of optical systems*

The dichroic mirror reflects a large part of the excitation light and orients it towards the sample on the microscope. Luminescence light from the sample is then transmitted by the dichroic mirror and also by the green longpass emission filter (OG 515).

4.3.3.2 Spectral characterisation

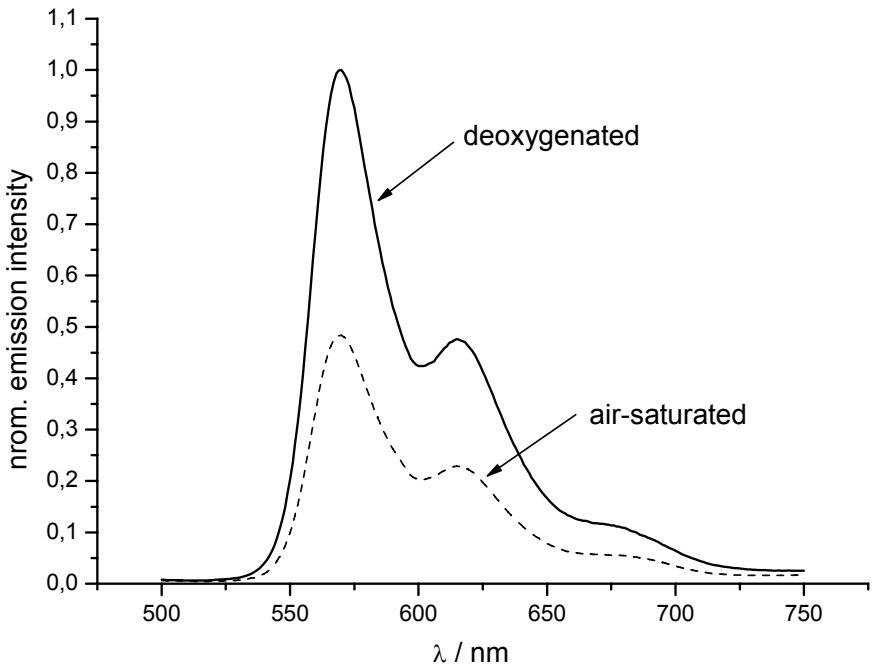

figure 4.24: Emission spectra of magnetic nanosensor particles in air-saturated (dashed line) and deoxygenated (solid line) solution; λ_{EX} = 475 nm. Ratio of deoxygenated to air-saturated intensity at 570 nm = 2.07

4.3.3.3 Calibration:

Calibration data were provided by Günter Mistlberger.

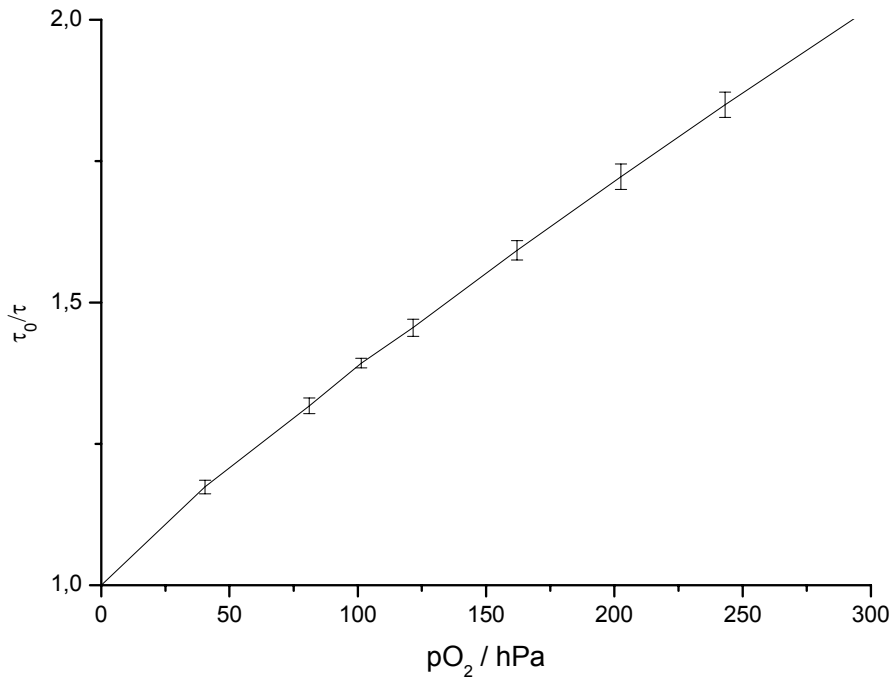

figure 4.25: Calibration curve of oxygen-sensitive nano sensor particles at various concentrations of dissolved oxygen
τ_0 = 10.5 µs τ0/τ = 1.75 and K_{SV} = 0.00353 hPa^{-1}

The Stern-Volmer-plot shows an almost linear increase. Characteristic values of the oxygen-sensitive nano sensor particles are τ_0 = 10.5 µs and K_{SV} = 0.00353 hPa^{-1}.

4.3.3.4 Application

Application in a flow-through-cell

Before the magnetic nanosensor particles were applied in microfluidic systems, they were tested in the flow-through-cell described in chapter 0. The hole of the flow-through-cell was closed from above with a glass slide covered with immobilized glucose oxidase (preparation see chapter 0) to simulate a biofilm which consumes oxygen.

40 µl particle suspension were dispersed in 0.5 ml deionised H_2O. The particle suspension was then injected into the flow-through-cell that was closed with a glass slide. Sensor signals

were read out on the fluorescence microscope using lifetime-imaging via rapid lifetime determination.

Then the cell was flushed by air-saturated solutions containing different concentrations of glucose using a syringe pump (v = 1 ml/min).

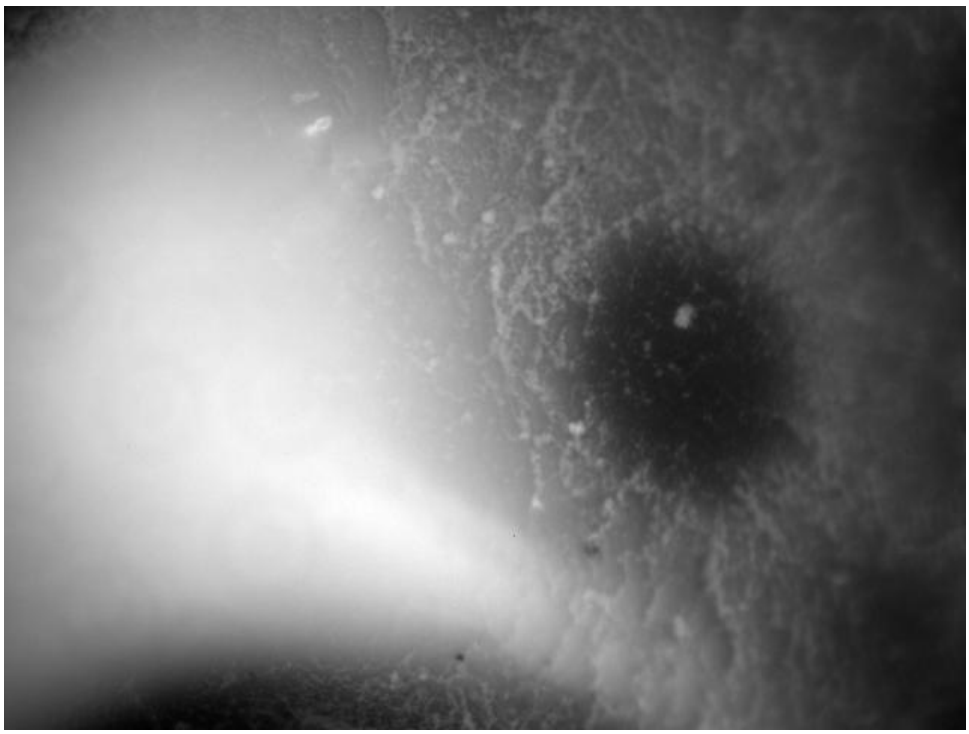

figure 4.26: Original image of the preliminary tests in the flow-trough-cell containing magnetic nano sensor particles and flushed with deionised H2O
T_{EX} = 20µs; dI = 3µs; d1 = 1µs; d2 = -1µs; averaging 8 images

(A) **(B)**

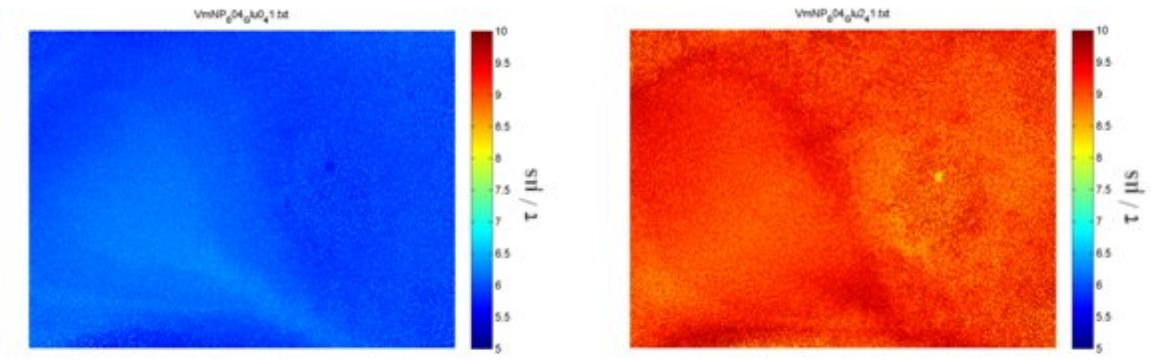

figure 4.27: Lifetime images of the preliminary tests in the flow-trough-cell containing magnetic nano sensor particles (A) flushed with deionised H_2O and (B) flushed with 2 mM glucose solution
T_{EX} = 20µs; dI = 3µs; d1 = 1µs; d2 = -1µs; averaging 8 images

In the original image in figure 4.26 one can see a very inhomogeneous distribution of the magnetic nano sensor particles because of the rough textured glucose oxidase surface. Lifetime images (figure 4.27 (A) and (B)) show a higher homogeneity than the original image, but especially the image acquired when the flow-through-cell was flushed with 2 mM glucose solution shows slight inhomogenities. It is assumed that these inhomogeneties arise from turbulent flow that is caused by the rough surface of the coating. Different flow rates on the surface lead to different oxygen levels.

Average pO_2 levels were obtained averaging a region of interest (x = 1-130 pixel; y = 100-190 pixel; see figure 4.28 (A)) and calculated using the Stern-Volmer-equation with τ_0 = 10.5 µs and K_{SV} = 0.00353 hPa^{-1}.

(A)

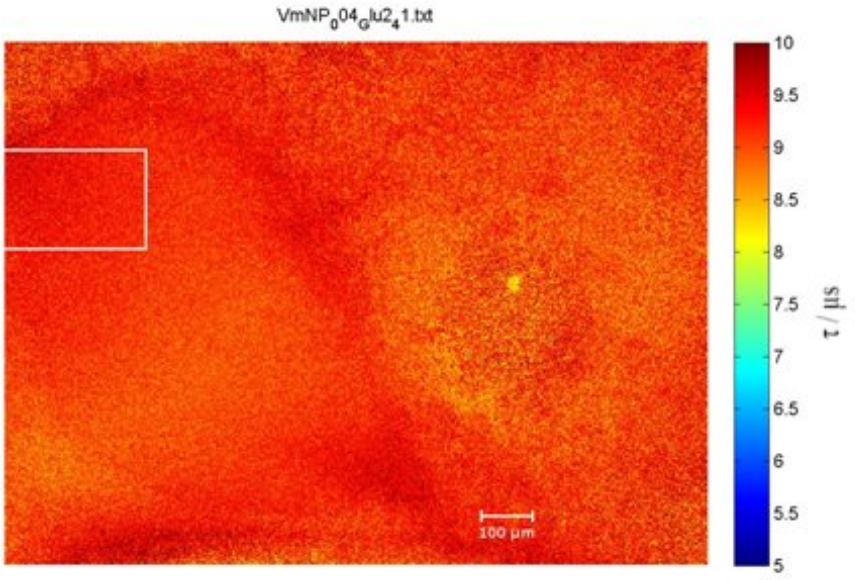

(B)

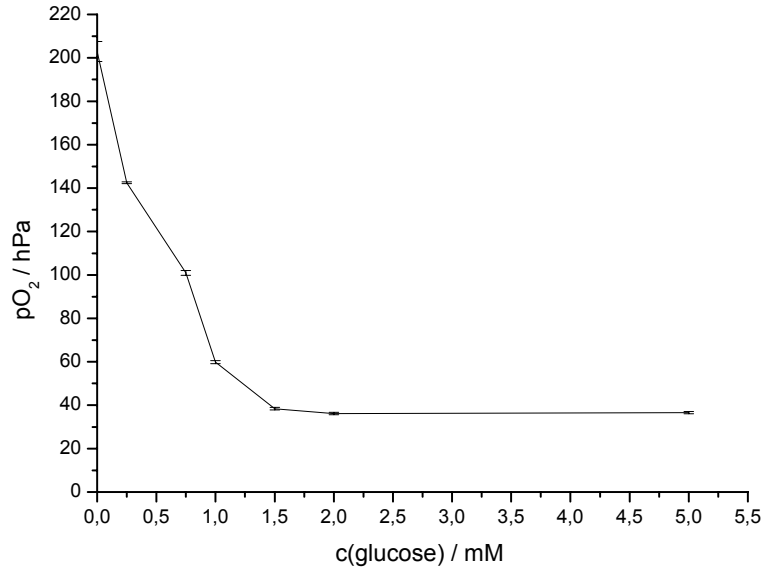

figure 4.28: (A) region of interest (white rectangle) and (B) pO2 vs. glucose concentration in the flow-trough-cell containing magnetic nano sensor particles flushed with solutions containing different concentrations of glucose

It was expected that the calculated pO_2 at high glucose concentrations the pO_2 level is zero. Unfortunately pO_2 remains static at values around 35 hPa. Perhaps this phenomenon can be traced back to the fact that the activity of the immobilized glucose oxidase is not high enough to transform all the oxygen on the surface of the coating. However, it is also possible that τ_0

takes another value than in the calibration because of different layer thickness of magnetic nano sensor particles or because of effects of the modified surroundings.

The investigated particles were shown to be applicable in flow-through-systems. It can be expected that their application in microfluidic systems will provide better experimental results because of the better controllability and the laminar flow found in these systems.

Application in microfluidic systems:

Oxygen-sensitive magnetic nano sensor particles were applied in microfluidic devices made from different materials (PDMS and SU8) and read out on the fluorescence microscope using lifetime-imaging via rapid lifetime determination. The chips were inoculated with pichia pastoris.

Microfluidic chip made from SU8:

5 µl of the particle suspension were added to the cultivation media with active cell material and then inserted into a microfluidic chip made from SU8. Then the nanosensor particles were separated from the media from the outside with a magnet.

Following figures show one fluorescence intensity image and the associated lifetime image.

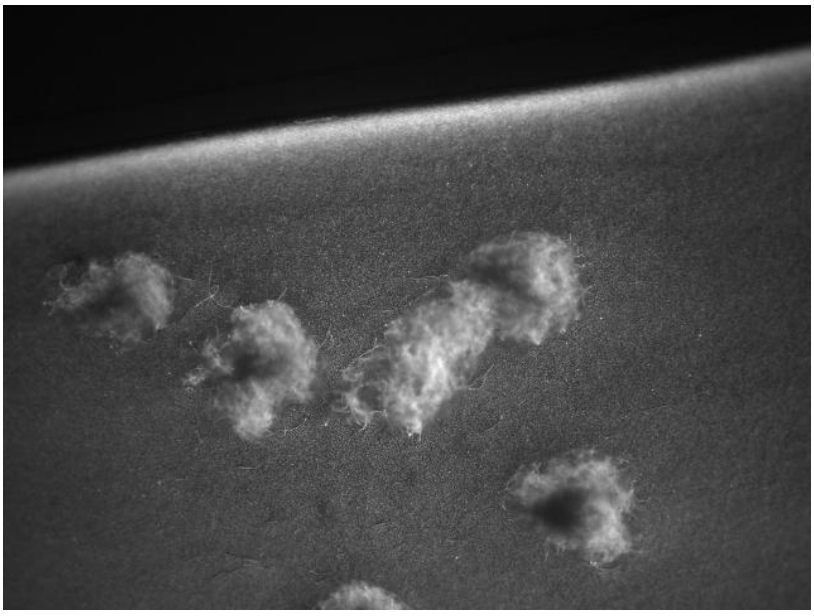

figure 4.29: fluorescence intensity image of pichia pastoris in a SU8 microfluidic device with magnetic nanosensor particles
T_{EX} = 20µs; dI = 3µs; d1 = 1µs; d2 = -1µs; averaging 16 images

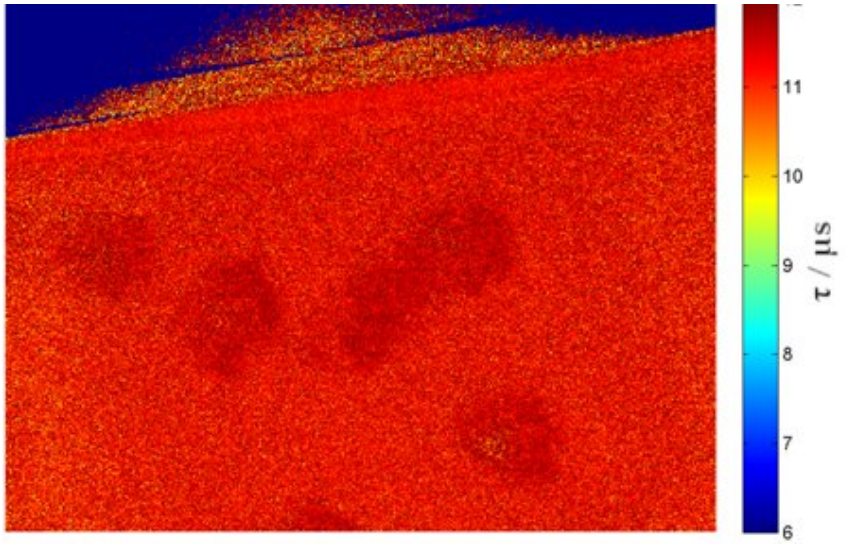

figure 4.30: Calculated lifetime image of pichia pastoris in a SU8 microfluidic device with magnetic nanosensor particles
T_{EX} = 20µs; dI = 3µs; d1 = 1µs; d2 = -1µs; averaging 16 images

In the fluorescence intensity image (figure 4.29) the highest intensity is located directly at the yeast colonies. Supposably this phenomenon can be traced back to the fact that the nanosensor particles accumulate at the cell walls and are integrated into the colonies.

In figure 4.30 it appears that the microfluidic channel is almost anoxic. The respiratory activity of pichia pastoris is only visible at the darker spots. Due to scattering of light at the channel walls there are values different from zero also outside of the microfluidic channel, where no particles can be found.

To investigate the monitoring of oxygen over time the channel was flushed with fresh, air-saturated media and a decrease of pO_2 was observed.

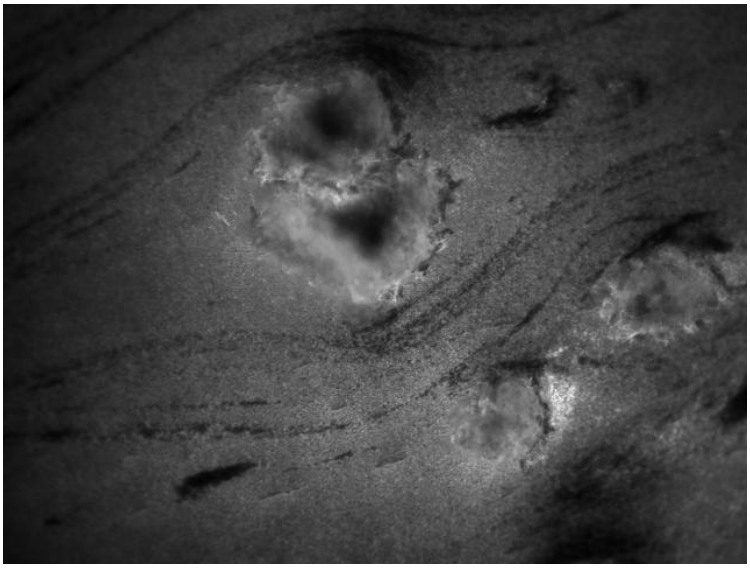

figure 4.31: fluorescence intensity image of pichia pastoris in a SU8 microfluidic chip inoculated with pichia pastoris following the decrease of pO2
T_{EX} = 20µs; dI = 3µs; d1 = 1µs; d2 = -1µs; averaging 16 images

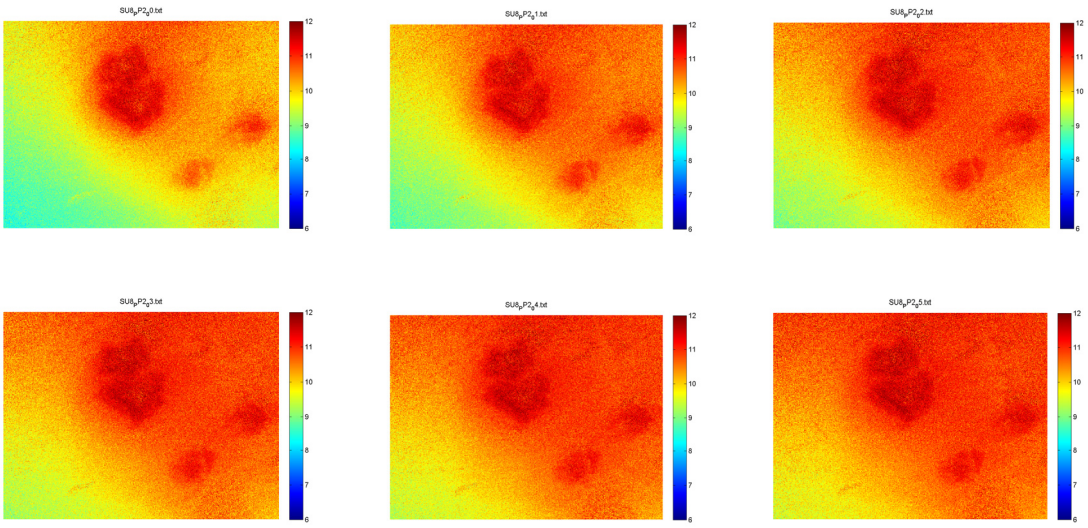

figure 4.32: lifetime images monitoring pO2 after flushing the microfluidic channel with air-saturated media; 1 image/20 s; first 6 images
T_{EX} = 20µs; dI = 3µs; d1 = 1µs; d2 = -1µs; averaging 16 images

Apart from the above already mentioned inhomogenities of the intensity figure 4.31 shows dark traces that are oriented along the direction of flow (horizontal). These traces are caused by loosened pichia pastoris colonies that were moved along the direction of flow and carried away some magnetic nanoparticles when the channel was flushed with fresh media. However, these traces don't influence the calculated lifetime images.

A constant increase of the lifetime (and the associated decrease of pO_2) can be observed in figure 4.32.

To demonstrate the development of pO_2 quantitatively an image section in the left, lower corner of the image was chosen (x = 15 – 220; y = 285 – 465) and the mean values were calculated using Matlab.

(A)

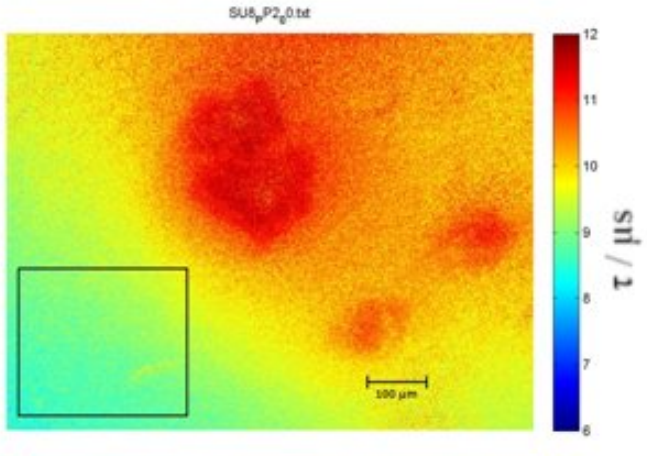

(B)

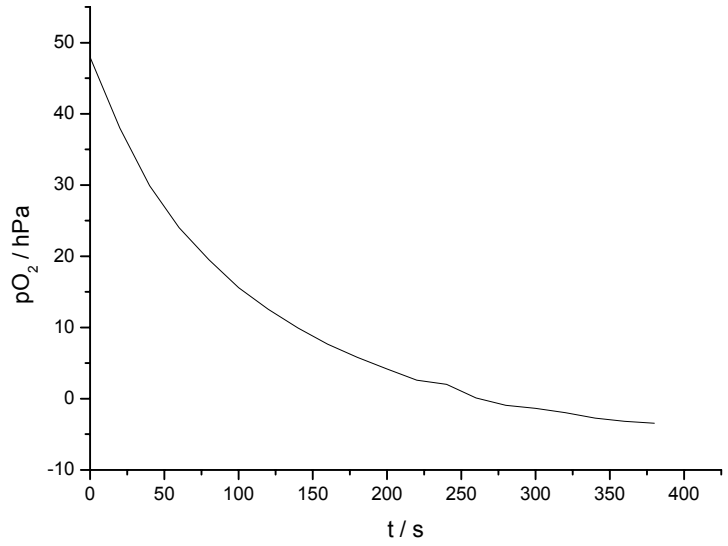

figure 4.33: (A) Region of interest (black rectangle) and (B) pO2 vs. t after flushing the microfluidic channel with air-saturated media; Pichia pastoris, mNSP, SU8

At the beginning of the measurement a sharp decrease of pO_2 was observed. Due to lower oxygen levels the graph later flattens because of a decrease of the concentration gradient.

At the end of the measurement pO_2 takes slightly negative values. Again it must be mentioned that calibration data were obtained under other conditions so that supposably the calibration data do not fit to the measurements carried out in the microfluidic chips.

Microfluidic chip made from PDMS:

In contrast to the measurements in the microfluidic chip made from SU8 20 µl magnetic particle suspension were inserted into the chip and collected by a magnet from outside before the chip was inoculated with E. coli to reduce the uptake of the nano particles by the microorganisms.

The figures figure 4.34 and figure 4.35 show original and lifetime images of these measurements.

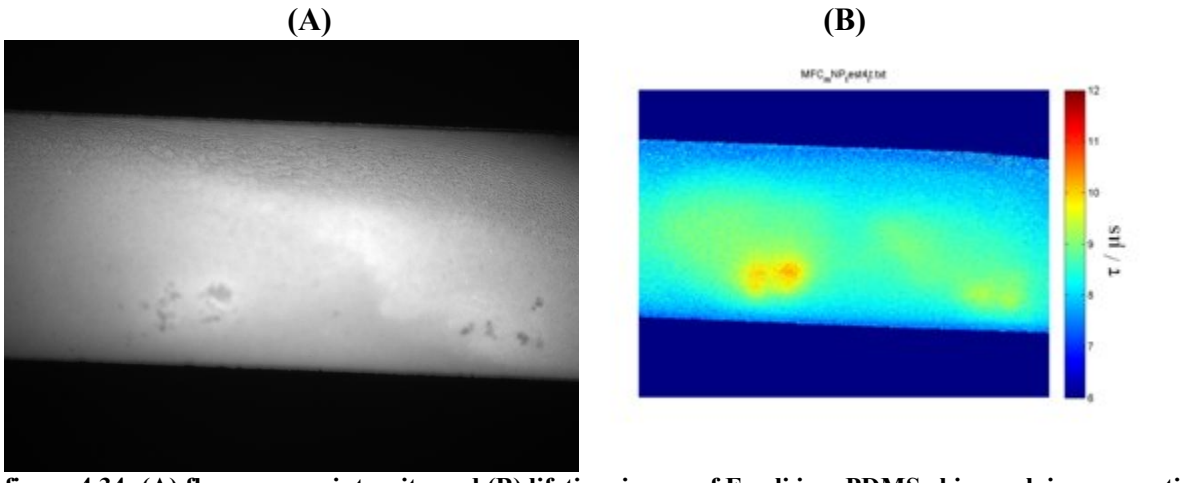

figure 4.34: (A) fluorescence intensity and (B) lifetime image of E.coli in a PDMS chip applying magnetic nanosensor particles
T_{EX} = 20µs; dI = 3µs; d1 = 1µs; d2 = -1µs; averaging 16 images

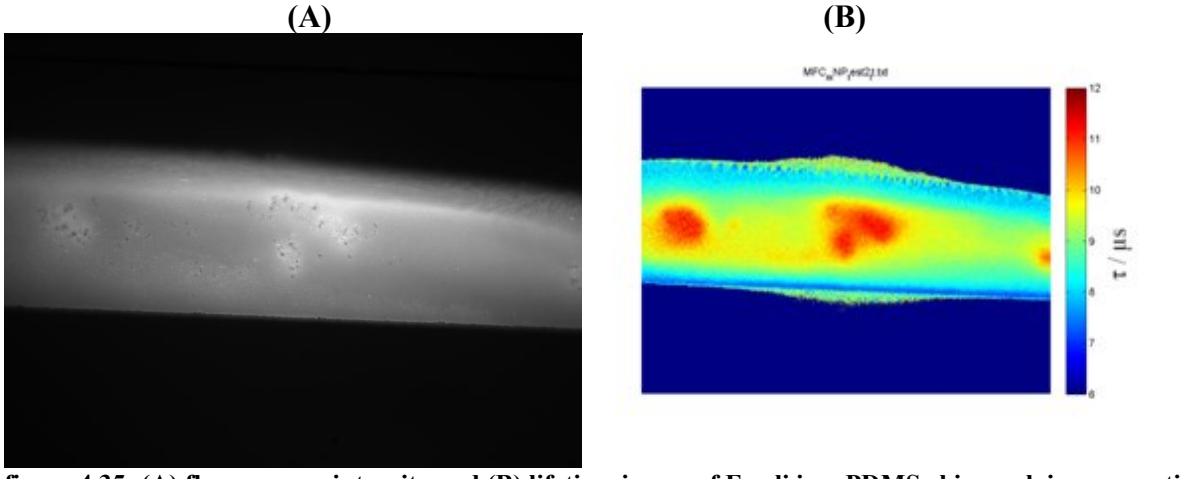

figure 4.35: (A) fluorescence intensity and (B) lifetime image of E.coli in a PDMS chip applying magnetic nanosensor particles; different spot
T_{EX} = 20µs; dI = 3µs; d1 = 1µs; d2 = -1µs; averaging 16 images

The insertion of the particle suspension into the microfluidic device before inoculation with E.coli results in a more homogeneous distribution of intensity. Highest values of intensity in the original images were not located at the E. coli colonies. High values of the lifetime (low pO_2 levels were observed at spots, where E. coli were located.
For that reason it can be assumed that nanoparticles are not taken up by the microorganisms.
Again lifetime can be calculated outside the microfluidic channel.

4.3.4 Conclusion

Integration of magnetic nanosensor particles into microfluidic devices seems to be a promising method for monitoring the oxygen level in these devices. Low oxygen-levels can be observed exactly at the spots, where active microorganisms are located. Monitoring oxygen over time seems to be possible as well.
However, there is the need to further optimise the employment of magnetic particles. Caused by the very narrow channels in microfluidic devices flow rates and shear forces often are relatively high. Low adhesion of the particles by the magnet from the outside can cause that the magnetic particles are flushed away during the measurement.
Further investigations must be made about the uptake of nanosensor particles by microorganisms. When sensor particles are integrated into bacterial networks, one of the most important advantages of applying magnetic nanosensor particles gets lost: the possibility to move the particles from the outside of the microfluidic device by a magnet.
It is also important to probe whether conduction of light in SU8 or PDMS plays an important role. Conduction may lead to wrong interpretation of the obtained images.
Unfortunately calibration data did not seem to be adaptable for measurements made in the microfluidic systems. At least a way must be found to determine τ_0 directly in the observed system.

The integration of magnetic nano sensor particles into microfluidic devices seems to be a promising method for monitoring oxygen levels. They are easy to handle and especially combined with ultra bright luminescence dyes high emission intensities can be obtained at low material usage. Developing of oxygen levels can be observed and images can be acquired where local differences of oxygen can be seen.

4.4 Optical pH-sensing films

4.4.1 Introduction

In life sciences it is of high importance to have information about the pH value. For instance the pH influences cell activity and stability in a bioreactor. Moreover the knowledge of pH in addition to the knowledge of other important metabolites can help understanding the complex processes in heterogeneous living communities [42].

Different principles of optical pH-sensing exist; for instance pH-dependency of absorption spectra and dependency of the luminescent lifetime [10]. Also in microfluidic systems the basic principle of optical sensing of pH is the change of the fluorescent response of a pH-sensitive dye [43].

Typical pH-sensitive dyes are for example fluorescein and HPTS (1-hydroxypyrene-3,6,8-trisulfonate). These substances are wavelength-ratiometric pH-indicators which show different absorption spectra in their acidic and basic form.

For the investigations on optical pH-sensing films a new synthesized pH-indicator (7-hydroxy-4-cyanocoumarin S) was selected with a pK_a around 7. The protonated (in acidic surrounding) form of the indicator is excited and emits at lower wavelengths than the deprotonated form (in basic surrounding). The ratio of these two forms changes depending on the pH of the surrounding, hence the ratio of the emission intensity of the deprotonated and protonated form can serve as a measurement of pH.

In order to enhance signal intensity of the basic form, the concept of light harvesting was employed using Macrolex Yellow as the antenna dye.

The pK_a around 7 makes the indicator well suited for biological applications since it exhibits high sensitivity at physiological conditions (pH 7.4) [55].

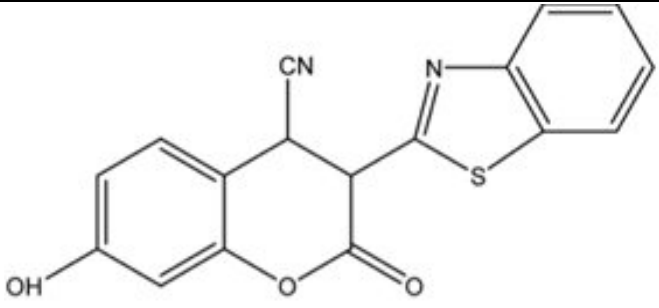

figure 4.36: molecular structure of 7-hydroxy-4-cyanocoumarin S

(A)

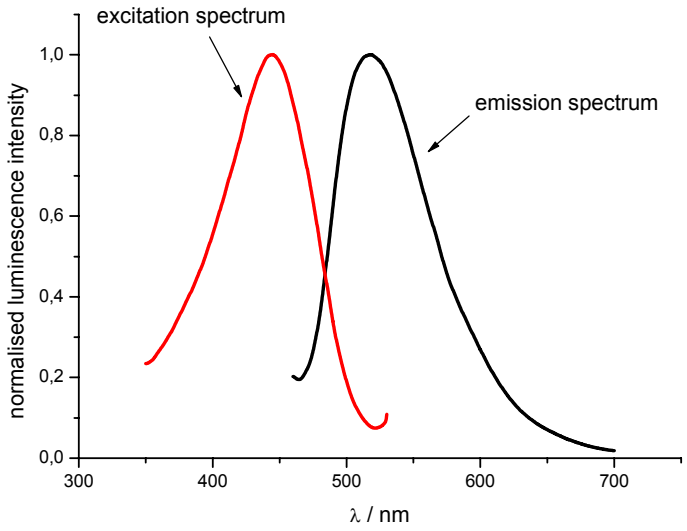

(B)

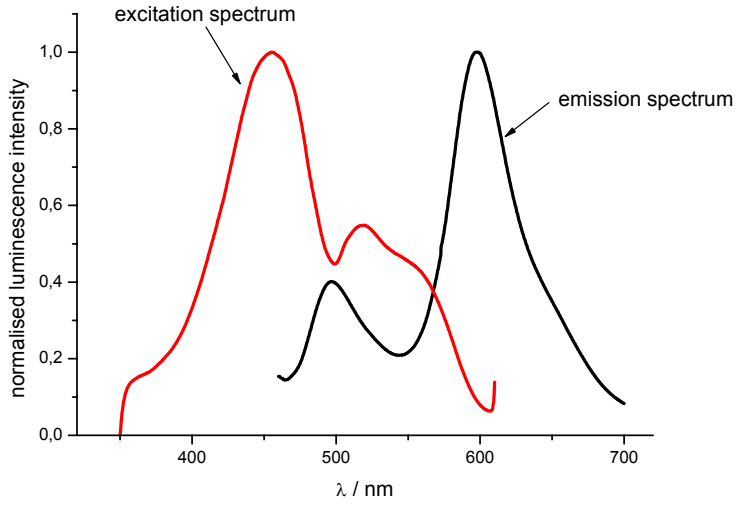

figure 4.37: normalised excitation and emission spectra of 7-hydroxy-4-cyanocoumarin S (HCS) with Macrolex Yellow in a D4 hydrogel in (A) strong acid and (B) base (pH = 8.00)

4.4.2 Experimental procedure

4.4.2.1 Preparation of sensor films

The respective amounts of the dyes Macrolex Yellow (MY) and 7-hydroxy-4-cyanocoumarin S (HCS) and of D4-hydrogel were weighed in, filled to overall 3 g of EtOH/H_2O (9:1) and dissolved carefully under sonication at maximum strength (100) for about 15 minutes. These stock-solutions then were diluted to the finally wanted concentration of D4.
Mylar-foils and microscope slides were cleaned carefully with acetone and lint-free tissues.
200 ml of the mixtures then were coated on these carriers with a very precise doctor knife (15 µm).
The solvent was allowed to evaporate in a 60˚C oven for approximately 1 hour. The films were then either used or stored in a dark, dust-free place overnight.

4.4.2.2 Calibration curve measurements

Prior to all calibration curve measurements, the sensor foil was soaked in a buffer of pH 7.55 for 45-60 minutes in the dark (to condition the sensor layer). The sensor foil was then immediately soaked in a buffer of pH 2.40 for 5 minutes.
The sensor foil was placed into a "flow-through" apparatus, which was then positioned on the fluorescence microscope.

The first measurement was obtained using the buffer of the lowest pH. Using a 10mL syringe, 8mL of buffer were sucked up into the syringe and the syringe was inserted into the tubing of the apparatus. The syringe first delivered 5mL of buffer to the apparatus, and the sensor foil was then given two minutes to equilibrate. After these two minutes the remaining 3mL of buffer was delivered to the apparatus. A measurement was then taken with the fluorescence spec 15 seconds after this last injection.

After a measurement was obtained, the syringe was emptied and 10mL of air was blown through the apparatus to clear the system of the previous buffer. The method outlined in the above paragraph is then repeated using the subsequent buffers.

4.4.2.3 Phosphate buffer preparation

Phosphate buffers ranging from pH 3 to 9 were prepared using salt solutions of Citric acid, Na_2HPO_4 and NaH_2PO_4. Ionic strength was adjusted with NaCl and pH was measured using a pH glass electrode.

4.4.3 Results and Discussion

4.4.3.1 Adaption of optical system

Due to the pH dependent spectral shift of 7-hydroxy-4-cyanocoumarin S (HCS) the dye system lends itself to pH-imaging using the color camera. Thus investigations on the applicability of the color camera must be made.

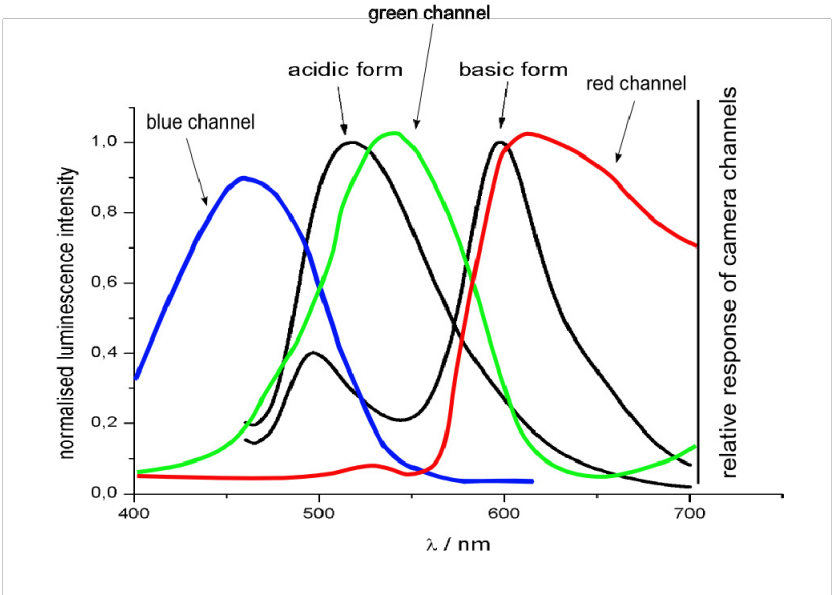

figure 4.38: comparison of the color channels of the camera with emission spectra of 7-hydroxy-4-cyanocoumarin S (HCS) with Macrolex Yellow in a D4 hydrogel; relative response of blue, green and red channel are displayed in the respective color

The color camera turned out to be perfectly convenient for the applied dye system. The green channel covers the range of wavelengths where Macrolex Yellow emits and detects high signals in acidic surrounding, while luminescence emission of the basic form can be detected by the red channel. However, it must be mentioned that there is some cross-sensitivity. Green and red channel are not totally separated.

4.4.3.2 pH dependency of emission spectra

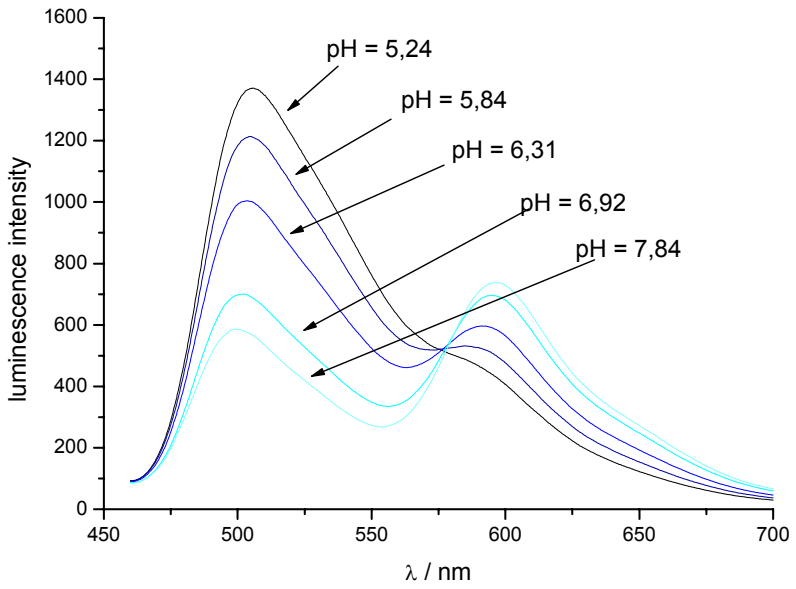

figure 4.39: change of emission spectra with changing pH; λ_{EX} = 450 nm; 0.5% HCS, 0.50%MY, 2.5%D4 hydrogel

Figure figure 4.39 illustrates how emission spectra change with changing pH. As pH increases the HCS emission peak also increases while MY emission decreases.

4.4.3.3 Calibration using the color camera

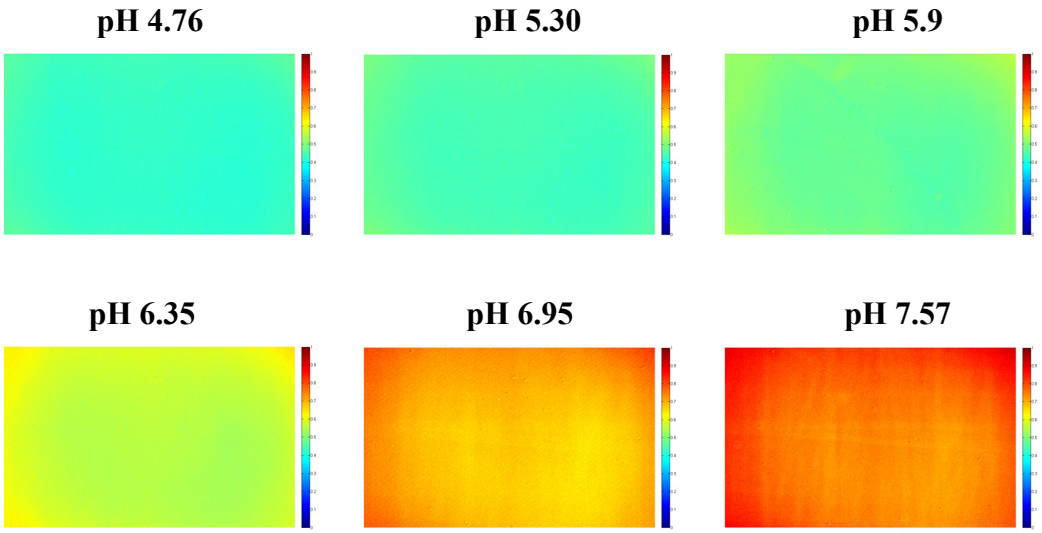

figure 4.40: images of intensity ratio (red to green channel) of pH-sensitive film;

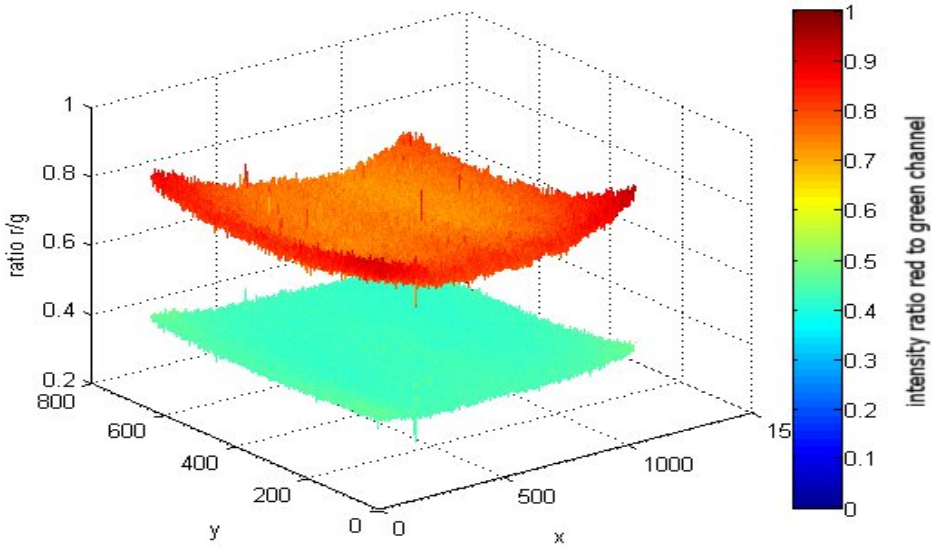

figure 4.41: surface plot of intensity ratio (red to green channel) of pH sensitive film

Different pH values are clearly distinguishable by their intensity ratio. Unfortunately scratches of the films can be seen in the intensity image. Figurefigure 4.42 shows that edges of the images show a higher intensity ratio than the middle of the image. Possibly this can be traced back to an inhomogeneous camera sensitivity over the CCD-chip surface. To inhibit effects of camera sensitivity investigations should be made how to correct images for the camera sensitivity.

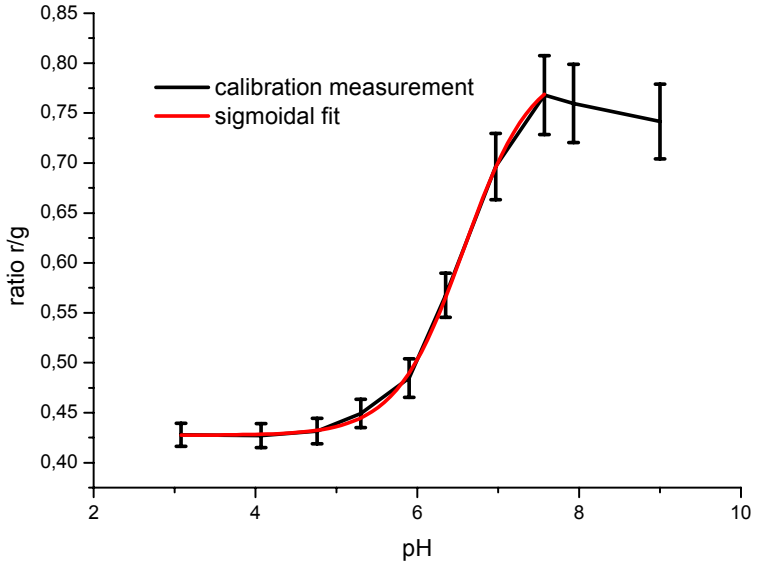

figure 4.42: calibration curve of pH sensitive foil; pK_a (= 6.58) was obtained applying a sigmoidal fit

A sigmoidal fit determined the pK_a to be 6.58 ± 0.22. The sensor foil shows the highest sensitivity at physiological conditions.

Above pH 7.5 the curve shows a decrease of the intensity ratio of red to green channel. This can be traced back to the general low stability of the dye in basic media. During investigations using the color camera we found out that HCS strongly bleaches, especially when sensing films are irradiated under basic conditions. When a film containing the basic form of the dye was illuminated for longer time using the HBO lamp (e.g. during focussing) a sharp decrease of luminescence intensity could be observed. Thus focussing was accomplished in the acid form of the dye. For calibration other film spots were selected and illumination time was reduced as much as possible.

4.4.4 Conclusion

Generally the investigated dye system is nearly ideal for pH-imaging using the color camera due to the great overlap of emission spectra and sensitivity of the color channels. Moreover intensity ratio images showed high homogeneity and a convenient pK_a for biological investigations. However, it is important to further investigate the possibility to correct the obtained images.

Though spectral feature of the investigated dye system are promising, we had to notice that HCS is strongly affected by bleaching effects, especially when exposed to pH values above 7.5.

5 Conclusion and Future Outlook

5.1 FLIM

Application of FLIM using RLD seems to be an appropriate referencing method to monitor oxygen-consumption of cells. Inhomogeneities of dye distribution can easily be referenced out and the lifetime is barely affected by photobleaching.

However, there is one important limiting factor. Due to short measuring time frames difficulties concerning the emission intensity can occur. For that reason TiO_2 (to enhance the optical pathway) must be added to sensor films, PSPVP-nanosensor particles have to be applied in high concentration or ultrabright dyes have to be used.

Despite the application of signal enhancing methods (use of the light harvesting principle and use of ultrabright dye $Ir(Cs)_2(acac)$) the lack of sufficiently high signal intensities sometimes leads to relatively high signal-to-noise ratios.

Moreover we must keep in mind that a possible commercial success of microfluidic systems can mainly be traced back to the simplicity and low costs of these systems. The measurement set-up for FLIM measurements, however, is rather complicated as it consists of highly sensitive and gateable cameras and additional instruments like a triggerbox.

Prospective ambitions comprise further investigations concerning the correctness of the obtained lifetime images and investigations on the possibility of parallelized measurements.

5.2 FRIM applying a monochrome camera

Unfortunately preliminary tests of FRIM applying a monochrome camera failed because images obtained with red and green emission filters were slightly shifted. The movement of the images can be traced back to a dissimilar assembly of the filter cubes and a resulting dissimilar orientation of the dichroic mirror.

On account of the mentioned shift the inhomogeneities of the original images can not be referenced out and invalid resulting ratio images are obtained.

However, preliminary tests also show that an important advantage of this method is the high flexibility of the integrated sensor materials because less attention must be paid on the lack of signal intensity. For instance senor films can be prepared without the addition of TiO_2 and nanosensor particles could be applied in lower concentration.

Perhaps difficulties with the shift of the original images could be solved when appropriate corrections are invented. Hence further investigations should concentrate on convenient correction methods.

5.3 FRIM applying a color camera

In contrast to FRIM applying a monochrome camera the application of a color camera was easier to handle. On the one hand images can be obtained taking only one picture hence additional personal effort is reduced. On the other hand sliding of the filter cubes can be omitted. This leads to the abolition of one error source.

As the application of color cameras represent a versatile and simple method to obtain 2D information on the oxygen distribution in a microfluidic system it is important to further investigate the applicability of color cameras for imaging purposes. However, further investigations concerning the correctness of the obtained lifetime images and investigations on the possibility of parallelization have to be made.

5.4 Integration of different sensor materials

Three different designs of optical sensors (films, PSPVP nano particles and magnetic nano particles) based on collisional quenching principle for monitoring dissolved oxygen and pH were applied in microfluidic systems. All of them showed to have their particular advantages but also exhibited their own drawbacks.

Sensor films showed high homogeneities of the obtained ratio and lifetime images. Compared to the other designs they exhibit reduced dye consumption and no interactions with microorganisms or media.

However, integration of films causes one additional fabrication step and adhesion on the substrate depends on the used material. Moreover frequently applied fabrication techniques like photolithography may lead to a strong reduction or even a loss of emission intensity. Generally the application of sensor films makes high demands on the photostability of the applied dye system.

The application of nano particles poses an easy-to-handle possibility to integrate sensors into microfluidic devices because they can be integrated into the completed device. That way they exhibit a high flexibility. For instance a variety of nano particles could be prepared detecting different analytes that permit the detection of these analytes consecutively.

However, the investigated PSPVP-nanosensor particles had to be applied in high concentrations due to low emission intensities that especially effected FLIM. Moreover leaching of the dye to the PDMS of the chip could be observed. Hence, further improvements must be made concerning the dye transfer from the particle to the PDMS.
In contrast to intensity and leaching problems concerning the application of stained nanobeads the application of magnetic nanosensor particles combines the advantages of solid sensor spots with high intensities and relatively low consumption of dyes and the general flexibility of nanosensor particles. Collecting the particles with a magnet from the outside entails that very low concentrations of the particles can be applied.
However, further investigations must be made about the uptake of nanosensor particles by microorganisms. When sensor particles are integrated into bacterial networks, one of the most important advantages of applying magnetic nanosensor particles gets lost: the possibility to move the particles from the outside of the microfluidic device by a magnet.

All of the presented sensor materials allow 2D monitoring of the very important metabolic parameters oxygen and pH in microfluidic devices. Even if each of the sensor materials exhibits particular drawbacks they represent promising methods for integration in microfluidic systems.

6 Appendix

6.1 References

[1] D. Li, *Encyclopedia of Microfluidics and Nanofluidics*, 2008.

[2] S. Terry, J. Jerman, and J. Angell, "A gas chromatographic air analyzer fabricated on a silicon wafer," *Electron Devices, IEEE Transactions on*, vol. 26, 1979, pp. 1880-1886.

[3] A. Manz, N. Graber, and H. Widmer, "Miniaturized total chemical analysis systems: A novel concept for chemical sensing," *Sensors and Actuators B: Chemical*, vol. 1, Jan. 1990, pp. 244-248.

[4] G.M. Whitesides, "The origins and the future of microfluidics," *Nature*, vol. 442, Jul. 2006, pp. 368-373.

[5] H. Becker and C. Gärtner, "Polymer microfabrication methods for microfluidic analytical applications," *Electrophoresis*, vol. 21, 2000, pp. 12-26.

[6] B. Kuswandi, Nuriman, J. Huskens, and W. Verboom, "Optical sensing systems for microfluidic devices: A review," *Analytica Chimica Acta*, vol. 601, Oct. 2007, pp. 141-155.

[7] R. Yotter, L. Lee, and D. Wilson, "Sensor technologies for monitoring metabolic activity in single cells-part I: optical methods," *Sensors Journal, IEEE*, vol. 4, 2004, pp. 395-411.

[8] M. Brischwein, E.R. Motrescu, E. Cabala, A.M. Otto, H. Grothe, and B. Wolf, "Functional cellular assays with multiparametric silicon sensor chips," *Lab on a Chip*, vol. 3, 2003, pp. 234-240.

[9] D. Sud, G. Mehta, K. Mehta, J. Linderman, S. Takayama, and M. Mycek, "Optical imaging in microfluidic bioreactors enables oxygen monitoring for continuous cell culture," *Journal of Biomedical Optics*, vol. 11, 2006, p. 050504.

[10] J.R. Lakowicz, *Principles of Fluorescence Spectroscopy*, Springer, Berlin, 2006.

[11] B. Valeur, *Molecular Fluorescence: Principles and Applications*, Wiley-VCH, 2001.

[12] G. Liebsch, "Time-resolved Luminescence Lifetime Imaging with Optical Chemical Sensors," Universität Regensburg, 2000.

[13] T. Mayr, S.M. Borisov, T. Abel, B. Enko, K. Waich, G. Mistlberger, and I. Klimant, "Light Harvesting as a Simple and Versatile Way to Enhance Brightness of Luminescent Sensors," *Analytical Chemistry*, vol. 81, 2009, pp. 6541-6545.

[14] M.J.E. Golay, "Vapor Phase Chromatography and Telegrapher's Equation," *Analytical Chemistry*, vol. 29, Jun. 1957, pp. 928-932.

[15] J.J. van Deemter, "Longitudinal diffusion and resistance to mass transfer as causes of nonideality in chromatography : J. J. van Deemter, F. J. Zuiderweg and A. Klinkenberg, Chem. Engng Sci. 5 271-289, 1956," *Chemical Engineering Science*, vol. 50, Dec. 1995, p. 3867.

[16] A. Manz, N. Graber, and H. Widmer, "Miniaturized total chemical analysis systems: A novel concept for chemical sensing," *Sensors and Actuators B: Chemical*, vol. 1, 1990, pp. 244-248.

[17] *Microfluidics for Biological Applications*, 2009.

[18] A. Manz, J. Fettinger, E. Verpoorte, H. Lüdi, H. Widmer, and D. Harrison, "Micromachining of monocrystalline silicon and glass for chemical analysis systems A look into next century's technology or just a fashionable craze?," *TrAC Trends in Analytical Chemistry*, vol. 10, May. 1991, pp. 144-149.

[19] D.J. Harrison, K. Fluri, K. Seiler, Z. Fan, C.S. Effenhauser, and A. Manz, "Micromachining a Miniaturized Capillary Electrophoresis-Based Chemical Analysis System on a Chip," *Science*, vol. 261, Aug. 1993, pp. 895-897.
[20] S.C. Jacobson, R. Hergenroder, A.W.J. Moore, and J.M. Ramsey, "Precolumn Reactions with Electrophoretic Analysis Integrated on a Microchip," *Analytical Chemistry*, vol. 66, Dec. 1994, pp. 4127-4132.
[21] Heckele M. and Schomburg W.K., "Review on micro molding of thermoplastic polymers," *Journal of Micromechanics and Microengineering*, vol. 14, Mar. 2004, pp. R1-R14.
[22] V. Piotter, T. Hanemann, R. Ruprecht, and J. Haußelt, "Injection molding and related techniques for fabrication of microstructures," *Microsystem Technologies*, vol. 3, May. 1997, pp. 129-133.
[23] R. Pethig, J.P.H. Burt, A. Parton, N. Rizvi, M.S. Talary, and J.A. Tame, "Development of biofactory-on-a-chip technology using excimer laser micromachining," *Journal of Micromechanics and Microengineering*, vol. 8, 1998, pp. 57-63.
[24] M.A. Roberts, J.S. Rossier, P. Bercier, and H. Girault, "UV Laser Machined Polymer Substrates for the Development of Microdiagnostic Systems," *Analytical Chemistry*, vol. 69, Jun. 1997, pp. 2035-2042.
[25] J.N. Lee, C. Park, and G.M. Whitesides, "Solvent Compatibility of Poly(dimethylsiloxane)-Based Microfluidic Devices," *Analytical Chemistry*, vol. 75, Dec. 2003, pp. 6544-6554.
[26] G.T. Roman, T. Hlaus, K.J. Bass, T.G. Seelhammer, and C.T. Culbertson, "Sol−Gel Modified Poly(dimethylsiloxane) Microfluidic Devices with High Electroosmotic Mobilities and Hydrophilic Channel Wall Characteristics," *Analytical Chemistry*, vol. 77, Mar. 2005, pp. 1414-1422.
[27] J. El-Ali, P.K. Sorger, and K.F. Jensen, "Cells on chips," *Nature*, vol. 442, Jul. 2006, pp. 403-411.
[28] J. Gottschamel, L. Richter, A. Mak, C. Jungreuthmayer, G. Birnbaumer, M. Milnera, H. Brücкl, and P. Ertl, "Development of a Disposable Microfluidic Biochip for Multiparameter Cell Population Measurements," *Analytical Chemistry*, vol. 81, Oct. 2009, pp. 8503-8512.
[29] P. Auroux, D. Iossifidis, D.R. Reyes, and A. Manz, "Micro Total Analysis Systems. 2. Analytical Standard Operations and Applications," *Analytical Chemistry*, vol. 74, Jun. 2002, pp. 2637-2652.
[30] D. Janasek, J. Franzke, and A. Manz, "Scaling and the design of miniaturized chemical-analysis systems," *Nature*, vol. 442, Jul. 2006, pp. 374-380.
[31] R. Jindal and S.M. Cramer, "On-chip electrochromatography using sol-gel immobilized stationary phase with UV absorbance detection," *Journal of Chromatography A*, vol. 1044, Jul. 2004, pp. 277-285.
[32] J. Park, K. Park, K. Shin, H. Park, M. Kim, J. Kim, S. Park, and Y. Song, "Design, fabrication and characterization of an integrated micro ammonia analysis system (IMAAS) with microreactor and in-plane type optical detector based on the Berthelot reaction," *Sensors and Actuators B: Chemical*, vol. 117, Oct. 2006, pp. 516-522.
[33] J. Gao, X. Yin, and Z. Fang, "Integration of single cell injection, cell lysis, separation and detection of intracellular constituents on a microfluidic chip," *Lab on a Chip*, vol. 4, 2004, pp. 47-52.
[34] L. Basabe-Desmonts, J. Beld, R.S. Zimmerman, J. Hernando, P. Mela, M.F. Garcia Parajo, N.F. van Hulst, A. van den Berg, D.N. Reinhoudt, and M. Crego-Calama, "A Simple Approach to Sensor Discovery and Fabrication on Self-Assembled Monolayers on Glass," *Journal of the American Chemical Society*, vol. 126, Jun. 2004, pp. 7293-7299.

[35] P. Mela, S. Onclin, M.H. Goedbloed, S. Levi, M.F. Garcia-Parajo, N.F.V. Hulst, B.J. Ravoo, D.N. Reinhoudt, and A.V.D. Berg, "Monolayer-functionalized microfluidics devices for optical sensing of acidity," *Lab on a Chip*, vol. 5, 2005, pp. 163-170.
[36] P. Caglar, S. Tuncel, N. Malcik, J. Landers, and J. Ferrance, "A microchip sensor for calcium determination," *Analytical and Bioanalytical Chemistry*, vol. 386, Nov. 2006, pp. 1303-1312.
[37] A. Ymeti, J.S. Kanger, J. Greve, G.A.J. Besselink, P.V. Lambeck, R. Wijn, and R.G. Heideman, "Integration of microfluidics with a four-channel integrated optical Young interferometer immunosensor," *Biosensors and Bioelectronics*, vol. 20, Jan. 2005, pp. 1417-1421.
[38] A. Sin, K.C. Chin, M.F. Jamil, Y. Kostov, G. Rao, and M.L. Shuler, "The Design and Fabrication of Three-Chamber Microscale Cell Culture Analog Devices with Integrated Dissolved Oxygen Sensors," *Biotechnology Progress*, vol. 20, 2004, pp. 338-345.
[39] Y. Kostov, P. Harms, L. Randers-Eichhorn, and G. Rao, "Low-cost microbioreactor for high-throughput bioprocessing," *Biotechnology and Bioengineering*, vol. 72, 2001, pp. 346-352.
[40] V. Nock, R.J. Blaikie, and T. David, "Patterning, integration and characterisation of polymer optical oxygen sensors for microfluidic devices," *Lab on a Chip*, vol. 8, 2008, pp. 1300-1307.
[41] Q.L. Chen, H.P. Ho, L. Jin, B.W. Chu, M.J. Li, and V.W. Yam, "Dissolved oxygen sensing using organometallic dyes deposited within a microfluidic environment," *Microfluidics, BioMEMS, and Medical Microsystems VI*, San Jose, CA, USA: SPIE, 2008, pp. 68860O-8.
[42] G. Liebsch, I. Klimant, B. Frank, G. Holst, and O.S. Wolfbeis, "Luminescence Lifetime Imaging of Oxygen, pH, and Carbon Dioxide Distribution Using Optical Sensors," *Applied Spectroscopy*, vol. 54, Apr. 2000, pp. 548-559.
[43] P. Mela, S. Onclin, M.H. Goedbloed, S. Levi, M.F. Garcia-Parajo, N.F.V. Hulst, B.J. Ravoo, D.N. Reinhoudt, and A.V.D. Berg, "Monolayer-functionalized microfluidics devices for optical sensing of acidity," *Lab on a Chip*, vol. 5, 2005, pp. 163-170.
[44] G. Holst, O. Kohls, I. Klimant, B. König, M. Kühl, and T. Richter, "A modular luminescence lifetime imaging system for mapping oxygen distribution in biological samples," *Sensors and Actuators B: Chemical*, vol. 51, Aug. 1998, pp. 163-170.
[45] C. Moser, "Multiplexed Bioanalysis: Sedimentation Arrays Based on Luminescently Encoded Magnetic Microspheres," Graz University of Technology, 2006.
[46] T.L. Andrew and T.M. Swager, "Reduced Photobleaching of Conjugated Polymer Films through Small Molecule Additives," *Macromolecules*, vol. 41, Nov. 2008, pp. 8306-8308.
[47] I. Klimant, F. Ruckruh, G. Liebsch, A. Stangelmayer, and O.S. Wolfbeis, "Fast Response Oxygen Micro-Optodes Based on Novel Soluble Ormosil Glasses," *Microchimica Acta*, vol. 131, Jun. 1999, pp. 35-46.
[48] E.R. Carraway, J.N. Demas, and B.A. DeGraff, "Luminescence quenching mechanism for microheterogeneous systems," *Analytical Chemistry*, vol. 63, Feb. 1991, pp. 332-336.
[49] E. Leclerc, Y. Sakai, and T. Fujii, "Cell Culture in 3-Dimensional Microfluidic Structure of PDMS (polydimethylsiloxane)," *Biomedical Microdevices*, vol. 5, Jun. 2003, pp. 109-114.
[50] G.T. Roman, T. Hlaus, K.J. Bass, T.G. Seelhammer, and C.T. Culbertson, "Sol−Gel Modified Poly(dimethylsiloxane) Microfluidic Devices with High Electroosmotic Mobilities and Hydrophilic Channel Wall Characteristics," *Analytical Chemistry*, vol. 77, 2005, pp. 1414-1422.
[51] Y. Cao, Y.L. Koo, and R. Kopelman, "Poly(decyl methacrylate)-based fluorescent

PEBBLE swarm nanosensors for measuring dissolved oxygen in biosamples," *The Analyst*, vol. 129, 2004, pp. 745-750.
[52] S. Borisov and I. Klimant, "Luminescent nanobeads for optical sensing and imaging of dissolved oxygen," *Microchimica Acta*, vol. 164, Jan. 2009, pp. 7-15.
[53] S.M. Borisov and I. Klimant, "Ultrabright Oxygen Optodes Based on Cyclometalated Iridium(III) Coumarin Complexes," *Analytical Chemistry*, vol. 79, Oct. 2007, pp. 7501-7509.
[54] G. Mistlberger, S.M. Borisov, and I. Klimant, "Enhancing performance in optical sensing with magnetic nanoparticles," *Sensors and Actuators B: Chemical*, vol. 139, May. 2009, pp. 174-180.
[55] J. Shao, X. Yu, X. Xu, H. Lin, Z. Cai, and H. Lin, "Colorimetric and fluorescent sensing of biologically important fluoride in physiological pH condition based on a positive homotropic allosteric system," *Talanta*, vol. 79, Jul. 2009, pp. 547-551.

6.2 List of figures

FIGURE 1.1: GENERAL OVERVIEW 6
FIGURE 2.1: JABLONSKI DIAGRAM WITH POSSIBLE TRANSITIONS 7
FIGURE 2.2: DEFINITION OF RATE CONSTANTS 9
FIGURE 2.3: DECAY OF LUMINESCENCE INTENSITY 10
FIGURE 2.4: POSSIBLE DE-ECXITATION PATHWAYS OF EXCITED MOLECULES 11
FIGURE 2.5: ASSEMBLY OF AN EPIFLUORESCENT MICROSCOPE 14
FIGURE 2.6: TIME-DOMAIN AND FREQUENCY-DOMAIN APPROACH 16
FIGURE 2.7: SCHEME OF RAPID LIFETIME DETERMINATION 16
FIGURE 2.8: PRINCIPLE OF LIGHT HARVESTING: 17
FIGURE 3.1: OPTICAL FILTERS USED FOR MEASURMENTS ON THE FLUORESCENCE MICROSCOPE 27
FIGURE 3.2: MICROFLUIDIC DEVICES (DIFFERENT DESIGNS) WITH INTEGRATED OXYGEN SENSING FILM 28
FIGURE 3.3: FLOW-THROUGH-CELL USED FOR EXPERIMENTS WITH NANO SENSOR PARTICLES 29
FIGURE 3.4: (A) MONOCHROME CCD CAMERA (SENSIMOD), (B) COLOR CCD CAMERA (AVT MARLIN F-201C) AND (C) SPECTRAL SENSITIVITY OF MARLIN F-201C WITHOUT CUT FILTER AND OPTICS 30
FIGURE 3.5: SREENSHOT LOOK@MOLLI V.1.83 31
FIGURE 4.1: EXCITATION AND EMISSION SPECTRA OF OXYGEN-SENSITIVE FILM (4% MY, 1% PTTFPP AND 30% TIO_2 IN PS COATED FROM 2% PS IN $CHCL_3$) IN AIR-SATURATED (DASHED LINE) AND DEOXYGENATED (SOLID LINE) SOLUTION; Λ_{EM} = 650 NM; Λ_{EX} = 450 NM. RATIO OF DEOXYGENATED TO OXYGENATED INTENSITY AT 655 NM = 3,10 35
FIGURE 4.2: EXCITATION AND EMISSION SPECTRA OF OXYGEN-SENSITIVE FILM (4% MY, 1% PTTFPP AND 30% TIO2 IN PS COATED FROM 2% PS IN CHCL3) WITH ADEQUATE OPTICAL FILTERS (BLUE BP AND RG 610) AND DICHROIC MIRROR; Λ_{EM} = 650 NM; Λ_{EX} = 450 NM 36
FIGURE 4.3: COMPARISON OF THE COLOR CHANNELS OF THE CAMERA WITH AN EXCITATION SPECTRUM (F12); RELATIVE RESPONSE OF BLUE, GREEN AND RED CHANNEL ARE DISPLAYED IN THE RESPECTIVE COLOR 37
FIGURE 4.4: PHOTOBLEACHING AT VARIABLE FILM THICKNESS; 39
FIGURE 4.5: PHOTOBLEACHING AT VARIABLE MY CONCENTRATIONS; 40
FIGURE 4.6: PHOTOBLEACHING AT VARIABLE PTTFPP CONCENTRATIONS; 41
FIGURE 4.7: PHOTOBLEACHING AT VARIABLE TIO_2 CONCENTRATION 42
FIGURE 4.8: LIFETIME IMAGES OF (A) DEOXYGENATED (N2 100 ML/MIN) AND (B) AIR-SATURATED (SYNTHETIC AIR 100 ML/MIN) OXYGEN-SENSITIVE FILM FIXED IN A FLOW-THROUGH CELL 43
FIGURE 4.9: STERN-VOLMER PLOT OF THE CALIBRATION DATA OBTAINED USING THE SENSICAM; 44
FIGURE 4.10: ORIGINAL IMAGES AFTER BACKGROUND CORRECTION OF THE (A) RED AND THE (B) GREEN CHANNEL 45

FIGURE 4.11: RATIOMETRIC SURFACEPLOTS OF (A) DEOXYGENATED (N2 100 ML/MIN) AND (B) AIR-SATURATED (SYNTHETIC AIR 100 ML/MIN) OXYGEN-SENSITIVE FILM 46
FIGURE 4.12: STERN-VOLMER PLOT OF THE CALIBRATION DATA OBTAINED USING THE COLOR CAMERA 47
FIGURE 4.13: LIFETIME IMAGES OF A MICROFLUIDIC CHANNEL FLUSHED WITH (A) NITROGEN AND (B) SYNTHETIC AIR; (C) SURFACE PLOT OF (A) AND (B) 48
FIGURE 4.14: (A) TRANSMITTED LIGHT AND (B) LIFETIME IMAGE OF CANDIDA ALBICANS IN MICROFLUIDIC CHIP 49
FIGURE 4.15: LIFETIME IMAGES TAKEN 20 MIN, 1 H 5 MIN, 4 H 55 MIN AND 7 H 50 MIN AFTER INOCULATION WITH CANDIDA ALBICANS 50
FIGURE 4.16: PO_2 VS. TIME DURING CULTIVATION OF CANDIDA ALBICANS 51
FIGURE 4.17: EXCITATION AND EMISSION SPECTRA OF P2 (2% MY AND 2% PTTFPP) IN AIR-SATURATED (SOLID LINE) AND DEOXYGENATED (DASHED LINE) SOLUTION; 54
FIGURE 4.18: PRELIMINARY TEST APPLYING NANOSENSOR PARTICLES P3 (4% MY AND 2% PTTFPP) IN A MICROFLUIDIC CHIP; LIFETIME IMAGE 55
FIGURE 4.19: (A) ORIGINAL IMAGE AND (B) LIFETIME IMAGE OF NANOSENSOR PARTICLES DURING CULTIVATION OF PICHIA PASTORIS 56
FIGURE 4.20: (A) ORIGINAL IMAGE AND (B) LIFETIME IMAGE OF NANOSENSOR PARTICLES DURING CULTIVATION OF PICHIA PASTORIS 57
FIGURE 4.21: LUMINESCENCE INTENSITY IMAGES OF THE (A) GREEN AND (B) RED CHANNEL OF THE COLOR CAMERA AND (C) RATIO (GREEN TO RED CHANNEL) OF A MICROFLUIDIC CHANNEL FILLED WITH AIR-SATURATED (LEFT) AND DEOXYGENATED (RIGHT) PARTICLE SUSPENSIONS P3 (4% MY AND 2% PTTFPP) 58
FIGURE 4.22: (A) STRUCTURE OF IR(CS)2(ACAC) PROVIDED BY SERGEY BORISOV AND (B) CORRECTED AND NORMALISED EMISSION (Λ_{EX} = 475 NM)AND EXCITATION SPECTRA (Λ_{EM} = 565 NM) OF MAGNETIC NANOSENSOR PARTICLES; 61
FIGURE 4.23: CORRECTED AND NORMALISED EMISSION (Λ_{EX} = 475 NM)AND EXCITATION SPECTRA (Λ_{EM} = 565 NM) OF MAGNETIC NANOSENSOR PARTICLES WITH APPROPRIATE OPTICAL FILTERS (BP BLUE, OG 515 AND DICHROIC MIRROR; 63
FIGURE 4.24: EMISSION SPECTRA OF MAGNETIC NANOSENSOR PARTICLES IN AIR-SATURATED (DASHED LINE) AND DEOXYGENATED (SOLID LINE) SOLUTION; Λ_{EX} = 475 NM. RATIO OF DEOXYGENATED TO AIR-SATURATED INTENSITY AT 570 NM = 2.07 64
FIGURE 4.25: CALIBRATION CURVE OF OXYGEN-SENSITIVE NANO SENSOR PARTICLES AT VARIOUS CONCENTRATIONS OF DISSOLVED OXYGEN 65
FIGURE 4.26: ORIGINAL IMAGE OF THE PRELIMINARY TESTS IN THE FLOW-TROUGH-CELL CONTAINING MAGNETIC NANO SENSOR PARTICLES AND FLUSHED WITH DEIONISED H2O 66
FIGURE 4.27: LIFETIME IMAGES OF THE PRELIMINARY TESTS IN THE FLOW-TROUGH-CELL CONTAINING MAGNETIC NANO SENSOR PARTICLES (A) FLUSHED WITH DEIONISED H_2O AND (B) FLUSHED WITH 2 MM GLUCOSE SOLUTION 66
FIGURE 4.28: (A) REGION OF INTEREST (WHITE RECTANGLE) AND (B) PO2 VS. GLUCOSE CONCENTRATION IN THE FLOW-TROUGH-CELL CONTAINING MAGNETIC NANO SENSOR PARTICLES FLUSHED WITH SOLUTIONS CONTAINING DIFFERENT CONCENTRATIONS OF GLUCOSE 68
FIGURE 4.29: FLUORESCENCE INTENSITY IMAGE OF PICHIA PASTORIS IN A SU8 MICROFLUIDIC DEVICE WITH MAGNETIC NANOSENSOR PARTICLES 69
FIGURE 4.30: CALCULATED LIFETIME IMAGE OF PICHIA PASTORIS IN A SU8 MICROFLUIDIC DEVICE WITH MAGNETIC NANOSENSOR PARTICLES 70
FIGURE 4.31: FLUORESCENCE INTENSITY IMAGE OF PICHIA PASTORIS IN A SU8 MICROFLUIDIC CHIP INOCULATED WITH PICHIA PASTORIS FOLLOWING THE DECREASE OF PO2 71
FIGURE 4.32: LIFETIME IMAGES MONITORING PO2 AFTER FLUSHING THE MICROFLUIDIC CHANNEL WITH AIR-SATURATED MEDIA; 1 IMAGE/20 S; FIRST 6 IMAGES 71
FIGURE 4.33: (A) REGION OF INTEREST (BLACK RECTANGLE) AND (B) PO2 VS. T AFTER FLUSHING THE MICROFLUIDIC CHANNEL WITH AIR-SATURATED MEDIA; PICHIA PASTORIS, MNSP, SU8 72
FIGURE 4.34: (A) FLUORESCENCE INTENSITY AND (B) LIFETIME IMAGE OF E.COLI IN A PDMS CHIP APPLYING MAGNETIC NANOSENSOR PARTICLES 73
FIGURE 4.35: (A) FLUORESCENCE INTENSITY AND (B) LIFETIME IMAGE OF E.COLI IN A PDMS CHIP APPLYING MAGNETIC NANOSENSOR PARTICLES; DIFFERENT SPOT 73
FIGURE 4.36: MOLECULAR STRUCTURE OF 7-HYDROXY-4-CYANOCOUMARIN S 75

FIGURE 4.37: NORMALISED EXCITATION AND EMISSION SPECTRA OF 7-HYDROXY-4-CYANOCOUMARIN S (HCS) WITH MACROLEX YELLOW IN A D4 HYDROGEL IN (A) STRONG ACID AND (B) BASE (PH = 8.00) 76
FIGURE 4.38: COMPARISON OF THE COLOR CHANNELS OF THE CAMERA WITH EMISSION SPECTRA OF 7-HYDROXY-4-CYANOCOUMARIN S (HCS) WITH MACROLEX YELLOW IN A D4 HYDROGEL; RELATIVE RESPONSE OF BLUE, GREEN AND RED CHANNEL ARE DISPLAYED IN THE RESPECTIVE COLOR 79
FIGURE 4.39: CHANGE OF EMISSION SPECTRA WITH CHANGING PH; Λ_{EX} = 450 NM; 0.5% HCS, 0.50%MY, 2.5%D4 HYDROGEL 80
FIGURE 4.40: IMAGES OF INTENSITY RATIO (RED TO GREEN CHANNEL) OF PH-SENSITIVE FILM; 80
FIGURE 4.41: SURFACE PLOT OF INTENSITY RATIO (RED TO GREEN CHANNEL) OF PH SENSITIVE FILM 81
FIGURE 4.42: CALIBRATION CURVE OF PH SENSITIVE FOIL; PK_A (= 6.58) WAS OBTAINED APPLYING A SIGMOIDAL FIT 81

6.3 List of tables

TABLE 1: LIST OF USED CHEMICALS 26
TABLE 2: MEASURING SETUP FOR PHOTOBLEACHING 33
TABLE 3: COMPOSITION OF THE NANOSENSOR PARTICLES 54
TABLE 4: PROPERTIES OF MAGNETIC NANOSENSOR PARTICLES 62

6.4 Matlab-scripts

alltau.m

```
function erg=alltau();

% liest alle Bildsätze im Verzeichnis gibt das Lebenszeitbild aus
% Es werden nur 2-windows-Bilder von Molli verarbeitet


dirdata=dir('*.txt');
dirsize=size(dirdata);
warning off MATLAB:divideByZero

y=[];

if (size(dirdata)>0)
    for i=1:dirsize(1)
        imname=dirdata(i).name;
        fid=fopen(imname);
        disp(['--------',imname]);
        a=fscanf(fid,'%c');
        % Art der Messung ermitteln (nur 2 windows erlaubt)
        searchstr='measurement:';
        startpunkt= findstr(a,searchstr)+size(searchstr,2);
        teststr = a(startpunkt:startpunkt+6 );
```

```
if teststr==' 2 wind'
    disp('2 Windows, ok');
    tiffs=findstr(a,'.tif');

    % 1. Bild laden
    searchstr='window 1: ';
    startpunkt= findstr(a,searchstr)+size(searchstr,2);
    fname1=a(startpunkt(1):tiffs(1)+3);
    im1=imread(fname1);
    im1=double(im1)./4095;

    % 2. Bild laden
    searchstr='window 2: ';
    startpunkt= findstr(a,searchstr)+size(searchstr,2);
    fname2=a(startpunkt(1):tiffs(2)+3);
    im2=imread(fname2);
    im2=double(im2)./4095;

    % t1 aus Datei lesen
    searchstr='d1   :';
    startpunkt= findstr(a,searchstr)+size(searchstr,2);
    searchstr='µs';
    endpunkt= findstr(a,searchstr);
    d1=str2num(a(startpunkt(end):endpunkt(end-1)-1));

    % t2 aus Datei lesen
    searchstr='d2   :';
    startpunkt= findstr(a,searchstr)+size(searchstr,2);
    searchstr='µs';
    endpunkt= findstr(a,searchstr);
    d2=str2num(a(startpunkt(end):endpunkt(end)-1));

    % dI aus Datei lesen
    searchstr='dI   :';
    startpunkt= findstr(a,searchstr)+size(searchstr,2);
    searchstr='µs';
    endpunkt= findstr(a,searchstr);
    dI=(str2num(a(startpunkt(end):endpunkt(end-2)-1)));

    t1=d1;
    t2=d1+d2+dI;

    if max(im1(:))==1
        disp ('Einige Pixel in Bild 1 sind gesättigt');
    end

    % im2=max(im2,50/4095);
    %im1=max(im1,50/4095);

    imtau=log(im1./im2);
    imtau=(t2-t1)./imtau;
    %    imtau=medfilt2(imtau,[3,3]);

    bwmaske=im2bw(im2,0.02);
    imtau=imtau.*bwmaske;
    disp('Stellen niedriger Intensität (<0,05) auf 0 gesetzt');
    h1=figure;
    imshow(imtau);
    %title(imname);
    colormap(jet);
    caxis([1 60]);
```

```
            colorbar;

            sname=['lt',imname(1:end-4),'.tif'];

            saveas(h1,sname);
            disp(['Gespeichert als: ',sname]);
            close(h1);
        else
            disp('letztes Bild nicht mit 2 Windows aufgenommen');
        end
        fclose(fid);
    end

else
    disp('kein file gefunden');
end
warning on MATLAB:divideByZero
```

ratio.m

```
 close all

erg=[];
rot=imread('test oO_r.tif');
rot = double(rot);
gr=imread('test oO_g.tif');
gr = double(gr);
r=rot ./gr;

r_roi = r(160:259, 250:349);
roi_mean = sum(sum(r_roi))/10000



  h1=figure


         imshow(r,[0 5]);
         colormap(jet);caxis([0 2]);colorbar



   %h1=figure;
  sname=['lt',rot(1:end-4),'.tif'];

            saveas(h1,sname);
            disp(['Gespeichert als: ',sname]);
            %close(r);
```

raw_to_tiff.m

```
a=dir('*.raw');

G1 = zeros(618,814);
```

```
G2 = zeros(618,814);
B = zeros(618,814);
R = zeros(618,814);


for i=1:numel(a)

    name=a(i).name;
    fid=fopen(name,'r','b');
    A=(fread(fid,[1628 1236],'ushort'))';
    t=fclose(fid);
    A=double(A./2^6)/1023;

    % channel separation
    for k=1:813
        for l=1:617

            B(l,k) = A(l*2,k*2);
            R(l,k) = A((l*2)+1,(k*2)+1);
            G1(l,k) = A((l*2)+1,k*2);
            G2(l,k) = A(l*2,(k*2)+1);

        end
    end

    % calculating virtual pixels
    I1 = zeros(1236,1628,3);
    I2 = zeros(1236,1628,3);
    I3 = zeros(1236,1628,3);
    I4 = zeros(1236,1628,3);

    % Teilbild 1 (rot-gruen-gruen-blau)
    for k=1:812
        for l=1:616

            I1(l*2,k*2,2) = R(l,k);
            I1(l*2,k*2,3) = B(l,k);
            gruen = (G1(l,k)+G2(l,k))/2;
            I1(l*2,k*2,1) = gruen;



            I2((l*2)+1,k*2,2) = R(l+1,k);
            I2((l*2)+1,k*2,3) = B(l,k);
            gruen = (G1(l,k)+G2(l+1,k))/2;
            I2((l*2)+1,k*2,1) = gruen;



            I3(l*2,(k*2)+1,2) = R(l,k+1);
            I3(l*2,(k*2)+1,3) = B(l,k);
            gruen = (G1(l,k+1)+G2(l,k))/2;
            I3(l*2,(k*2)+1,1) = gruen;


            I4((l*2)+1,(k*2)+1,2) = R(l+1,k+1);
            I4((l*2)+1,(k*2)+1,3) = B(l,k);
            gruen = (G1(l,k+1)+G2(l+1,k))/2;
            I4((l*2)+1,(k*2)+1,1) = gruen;
```

```
        end
    end

    I=I1+I2+I3+I4;
    I=im2uint16(I);
    name=name(1:numel(name)-4);
    imwrite(I,[name '.tif']);
    clear A
    disp(name)

end
```

allroithres

```
function [erg1,erg2]=allroi();

% liest alle Bilder im Verzeichnis und analysiert sie
% und zeigt sie an.
close all

dirdata=dir('*.tif');
dirsize=size(dirdata);
erg=[];
y=[];
s=[];

if (size(dirdata)>0)
   for i=[dirsize(1):-1:1]
       imname=dirdata(i).name;
       %figure
       im=imread(imname);
       im=double(im)./4095;
       %falsche Pixel ausgleichen
    %   im(352,340)=im(351,340);
      % im(297,188)=im(296,188);
     %  im(292,83)=im(291,83);
       h1=figure;
       if imname(end)=='f'

           %imshow(im,[0 1]);
           %colormap(jet);caxis([0 1]);colorbar
       else
           %imshow(im,[0 1]);
       end
      % ROI festlegen
       if i==dirsize(1)
           imshow(im,[0 1]);
           colormap(jet);caxis([0 1]);colorbar
           pixval
           disp('Taste drücken')
           pause
           disp('ROI festlegen')
           roip=roipoly;
           pixval
           grenze=input('Minimum-Grenzwert eingeben > ');
           grenzbild=im>grenze;
           roip=roip&grenzbild;
       end
        mittwert=mean(im(find(roip)));
        Stab=std(im(find(roip)));
```

```
        y=[y,mittwert];
        s=[s,Stab];

        close
       %title(imname,'Interpreter','none');
       %pixval
         %sname=['pc_',imname(1:end-4),'.tif'];

            %saveas(h1,sname);
            %disp(['Gespeichert als: ',sname]);
            %close(h1);

   end
       %pause
       %close all
    figure
    imshow(roip);
    title(num2str(sum(roip(:))))
    figure
    errorbar(dirsize(1):-1:1,y,s);
    %plot(dirsize(1):-1:1,y);
    erg1=y;
    erg2=s;
else
   disp('keine Datei gefunden');
end
```

average

```
%liest alle '.tif'-Dateien aus dem Verzeichnis aus und bildet den
%Durchschnitt


close all

a=dir('*.tif');
summe=zeros(1236,1628,3);

for i=1:numel(a)
    name=a(i).name;
    %liest 3-dim-Matrix aus
    A=imread(name);
    A=double(A);
    summe=summe+A;
end

durchschnitt=summe./numel(a);

%macht aus 3-dim-Matrix 2 2-dim
rot=durchschnitt(:,:,2);
gr=durchschnitt(:,:,1);

%ratio
r=rot ./gr;
r_roi=gr(330:870, 855:895);

Mittelwert=mean2(r_roi)
Standardabweichung=std2(r_roi)
```

```
h1=figure;


          imshow(gr,[0 5]);
          colormap(jet);caxis([0 10000]);colorbar

          %surf(r); figure(gcf);
          %colormap(jet);caxis([0 3]);colorbar
```